THE UNIVERSITY
of EDINBURGH

The role of eEF1A Isoforms in Neuritogenesis and Epilepsy

Faith Cathryn Joy Davies

THE UNIVERSITY
of EDINBURGH

A thesis submitted for the degree of

Doctor of Philosophy

The University of Edinburgh

2017

Declaration

I declare that this thesis has been composed by me and that all the work presented within is my own unless clearly stated. All sources of information and other individuals' contributions have been appropriately acknowledged. This work has not been submitted for any other degree or professional qualification

Faith Davies

Dedication

This thesis is dedicated to my wonderful dad, Hugh Quentin Davies, who died before my PhD began, but has and always will be an inspiration.

Acknowledgements

My first and deepest thanks to Cathy, an incredibly supportive, caring and inspiring supervisor and mentor. I count myself very lucky to have spent this time learning from you.

I'm also indebted to the members of the Abbott lab, past and present, who have taught me, helped me, and made the lab a lovely place to work and learn over the last five years.

To my friends and colleagues for commiserating and celebrating with me through the crazy ups and downs of PhD life, I'd be lost without you. Special thanks to Niamh, for always being there and being the most excellent of friends.

Matilda, my daughter, when I found out I was pregnant I felt like starting a family and doing a PhD might be incompatible. I needn't have worried. Having you has made life immeasurably richer, and forced me to develop some much-needed time-management skills.

Finally, to my family, most especially Leo – you have stuck with me and been my solid rock. You've kept me going and always believed in me, I could not ask for more, and certainly could not have got here without you.

List of Contents

List of Figures

List of Tables

Abstract

Eukaryotic Elongation Factor 1A (eEF1A) exists in two forms in vertebrates. The first form, eEF1A1, is expressed ubiquitously throughout development but is downregulated postdevelopmentally and replaced with eEF1A2, an isoform sharing 92% amino acid identity, in neurons and muscle. The primary function of eEF1A is to recruit amino-acylated tRNAs in a GTP-dependent manner to the A site of the ribosome during protein translation, but it also has non-canonical roles in the cell, some of which are isoform dependent.

The reasons for the cell-type dependent switch from eEF1A1 to eEF1A2 are poorly understood. The first aim of this project was to examine the role played by eEF1A isoforms in neuritogenesis. To do this I used RNAi to significantly reduce expression of one or other isoform in neuronal cells and measure the effects this had on neurite outgrowth. Neurite outgrowth was significantly reduced in cells depleted of eEF1A1, but not eEF1A2.

The complete loss of eEF1A2 is fatal, as has been demonstrated in the wasted mouse, an eEF1A2-null model characterised by muscle wastage, neurodegeneration and death at 4 weeks of age. Mice heterozygous for the wasted mutation have normal motor function. Recent work has found that heterozygous missense mutations in eEF1A2 can cause epilepsy and intellectual disability. It is not yet known whether the seven different *de novo* mutations identified to date confer loss or gain of function – a crucial piece of information required before possible treatments can be sought. The second aim of this project therefore was to investigate the role of eEF1A2 in epilepsy and intellectual disability. I achieved this by using CRISPR in two ways; firstly to model one of the mutations, D252H, *in vitro* in a neuronal cell line, and secondly to model another of the mutations, G70S, *in vivo.*

No mice that recapitulated the human disease condition of *EEF1A2*$^{G70S/+}$ were obtained however, due to the error-prone nature of the non-homologous end joining repair pathway activated by CRISPR-mediated DNA cleavage, 17 of the 35 mice born were found to be homozygous nulls at the *Eef1a2* locus. Nine of these had fatal audiogenic seizures caused by sudden loud noises within the animal unit. Three mice were *Eef1a2*$^{G70S/-}$ and one *Eef1a2*$^{G70S/G70S}$ but these nonetheless showed a wasted

phenotype, indicating that this mutant form of eEF1A2 has compromised function, at least in terms of translation elongation. Whether it has a toxic function ca not yet be known, but the severity of the phenotype in the G70S homozygous animal could suggest a gain of function.

In *in vitro* experiments with exogenous eEF1A2 carrying the epilepsy-causing mutation R423C, protein expression of the mutant construct in immortalised cell lines was significantly higher when cotransfected with the wildtype construct, which mirrors the condition in humans, than when transfected alone, so the mutant protein could be stabilised in the presence of wildtype eEF1A2.

I used CRISPR on LUHMES cells to make a mutant neuronal cell line containing the D252H mutation in eEF1A2. Due to time restraints no phenotypic differences between the wild type line and the D252H mutation line have yet been identified, but would form the focus of a future project.

List of abbreviations

AD	Alzheimer’s disease
AHA	L-Azidohomoalanine
AMPS	Ammonium persulphate
ANOVA	Analysis of variance
Arc	Activity-regulated cytoskeletal protein
BAC	Bacterial artificial chromosome
bp	base pairs
BRF	Biomedical research facility
cAMP	Cyclic adenosine monophosphate
cDNA	Complementary DNA
CRISPR	Clustered regularly interspaced short palindromic repeats
dB	Decibels
DNA	Deoxyribonucleic acid
DIC	Differential interference contrast
DMSO	Dimethyl sulphoxide
DMEM	Dulbecco's modified eagle medium
eEF1A	Eukaryotic elongation factor 1A
EEF1A1	Eukaryotic elongation factor 1A1 (Human gene)
EEF1A2	Eukaryotic elongation factor 1A2 (Human gene)
Eef1a1	Eukaryotic elongation factor 1A1 (Mouse gene)
Eef1a2	Eukaryotic elongation factor 1A2 (Mouse gene)
eEF1A1	Eukaryotic elongation factor 1A1 (protein)
eEF1A2	Eukaryotic elongation factor 1A2 (protein)
eEF1B	Eukaryotic elongation factor 1B
ERK	Extracellular signal-regulated kinase
FACS	Fluorescence-activated cell sorting
FBS	Foetal Bovine Serum
FGF	Fibroblast growth factors
FMRP	Fragile X mental retardation protein
FXS	Fragile X syndrome
gDNA	genomic DNA
GDP	Guanosine diphosphate
GEF	Guanine exchange factor
GFAP	Glial fibrillary scidic protein
GFP	Green fluorescent protein
GluR	Glutamate receptor
GTP	Guanosine triphosphate
gRNA	Guide RNA
HEK293ft	Human embryonic kidney 293
HDR	Homology directed repair
HRP	Horse radish peroxidase
HSF	Heat shock factor

iPSC	induced pluripotent stem cell
kD	kilodalton
LTD	Long term depression
LTP	Long term potentiation
LUHMES	Lund human Mesencephalic
mRNA	messenger RNA
NGF	Nerve growth factor
NHEJ	Non homologous end joining
NS1	Neuroscreen-1
PAGE	Polyacrylimide gel electrophoresis
PAM	Potospacer adjacent motif
Pcdh10	Protocadherin 10
PCR	Polymerase chain reaction
PDE	Phosphodiesterase
PND	Post natal day
qPCR	Quantitative PCR
RIPA	Radioimmunoprecipitation assay
RPE1	Retinal Pigment Epithelium 1
RNA	Ribonucleic acid
RNAi	RNA interference
RPMI	Roswell Park Memorial Institute
RT-PCR	Reverse transcriptase PCR
SDS	Sodium dodecyl sulphate
SILAC	Stable isotope labelling by amino acids in cell culture
shRNA	Small hairpin RNA
siRNA	Small interfering RNA
SOC	Super Optimal Broth
ssODN	single-stranded oligonucleotide
SUDEP	Sudden unexpected death in epilepsy
TEMED	Tetramethylethylenediamine
TBE	Tris Borate EDTA buffer
Tm	Melting temperature
TRIS	Tris(hydroxymethyl)aminomethane
tRNA	Transfer RNA
UBE3A	Ubuiqitin E3 Ligase
UTR	Untranslated region
Wst	Wasted
WT	Wildtype

Chapter 1 Introduction

1.1 eEF1A in translation

First identified in yeast (Pedersen et al., 2001), elongation factor eEF1A was so named for its role in protein translation. It is a GTP binding protein, and in its GTP-bound form delivers the aminoacylated tRNA to the A site of the ribosome. After codon-anticodon recognition, GTP is hydrolysed to GDP and eEF1A is released from the ribosome. It is then free to associate with nuclear exchange factor eEF1B, which causes exchange of GDP for GTP, reactivating the protein to begin the cycle again (Figure 1.1)

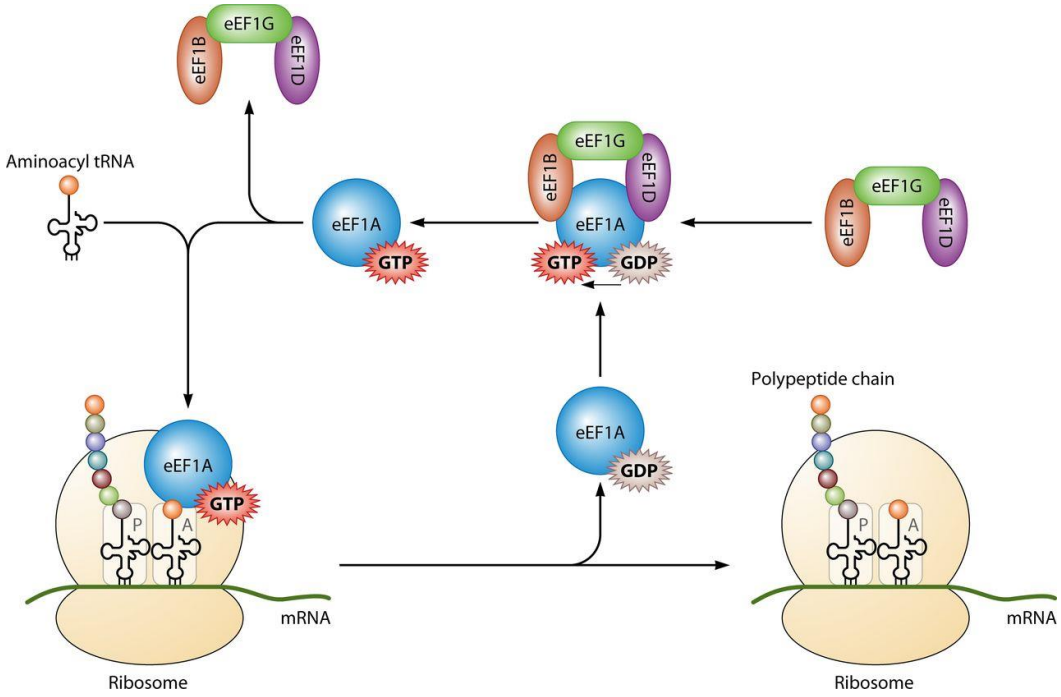

Figure 1.1 Translation elongation (not to scale) *Eukaryotic elongation factor 1A (eEF1A; blue circle) in complex with GTP (red star) delivers an aminoacylated tRNA to the A site of the ribosome (yellow). GTP is hydrolysed when codon-anticodon recognition occurs, and eEF1A-GDP is released from the ribosome. The GTP exchange factor for eEF1A is a complex with three subunits: eEF1B is shown in orange, eEF1G in green, eEF1D in purple. This complex promotes the exchange of the bound GDP for GTP. Taken from Li et al., 2013.*

1.1.1 eEF1A exists as two differentially expressed isoforms in vertebrates

In vertebrates two forms of the eEF1A gene are found encoded on different chromosomes. In humans *EEF1A1* maps to 6q14, whilst *EEF1A2* maps to 20q13.3 (Lund et al., 1996). The first isoform, eEF1A1, is ubiquitously expressed throughout the cells of the body during embryogenesis. In mice and rats, and probably humans, eEF1A1 is downregulated soon after birth in heart, muscle and neurons, and eEF1A2 is expressed in its place (Khalyfa et al., 2001; Lee et al., 1992). Pockets of eEF1A2 expression have also been identified in pancreatic islet cells and enteroendocrine cells in colon crypts (Newbery et al., 2007). The reasons for this tissue-specific developmental switch from one isoform to another are not yet well understood, although the cell types which experience the switch (skeletal muscle, heart, neurons) are notable for their longevity, being terminally differentiated. Interestingly, a study of muscle samples taken from trauma patients in a state of a hypercatabolic stress (the result of which is muscle breakdown) found a 165-fold increase in eEF1A1 mRNA not seen in healthy age-matched controls (Bosutti et al., 2007). Similarly, in rats subjected to permanent muscle denervation an upregulation of eEF1A1 is seen which lasts for at least 2 years after injury (Khalyfa et al., 2003).

A plausible hypothesis for the developmental switch is that certain cell types replace eEF1A1 with eEF1A2 to avoid certain functions performed by the former isoform whilst maintaining translation elongation function. The switch back to eEF1A1 identified in trauma patients and injured rat muscle may give a clue as to the functional differences between the two isoforms.

Structurally the two isoforms are very similar, 92% identical at the amino acid level (Figure 1.2A). 3-D modelling has shown most of the differences to be clustered in two regions across one face of the protein, not overlapping with the binding site for eEF1B (Figure 1.2B) (Soares et al., 2009).

The two isoforms possess different propensities to self-aggregate: eEF1A1 has been found to have a higher ability to self-associate than eEF1A2, and is more hydrophobic (Timchenko et al., 2013). They also have different affinities for GTP (Kahns et al., 1998).

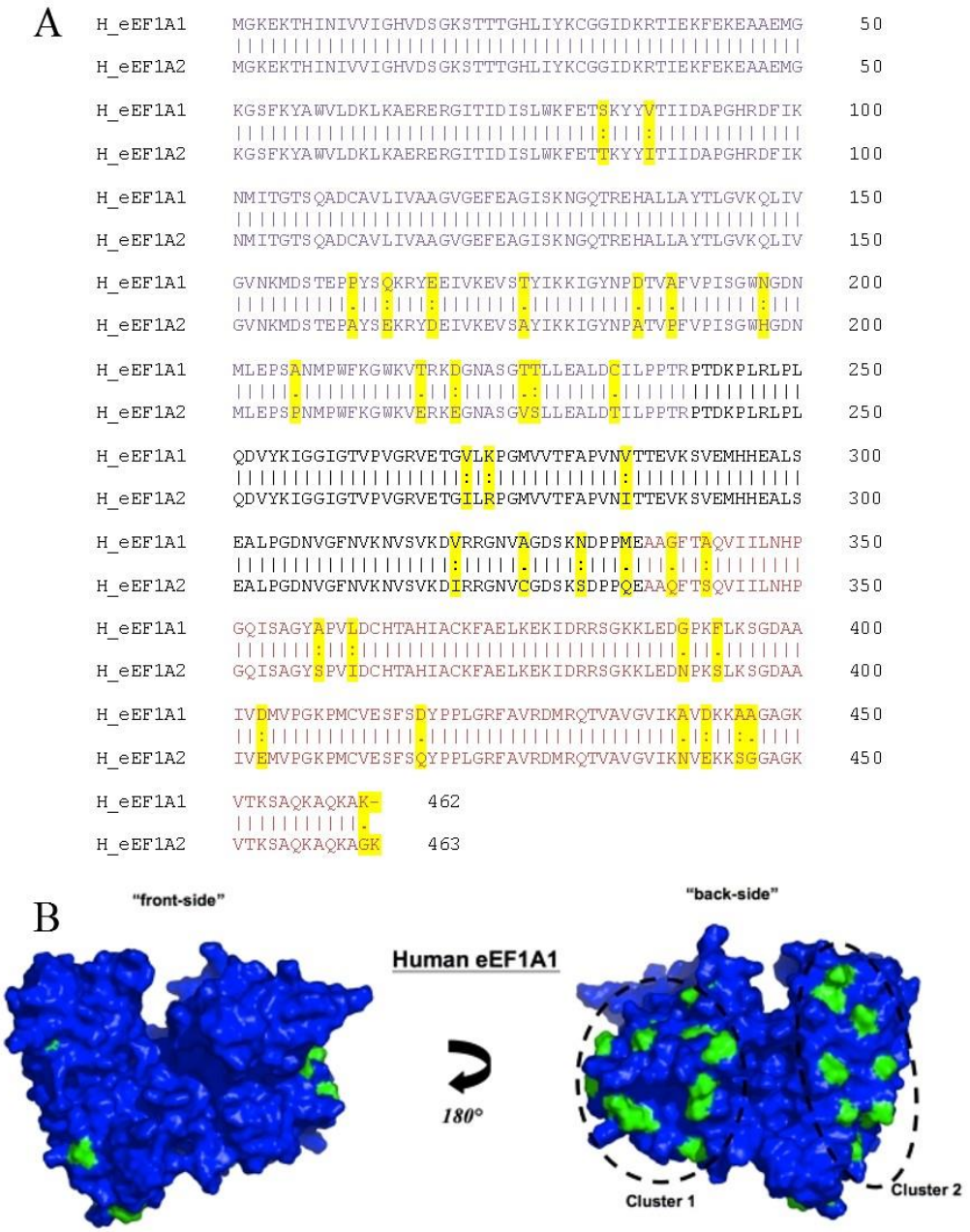

Figure 1.2 (A) Amino acid alignment of human EEF1A1 and EEF1A2*. Amino acid variation between the two isoforms is highlighted in yellow. A single dot indicates a semi-conservative change, a double dot is a conservative substitution. The three colours used indicate different domains of the protein, domain I is purple, domain II is black, domain III is red. (B) 3-D model of eEF1A1 Locations of exposed side-chains that vary in eEF1A2 are mapped onto the surface of the model (coloured green) Adapted from Soares et al., (2009).*

eEF1A1 binds GTP more strongly than GDP, whereas the reverse is true for eEF1A2. This may mean that eEF1A2 has a greater dependence on eEF1B, the nuclear exchange factor, than does eEF1A1. Post-translational modifications, when mapped onto 3D models of the proteins, are highly enriched on those surface regions of the

protein that correspond to the clusters of sequence variation, showing how two highly homologous proteins could still perform different functions (Soares et al., 2009).

Despite these differences, functionally speaking the two isoforms have indistinguishable abilities in terms of their canonical function in translation, when measured *in vitro*, (Kahns et al., 1998) so the structural and biochemical differences could account for differences in function apart from elongation translation.

1.1.2 Non-canonical Functions of eEF1A isoforms

Apart from its role in elongation translation, one or both isoforms of eEF1A are known to have a number of other non-canonical functions. These are summarised in table 1.1, and two of these, heat shock regulation and actin bundling, are discussed in greater depth below.

Table 1.1 A summary of non-canonical roles of eEF1A

Non-canonical role for eEF1A	Description	References
Heat shock regulation	Essential part of heat shock response pathway (expanded below)	Vera et al., 2014
Actin bundling	eEF1A has been shown to bind and bundle actin (expanded below)	Liu et al., 1996; Numata et al., 2000; Vlasenko et al., 2015
Nuclear export	Central role in transcription-dependent export of proteins from nucleus in mammalian cells	Khacho et al., 2008
Protein degradation	Interacts with the 26S proteasome, association increases when translation inhibited	Sanges et al., 2012 Chuang et al., 2005
Apoptosis	eEF1A2 is anti-apoptotic, it interacts with Pdrx-1 to confer cells with resistance to oxidative stress insult	Ruest et al., 2002 Chang and Wang, 2007

1.1.2.1 eEF1A1 and the heat shock response

In response to environmental stresses including but not limited to hypoxia, starvation, toxin exposure and elevated temperature, genes are activated that encode cytoprotective proteins able to rescue cells from damage caused by misfolded proteins or inappropriate protein accumulation. This is known as the heat shock response. Reviewed by Shamovsky et al. (2008). Heat shock factor 1 (HSF1) is the master regulator of the heat shock response in mammalian cells. Upon stress HSF1 is released from its inhibitory complex and localised to the nucleus. As a homotrimer, it binds heat shock response elements in the promotor region of genes that are upregulated as part of the response (Kugel and Goodrich, 2006). These transcribed genes must be stably transported out of the nucleus to the ribosome for translation.

eEF1A was first identified as playing a major role in heat shock response induction by Shamovsky et al., (2006), who found that eEF1A interacted with HSF1, and that this interaction was enhanced by heat shock. Although the isoform involved was not mentioned, the eEF1A molecule used was isolated from liver, which only expresses eEF1A1.

Dr Lowri Griffiths, from our laboratory group, investigated the separate roles of eEF1A1 and eEF1A2 in the heat shock response. By selectively knocking down eEF1A1 and eEF1A2 using RNAi, Griffiths showed that eEF1A2 alone was not sufficient to induce the heat-shocked cells to express HSP70 (Griffiths; Vera et al., 2014).

Work by Vera et al. (2014) has shown that eEF1A1 is more thoroughly involved with the heat shock response than previously thought. It was found that in the absence of stress eEF1A1 is bound to the promotor regions of heat shock proteins where it acts as a heat shock gene transcriptional repressor. Hence eEF1A1 both enables HSF1 binding to DNA upon stress, and also represses HS gene activation before stress. eEF1A1 was also found to stabilise heat shock mRNA transcripts and facilitate their export to the ribosome by binding to their 3'UTR.

1.1.2.2 Actin bundling and oligomeric state of eEF1A

Cytokinesis is the final step of the cell cycle in which a contractile ring containing actin filaments forms a division furrow and divides the cell into two daughter cells.

eEF1A and calmodulin had previously been found colocalised to the divison furrow (Numata et al., 2000), but more recently Bunai et al. (2006) used gel filtration chromatography to show that eEF1A exists in both monomeric and dimeric forms. They found through electron microscopy and a cosedimentation assay that dimeric eEF1A could bundle F-actin *in vitro*, but monomeric eEF1A could not, and that this bundling can be regulated by Ca^{2+}/Calmodulin: in the presence of Ca^{2+}/Calmodulin eEF1A the monomeric form of eEF1A is promoted and F-actin bundling is reduced, whilst in the absence of Ca^{2+}/Calmodulin eEF1A dimers can form and can bundle F-actin. Further to this, Timchenko et al. (2013) found that eEF1A1 has a higher ability to oligomerise than eEF1A2, and oligomeric state had no effect on translation elongation efficiency.

Although the first crystal structure for the bacterial homolog of eEF1A, EF-Tu, was resolved over 20 years ago, (Kjeldgaard et al., 1993) the X-ray crystal structure for eEF1A2*GDP was only recently reported fully by Crepin et al (2014). In this study, eEF1A2 crystallised as a dimer, however in a more recent study which used human *ex vivo* derived polysomes to examine, using cryo-electron microscopy, the actively translating polysomes in a variety of intermediate states, EEF1A was visualised as a monomer (Behrmann et al., 2015), indicating that when performing translation elongation, eEF1A probably functions as a monomer.

Vlasenko et al (2015) showed that a truncated form of eEF1A1 lacking the first 69 (of 462) amino acids at the N-terminal end (domain I) loses its ability to bind actin, however only domain III at the C-terminal end of the protein directly interacted with actin. This seeming contradiction can be resolved if eEF1A does indeed bundle actin as a dimer. In this case then the loss of the N-terminal amino acids would mean eEF1A domain I could no longer dimerise by contact with domain III of the counterpart molecule (Figure 1.3A), though domain III is still able to bind actin filaments. A proposed model of eEF1A actin binding (Figure 1.3B) illustrated which of the three domains of eEF1A contacts which of the counterpart molecule domains, in normal circumstances (Vlasenko et al., 2015). Taken together, these results could indicate that oligomeric status is a factor in the canonical and non-canonical roles of eEF1A isoforms, with eEF1A performing translation as a monomer, but actin-bundling as a dimer.

Given that eEF1A1 has a greater propensity to self-aggregate than does eEF1A2 (Timchenko et al., 2013), it is tempting to hypothesis that eEF1A1 is able to bundle actin as a dimer and perform many more secondary functions in early development, but is then switched off and replaced with eEF1A2. Much work remains to untangle

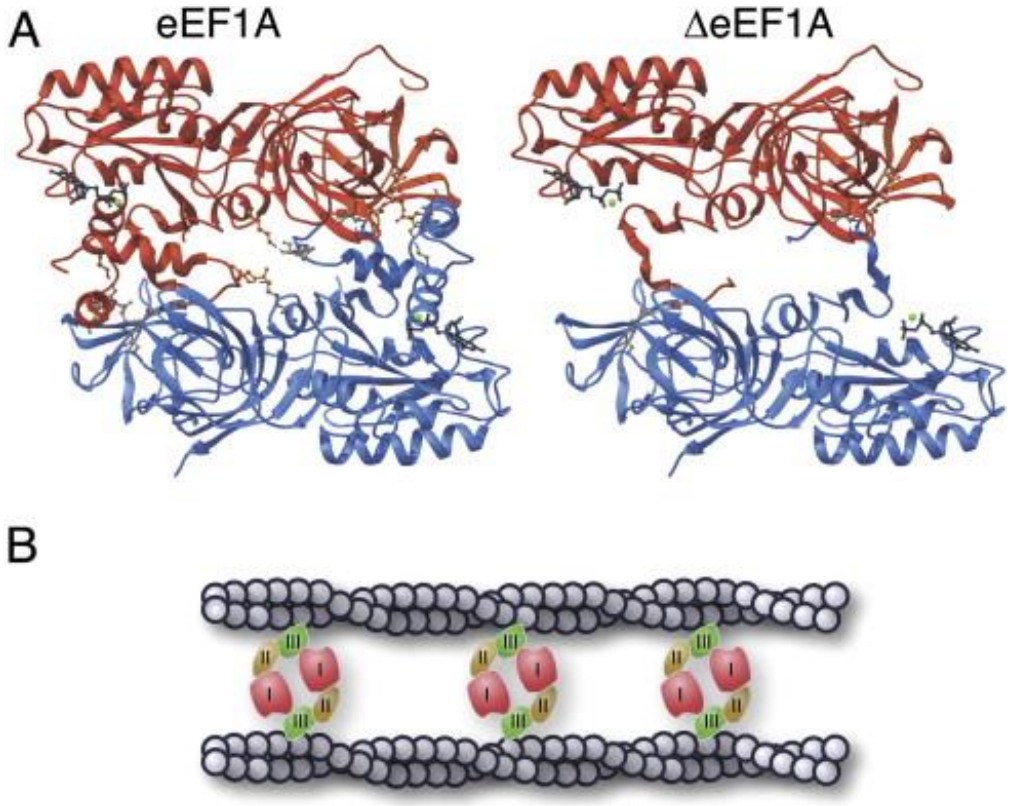

Figure 1.3 Dimeric structure of eEF1A is required for actin bundling*. (A) ΔeEF1A, lacking the first 69 amino acids, loses the structural elements responsible for dimerization of eEF1A. Chain A coloured in red, chain B coloured in blue. Removal of the N-terminal part of eEF1A disrupts hydrogen bonds contributing to the dimer formation. (B) Model of the eEF1A dimers involvement into actin bundling. Domain III of each dimer binds the actin filaments, whereas Domain I contacts Domain III of the counterpart chain to stabilize a dimer. Adapted from Vlasenko et al., (2015).*

which isoforms are involved in which functions.

1.1.3 eEF1A isoform expression in neuronal development

The tissue-specific developmental swap from eEF1A1 to eEF1A2 in muscle, neurons and heart is very well documented in mouse and rat (Khalyfa et al., 2001), in which eEF1A1 protein is almost undetectable in muscle by post-natal day 21, and in pig (Svobodová et al., 2015). Adult human samples tested also show the tissue-specific

isoform swap (Khalyfa et al., 2001), although the exact timing of the switch remains unknown in humans. A study using isoform-specific antibodies to probe mouse brain sections showed that eEF1A isoform expression is mutually exclusive in brain (Newbery et al., 2007). In cerebellum eEF1A2 is strongly expressed in Purkinje cells, eEF1A1 is expressed in white matter. Across the brain eEF1A2 predominates in neurons though eEF1A1 is found in some small neurons (Newbery et al., 2007).

Cajigas et al. (2012) identified the presence of eEF1A1 and eEF1A2 mRNA transcripts in both somata and neuropil taken from adult rat hippocampus, however the paper recognises that the neuropil sample microdissected from the hippocampus also contained glial cells, interneurons and endothelial cells. Since glial cells express eEF1A1, and most neurons express eEF1A2, lysates and other extracts from brain will include both isoforms. This was controlled for, with analysis of varying proportions of glial-derived and neuropil-derived samples showing a proportion of eEF1A1 mRNA to be of glial origin, though this would not account for all the eEF1A1 mRNA identified.

The presence of mRNA transcripts does not mean that the protein is necessarily translated, however eEF1A1 has been identified in the post synaptic densities (and not the presynaptic area) of adult rat brain in a proteomics study (Phillips et al., 2005). eEF1A1 mRNA and protein have been found in matured (13 days *in vitro*) cortical axons using fluorescent in situ hybridisation and immunocytochemistry (Taylor et al., 2009) though the antibody used to show presence of eEF1A1 protein may not have been specific to that isoform. Conversely, Cho et al. (2012) found that in 8-10 days *in vitro* (DIV) cortical neurons from rat, exogenous GFP-tagged eEF1A1 was localised to dendritic spines, but not localised to the axon. These differing results may reflect the different developmental stages of the neurons cultured, the different experimental methods employed – exogenous versus endogenous eEF1A1, or the difference between examination of tissue versus cell culture: all cells in culture and all immortalised cell lines so far examined express eEF1A1. In a study by Tsai et al. (2012) examining the role of eEF1A in fragile X syndrome, shRNAs specific to eEF1A1 were used in RNAi experiments in dissociated mouse neuronal culture and hippocampal slice preparations. eEF1A was found to be upregulated in neuronal and mouse models of Fragile X disease, and RNAi silencing of eEF1A1 was sufficient to

reverse some of the cellular phenotypes associated with the disease. (Tsai et al., 2012) Altogether the weight of evidence certainly suggests a role for eEF1A1 in neuronal development, particularly related to synapse function (explored further in section 1.2.4).

1.2 eEF1A2 and Neurological disease

1.2.1 The Wasted Mouse is eEF1A2-null.

A functional knockout for eEF1A2 was discovered in the wasted mouse, an autosomal recessive mutation which arose spontaneously in 1972 (Shultz et al., 1982). The wasted mutation is a 15.8 kilobase deletion which includes exon 1 and the entire promotor region of *Eef1a2*. Transgenic experiments have shown the wasted phenotype is due entirely to the loss of eEF1A2 (Newbery et al., 2007). Mice were engineered that carried a bacterial artificial chromosome (BAC) of approximately 65kB, which included the entire *Eef1a2* gene. When crossed with wasted mice, the presence of the BAC was found to be sufficient to rescue the wasted phenotype. A separate mouse line was then engineered which carried a mutated version of the same BAC with a deletion within the *Eef1a2* gene. The mutated BAC failed to correct any aspect of the wasted phenotype, so it was concluded that loss of eEF1A2 function alone was responsible for the wasted phenotype (Newbery et al., 2007).

Homozygous wasted mice develop tremors, gait abnormalities and weight loss starting from post-natal day (PND) 21. They rapidly deteriorate and die at around PND 28. Heterozygous wasted mice, despite expressing eEF1A2 at half the level of wild type mice (Khalyfa et al., 2001, 2003), display no neuromuscular deficits nor spinal cord pathology, and have comparable life spans to wildtype littermates (Griffiths et al., 2012).

The neuromuscular pathology of wasted mice starts as early as PND 17. A decrease in the number of innervated motor endplates is the first discernible abnormality, followed by reactive gliosis with increased GFAP staining in wasted mouse spinal cord sections initially in cervical sections but progressing rostrocaudally (Newbery et al., 2005). Motor neurons in the anterior horn develop vacuoles from PND 24, again with a rostrocaudal gradient. Motor impairment (as measured by performance on a rotarod)

is apparent in wasted mice from PND 21 and grip strength tests show reduced forelimb strength compared to wild type and heterozygous wasted littermates from PND 20 (Griffiths et al., 2012).

Weight loss in the mice is mostly accounted for by loss of muscle bulk (Newbery et al., 2005). Whether muscle atrophy is due to loss of muscle eEF1A2 or is neurologic in origin (denervation atrophy) was determined by the creation of transgenic animals expressing eEF1A2 driven by muscle-specific promotor HSA (human skeletal actin). Wasted mice expressing eEF1A2 in muscle but not in neurons were phenotypically indistinguishable from wasted mice expressing no eEF1A2 at all: muscle expression of eEF1A2 is not sufficient to rescue the phenotype.

Attempts to produce transgenic mice expressing eEF1A2 only in neurons were unsuccessful, with the mice resulting from this experiment unexpectedly expressing eEF1A2 in both nerve and muscle, though the transgene expressed in no other tissues, so the 'leaky' expression was limited only to muscle. The authors note that this could be due to positional effects or because of a change to the promotor introduced during preparation to facilitate cloning of the construct. Wasted mice expressing this transgene were phenotypically normal: muscle and nerve expression of eEF1A2 rescued the phenotype. In all, the evidence points to a neurological origin for muscle atrophy in the wasted mouse (Doig et al., 2013; Newbery et al., 2005).

1.2.2 Missense Mutations in eEF1A2 can cause epilepsy and intellectual disability

Since 2012, a total of 13 *de novo* heterozygous missense mutations of eEF1A2 have been identified in 22 patients suffering from epilepsy and intellectual disability (summarised in Table 1.2). Other features of many but not all cases include autistic behaviours, hypotonia, movement disorder, microcephaly, cerebral atrophy and characteristic facial features – a broad nasal bridge, tented upper lip, everted lower lip and downturned corners of the mouth.

None of the mutations are found in the Exome Aggregation Consortium (ExAc) database containing data from over 60000 different individuals, and there are no known coding polymorphisms. (Lam et al., 2016). eEF1A2 has been found to be

amongst the top 5% of constrained genes, as measured by comparing the difference between expected and observed synonymous mutation rates (Samocha et al., 2014).

It should be noted that four of the cases were displayed on a conference poster (Helbig et al., 2015), and have not yet been published. These cases should be treated with caution until such time as they have been published, since establishing likelihood of causation in cases of *de novo* mutation is part of the process of bringing such cases to publication. The cases identified from conference poster are marked as such in the table.

Of note is the variety in phenotype severity, which ranges from severe, daily intractable seizures, global developmental delay and cerebral atrophy for the patient with the F98L mutation, to no seizures (although an abnormal EEG), moderate ID and a normal MRI for the patient carrying the F98C mutation. The patient carrying the E124K mutation is also only mildly affected as her seizures are under control, she can speak in sentences and she has been in mainstream school, although will attend a special school at secondary level (Lam et al., 2016).

Mutation	Published	Age	Seizure phenotype	Intellectual disability/developmental delay/motor delay	Autistic Features	Microcephaly/ cerebral atrophy	Hypotonia	Facial features
G70S	(Veeramah et al., 2013) Proband B	14y, M	Infantile spasms from 8 months, myoclonic/tonic, GTCS, intractable	Severe ID, non-verbal, gait instability		Microcephaly	+	
G70S	(de Ligt et al., 2012) Case 91	22y, F	Absence, GTCS and myoclonic seizures from 4 months.	Severe ID, Non-verbal, global developmental delay	+	No microcephaly at 22y	+	+
G70S	(Lam et al., 2016) Case 1 (Yang et al., 2014)	3y, F	Myoclonic, tonic-clonic from 2 months, later developed absence	Global developmental delay		No microcephaly at 9m	+	+
G70S	Helbig (poster) Patient 1 Deceased (resp failure)	4y, M	Absence, GTCS, tonic, myoclonic	Severe ID, non-verbal	Stereotypies	Normal MRI	+	
G70S	Helbig (poster) Patient 2 (Helbig et al., 2016)	7y, F	Atypical, absence, myoclonic	Moderate ID, non-verbal	None	Cerebral atrophy	+	
E122K	(Nakajima et al., 2015) Case 2	12y, F	Infantile seizures, controlled	Severe ID, ataxic gait	+	Cerebral atrophy, progressive microcephaly	+	+
E122K	(Inui et al., 2015) Case 1	2y, F	Repetitive myoclonic from 10 months, atypical absence, intractable	Severe ID, non-verbal, cannot roll over		Normal head circumference at birth		+
E122K	(Inui et al., 2015) Case 2	2y, M	Repetitive myoclonic and myoclonic-atonic at 8 months, intractable	Severe ID, non-verbal, cannot stand unaided		Cerebral atrophy		+
E122K	(Lam et al., 2016) Case 5	6y, F	Infantile spasms from 10 weeks, controlled	Non-verbal, but uses signs. gross motor delay, unsteady gait	None	microcephaly	+	+
E124K	(Lam et al., 2016) Case 6	10y, F	Myoclonic seizures from 3 months, then absence, controlled	Language delay but speaks well. Mild ID	None	Normal MRI	-	+

Mutation	Published	Age, gender	Seizure phenotype	Intellectual disability/developmental delay/motor delay	Autistic Features	Microcephaly/ cerebral atrophy	Hypotonia	Facial features
D252H	(Nakajima et al., 2015) Case 1	8y, F	GTCS beginning at 8y	Moderate ID, non-verbal, Global developmental delay, cannot walk	+	Cerebral atrophy, progressive microcephaly	+	+
D252H	DDD	F		Severe global development delay	+	Microcephaly		
R266W	Helbig (poster) Patient 5	5m, M	Absence, GTCS, hemiclonic, controlled	Global developmental delay	None	Ventriculomegaly	+	
R266W	DDD	F	Seizures	Severe global development delay	+			+
R423C	(Lam et al., 2016) Case 7 also Helbig (poster) Patient 6	5y, M	Infantile spasms, myoclonic, tonic, intractable	Global developmental delay, moderate ID, non-verbal		Thin corpus callosum, cerebral atrophy	+	+
F98L	(Lam et al., 2016) Case 4	9y, F	Focal seizures as infant, now daily myoclonic, tonic, occasional tonic-clonic,	Severe global developmental delay, no head control, cannot sit, non-verbal		Progressive microcephaly	+	+
F98C	Helbig (poster) Patient 3	5y, F	No seizures, abnormal EEG	Moderate ID, non-verbal	Stereotypies	Normal MRI	+	
I71L	(Lam et al., 2016) Case 2	9y, M	Seizures	Severe global developmental delay, can walk independently, non-verbal but signs		Head circumference 25th centile at 5y		+
D91N	(Lam et al., 2016) Case 3	14y, F	Seizures from 2y, head drops, eye rolling, arm extension, intractable	Developmental delay, non-verbal, cannot walk independently		No microcephaly	+	+
M102V	Helbig (poster) Patient 4	8y, F	Febrile seizures, GTCS, hemiclonic	Moderate ID	None	Normal	_	
T432M	DDD	M		Severe ID, delayed speech & lang. development				
A92T	(Lopes et al., 2016) Proband 17	6y, F	Seizures (started at 1month old)	Severe ID, global developmental delay,	+	Generalised brain atrophy		

Table 1.2 Clinical features of patients with eEF1A2 mutations. *GTCS: generalised tonic-clonic seizures; ID: intellectual disability. DDD: Deciphering Developmental Disorders Study. Where a box is empty, this information was not included in case report. Helbig poster available at http://www.ambrygen.com/sites/default/files/web/scientific_posters/aes_2015_helbig.pdf*

The mutations are all found on amino acid residues that are conserved across both eEF1A isoforms, and evolutionarily conserved back to yeast. Modelling the mutations on a 3D surface representation of eEF1A2, (**Figure 1.4**), they are mostly seen to be close to either the eEF1Bα binding site, the GTP/GDP binding site or inter-domain contacts, indicating how the mutations may affect protein function. One of the mutations, E122K, is close to the GTP/GDP binding site. It happens to have been characterised in yeast eEF1A, in which it was found to reduce translational fidelity (Sandbaken and Culbertson, 1988). The patient suffering from the E124K mutation, which can be seen in **Figure 1.4** to be slightly further away from the GTP/GDP binding site, also suffers from a much milder phenotype, perhaps reflecting the lower impact this mutation has on the function of critical areas of eEF1A2.

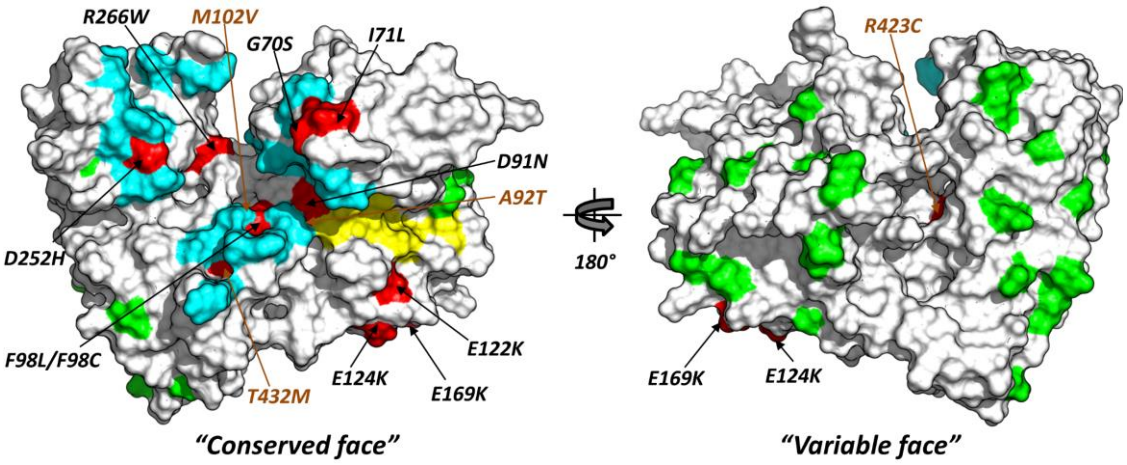

Figure 1.4 Location of known missense mutations and binding sites mapped on 3-D model of human eEF1A2. *The equivalent location of the eEF1Bα (cyan) and GTP/GDP binding site (yellow) from yeast eEF1A (Andersen et al., 2001) are indicated on a surface representation of the 3-D model of human eEF1A2 (Soares et al., 2009), and variant amino acid residues between eEF1A1 and eEF1A2 highlighted (green). Known epilepsy mutations (red) are mapped on the model to show proximity or overlap to the binding site of eEF1Bα (G70S, I71L, D91N, F98L/F98C, D252H, R266W), and/or to the GTP/GDP-binding site (D91N, E122K, E124K). Residues whose side-chains are largely buried (A92T, M102V, R423C, T432M) are highlighted in brown; in these instances, A92T, M102V, T432M are also located in close proximity to the eEF1Bα binding site, whereas M102V, R423C and T432M are located at or adjacent to inter-domain contacts. Structural modelling and figure by Dinesh Soares*

1.2.3 Translation Factor Mutations and Disease

Around a dozen translation factors are involved in translation initiation (Aitken and Lorsch, 2012). Mutations in several of these factors have been implicated in neurological disease: a missense mutation of translation initiation factor *EIF2γ* causes moderate to severe intellectual disability, microcephaly and facial dysmorphic features (Borck et al., 2012), mutations in any of the subunits encoded by another translation initiation factor, *EIF2B*, lead to a severe autosomal recessive neurodegenerative disorder known as vanishing white matter disease. This disorder is characterised by brain myelin loss upon physiological stress, and has an extremely wide phenotypic variation, varying from antenatal onset and early death to adult onset and slow disease progression (Reviewed in Scheper et al., 2007). A homozygous splice site mutation in *EEF1B2*, encoding eEF1Bα which acts as GTP-exchange factor for eEF1A, was the only mutation found within a consanguineous family with non-syndromic intellectual disability (Najmabadi et al., 2011).

Amino-acyl-tRNA synthetases are a group of enzymes which attach amino acids to tRNAs. Each amino acid has its own specific amino-acyl tRNA synthetase. Mutations in *GARS* and *YARS*, the genes encoding glycyl- and tyrosyl- tRNA synthetases respectively are linked to Charcot-Marie-Tooth peripheral neuropathies (Antonellis et al., 2003; Jordanova et al., 2006).

'Sticky mice' carry a homozygous point mutation in *Aars*, the alanyl-tRNA synthetase gene, and suffer from progressive cerebellar purkinje cell loss and ataxia (Lee et al., 2006). The mutation is located in an evolutionarily conserved editing domain of the alanyl-tRNA synthetase protein, which edits and corrects misaminoacylated tRNAAla. A reduction in the efficiency of this functional domain causes an increase in non-cognate amino acids becoming mistakenly incorporated into nascent proteins. This in turn leads to an accumulation of misfolded proteins, thought to be the cause of the sticky mouse phenotype (Lee et al., 2006). As mentioned above, one of the newly-identified epilepsy-causing mutations in eEF1A2, E122K, was previously modelled in yeast and found to cause translational infidelity (Sandbaken and Culbertson, 1988). Knowledge that reduced translational infidelity in mouse leads to cerebellar Purkinje

cell loss and ataxia may well give an indication of the disease mechanism here, especially considering ataxia is one of the observed phenotypes.

1.2.4 eEF1A in Neurological Disorders

There is growing evidence that eEF1A plays a role in synaptic plasticity. eEF1A mRNA was first identified *in vivo* in dendrites from Aplysia (sea slug) (Giustetto et al., 2003). In Aplysia sensory neurons, serotonin application produces long-term facilitation. One of the late genes responsible for maintenance of the long-term facilitation of this process is Aplysia (Ap) EF1A. Ap-eEF1A mRNA and protein are both translocated to the synapse in response to local serotonin signalling, and this translocation is essential for long-term facilitation to be maintained.

eEF1A has since been found *in vivo* in the dendrites of mammalian neurons that exhibit long term potentiation (LTP) or long term depression (LTD) (Huang et al., 2005). When levels of eEF1A mRNA were examined in mouse hippocampi using *in situ* hybridisation, eEF1A mRNA was found at highest levels in the brains of post-natal day (PND) 10-15 mice. By day 25, eEF1A mRNA localisation was similar to that found in adult mice (Huang et al., 2005). The author points out that most other dendritic mRNAs are present at low levels throughout development and increase in abundance as dendrites reach maturity, so it is tempting to speculate that local synthesis of eEF1A plays an important role in synaptic development.

In the same study, a form of LTD induced by metabotropic glutamate receptors (GluR) agonists, which depends on dendritic protein synthesis for induction (Huber et al., 2000) was studied in relation to eEF1A. Diffusion of an mGluR agonist, DHPG, into a dendritic lamina within the hippocampal CA1 of a mouse caused a large increase in eEF1A immunostaining in dendrites surrounding the micropipette tip 30 minutes after placement, but no change in eEF1A mRNA localisation. This immunostaining increase was totally blocked by pre-treatment with a protein synthesis inhibitor, illustrating regulation of eEF1A translation by GluR activation.

In a rat brain pull-down experiment eEF1A has been found associated with inhibitory glycine receptor subunit α2. Immunostaining showed partial overlap of eEF1A with glycine receptors in cultured spinal cord neurons and cultured hippocampal neurons. Interestingly, the distribution of eEF1A in cultured spinal cord and hippocampal neurons changed over five weeks in culture from co-localisation with receptors to the cytoskeleton in 45% of neurons. This redistribution could be induced at earlier time-points by inhibition of glycine receptors or the ERK1/2 pathway, and a simultaneous NMDA receptor activation (Bluem et al., 2007).

1.2.4.1 eEF1A1 and Fragile X

Fragile X syndrome (FXS) is the most common inherited form of intellectual disability and autism. The fragile X mental retardation protein (FMRP), an RNA-binding protein that regulates translation of its target mRNAs, is transcriptionally silenced in human FXS sufferers (Bassell and Warren, 2008). An excess of dendritic spines has been found in both human sufferers and the neurons of a mouse model of FXS, the *Fmr1* knockout (*Fmr1* KO). Work by Tsai et al. (2012) examines how a lack of synapse elimination in the *Fmr1* KO mouse could contribute to this excess. Transcription factor MEF2 induces excitatory synapse elimination in mouse neurons in an FMRP-dependent manner. In normal brain, MEF2 and FMRP together regulate the expression of protocadherin 10 (Pcdh10), a cell adhesion molecule. When MEF2 is activated, PSD95 is ubiquitinated by Mdm2 and then binds to Pcdh10, which links it to the proteasome for degradation.

Neurons that lack FMRP have higher levels of eEF1A protein (Sung et al., 2003). The higher levels of eEF1A sequester Mdm2 and prevent the MEF2-induced ubiquitination of PSD95, and so prevent synapse elimination (Tsai et al., 2012). Tsai et al. (2012) showed that RNAi of EF1A in *Fmr1* KO neurons didn't affect upstream MEF2 activation, but did restore synaptic localisation of Mdm2 and its reaction with PSD-95. A model of the normal and disease process of synapse elimination is shown in Figure 1.5.

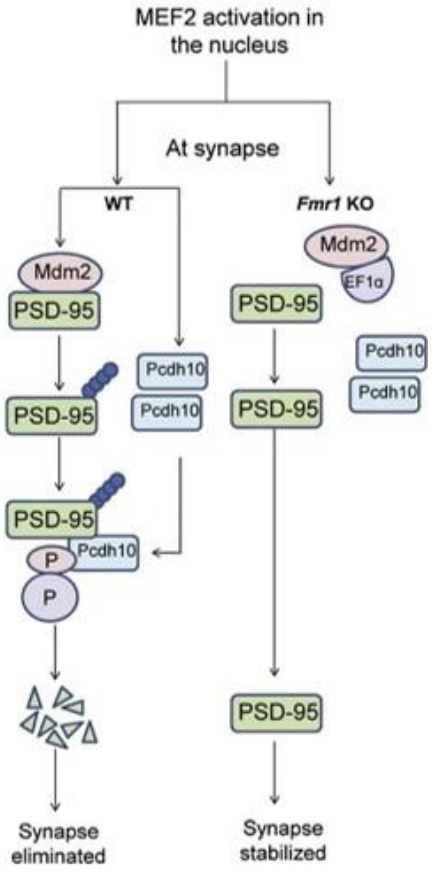

Figure 1.5 Working model of MEF2-induced synapse elimination *in WT neurons and the molecular basis of the deficit in synapse elimination in* Fmr1 *KO neurons. Adapted from Tsai et al., (2012)*

Although the paper does not specify which isoform is detected, the shRNAs used to knockdown eEF1A are specific to eEF1A1, and the GST-eEF1A recombinant protein used to show that EF1A can effectively compete with PSD-95 for binding to Mdm2 is likewise eEF1A1, so we can be confident the described interactions are related to eEF1A1.

1.2.4.2 eEF1A and other neuropsychiatric disorders

The brains of Alzheimer's sufferers have been found to have lower than expected levels of eEF1A in the CA1 and dentate gyrus of the hippocampus, (Beckelman et al., 2016), and also in a mouse model of Alzheimer's Disease, although this work is as yet unpublished (Beckelman and Ma, 2015). Likewise eEF1A was among one of several factors involved in protein synthesis found to be expressed at a lower level in post-

mortem frontal cortex tissue of Parkinson's disease sufferers than in those of control cases. eEF1A downregulation was linked to the severity of the disease, with the more severe cases expressing the least eEF1A (Garcia-Esparcia et al., 2015).

An increase in translation elongation and ribosomal proteins, including eEF1A1 and eEF1A2 was also found in four iPSC-derived neural progenitor cell lines isolated from schizophrenia sufferers relative to healthy controls (Topol et al., 2015).

Papers finding changes in eEF1A levels in neuropsychiatric disease often do not specify which isoform of eEF1A they are investigating. By examining siRNA and cDNA sequences it is possible to deduce, in some cases, which isoform they refer to (see Table 1.3). Antibodies used in Western blots are commonly referred to as detecting eEF1A. These most often detect either eEF1A1 or both isoforms, but without testing in the particular set of experimental conditions used in each investigation it is impossible to know which isoform(s) would be detected in each case.

Table 1.3 Isoforms of eEF1A Investigated in Neuropsychiatric Disease

Paper reference	**Techniques used**	**Isoform detected**	**eEF1A level compared to normal**
Parkinson's disease (Beckelman et al., 2016)	Western blot, IHC	unknown	↓
Alzheimer's disease (Garcia-Esparcia et al., 2015)	Western blot	unknown	↓
Schizophrenia (Topol et al., 2015)	SILAC on iPSCs	Both	↑
Fragile X (Sung et al., 2003)	IP	eEF1A1	↑
	Western blot	unknown	↑
	Northern blot	Probably both	↑
Fragile X (Tsai et al., 2012)	*In vitro* protein-protein binding followed by western blot	eEF1A1	↑

1.3 Other genetic disorders causing epileptic encephalopathies

Epileptic encephalopathies are a diverse group of neurological disorders characterised by severe seizures in infancy and/or childhood with accompanying developmental delay or regression. Comorbities often include behavioural or movement disorders such as autism, hypotonia or ataxia. In epileptic encephalopathies, such comorbidities are ascribed to neurological damage caused by the seizures (Engel and International League Against Epilepsy (ILAE), 2001), however it is also possible that where a genetic cause underlies a seizure disorder, comorbidities are due to seizure-independent effects of the genetic mutation.

An example of this is Dravet Syndrome, in which 80% of sufferers have a mutation in sodium channel SCN1A and a small proportion of cases have mutations in other genes such as GABRA1 and STXBP1 (Carvill et al., 2014). Dravet syndrome sufferers generally experience prolonged febrile generalised clonic seizures beginning in infancy, progressing to several different types of afebrile seizure through development. From the second year of life they experience cognitive decline and behavioural disorders, which until recently were believed to be due to cerebral damage caused by the epileptic episodes. Data from clinics on early cognitive deficiencies seen before full onset of the seizures characteristic of Dravet (Chieffo et al., 2011), plus recent work in a mouse model in which *in vivo* RNAi was used to selectively knock down expression of $Na_v1.1$ channels in a small region of the brain (Bender et al., 2012) are adding evidence to the hypothesis that Dravet syndrome is both an epileptic encephalopathy and channelopathy.

Ion channel mutations are a common cause of epileptic encephalopathy, since proper brain function relies on the proper balance of inhibitory and excitatory input, and disruption of ion channel function within neurons could easily provoke such an imbalance, leading, potentially, to the hyperexcitability of epilepsy (Steinlein, 2004). An example of this is found in the gene *ATP1A3*, which encodes the α3 subunit of the

Na^+/K^+-ATPase pump. Mutations of this gene have been identified in various neurological conditions including rapid-onset dystonia-parkinsonism and alternating hemiplegia of childhood (Dard et al., 2015), as well as, in two cases, epileptic encephalopathy (Paciorkowski et al., 2015). The two different heterozygous mutations found to cause this condition cause a loss of Na,K-ATPase activity *in vitro*. Immunostaining of the α3 subunit of the Na^+/K^+-ATPase pump show it to be present in cortical GABAergic interneurons, malfunctioning of which could lead to a lack of inhibition in the brain, predisposing to epilepsy (Reviewed in Bernard et al., 2000).

As well as mutations in several genes being able to cause one syndrome (as noted above in Dravet syndrome), mutations of one gene can be responsible for a range of phenotypic severities, depending on the precise nature of the mutation. Mutations of KCNQ2, a voltage-gated potassium channel, were originally linked to familial benign neonatal seizures (Claes et al., 2004) in which focal or generalised seizures begin around three days after birth but fade away within one to four months. More recently they have been found to cause epileptic encephalopathy with intellectual disability and motor impairment (Weckhuysen et al., 2012). As mentioned above, mutations in amino-acyl-tRNA synthetases can also produce a very wide range of phenotypic severity (Reviewed in Scheper et al., 2007).

Why do some mutations cause mild phenotypes, and others severe? In the case of KCNQ2, loss-of-function mutations that cause haploinsufficiency tend to cause a mild phenotype, whereas several mutations that give rise to the more severe epileptic encephalopathy have been found to act through dominant-negative effects on wildtype subunits: mutant and wildtype units coupling to form non-functional ion channels, leading to higher than the 50% drop in function expected for haploinsufficiency (Orhan et al., 2014).

1.4 Common Pathways in Epileptic Encephalopathies and Neurodevelopmental Disorders

With the recent surge in genetic profiling, a number of previously unknown genetic causes and contributors to epileptic encephalopathy have been identified (Veeramah et al., 2013). Amongst the genes so far linked to epilepsy a large proportion are, unsurprisingly, genes that code for ion channels and neurotransmitter receptors. A recent exome sequencing study of 263 cases of two particular epileptic encephalopathies, infantile spasms and Lennox-Gastaut syndrome, identified a large number of *de novo* mutations. A protein-protein interaction network of 93 of the genes with confirmed *de novo* mutations overlapped significantly with sets of genes regulated by the fragile X protein, and genes involved in autism spectrum disorder and intellectual disability (Epi4K Consortium et al., 2013).

This network appears to reflect a group of genes critical to normal neurodevelopment that when disrupted can lead to multiple neurological disorders. If these genes converge on common biochemical pathways then diverse genetic mutations could be amenable to common therapeutic treatment, so identification of common pathways in neurological conditions is of importance.

OMIM currently lists 47 genes that cause epileptic encephalopathy (data accessed November 2016), but the number of candidate genes for which there is some evidence of association with epileptic encephalopathy is much higher: de Kovel et al., (2016) screened patients using a panel of 351 candidate genes. This study found several pathogenic variants in genes currently annotated for intellectual disability, illustrating the overlap between various phenotypes.

Around 70% of people diagnosed with autism also have intellectual disability (Zoghbi et al., 2012), and autism sufferers have a heightened risk of epilepsy (Tuchman et al., 2002), it is unsurprising that pathogenic mutations causing these phenotypes affect converging pathways.

One common pathway upon which cases of intellectual disability and autism can converge is synaptic structure and function. Figure 1.6 shows components of the

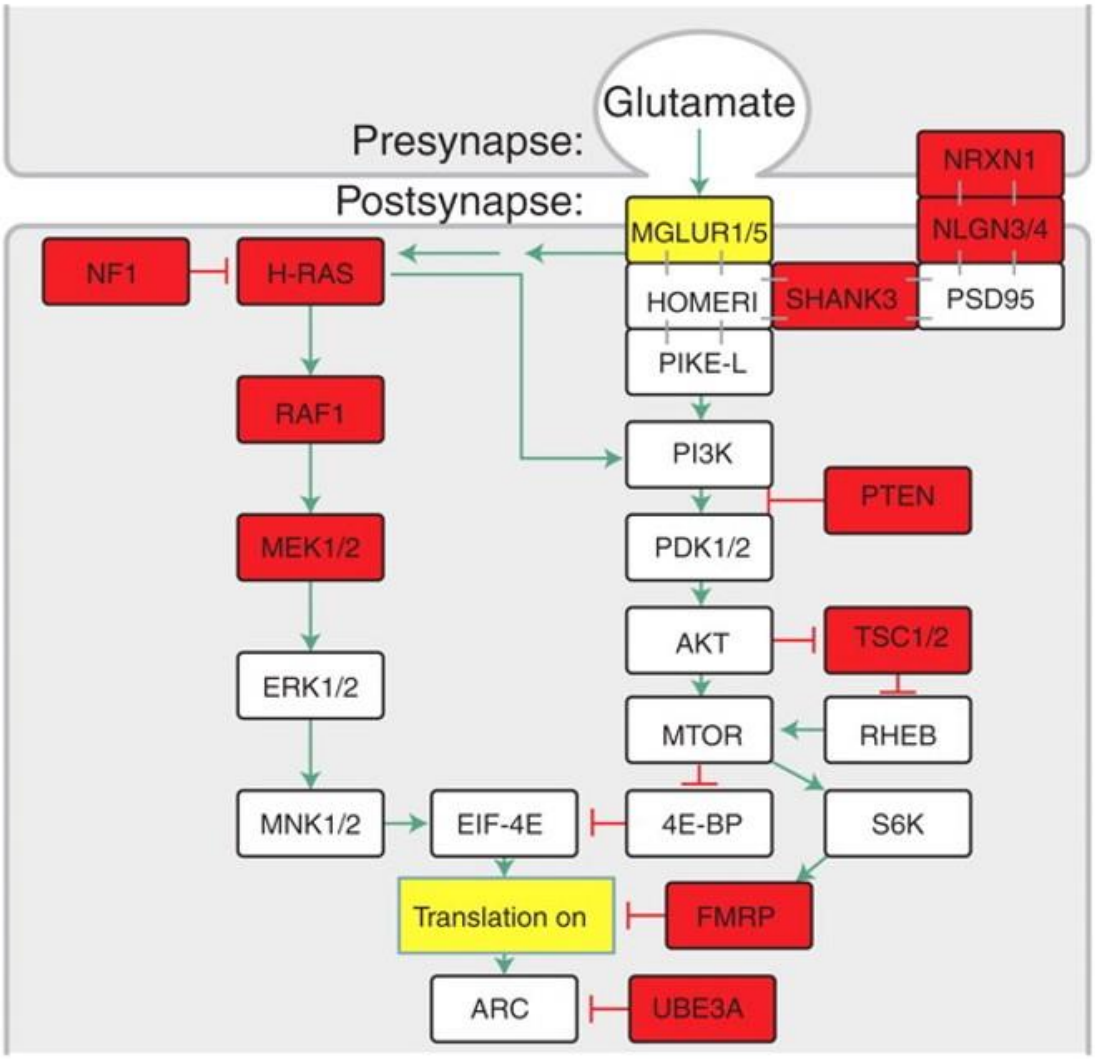

Figure 1.6 Disruption of genes involved in glutamate-dependent protein synthesis at an excitatory synapse increase the risk of ASD/ID. *Coloured boxes indicate genes which, when gene products are disrupted, cause disorders with increased prevalence of ASD. Adapted from Zoghbi et al., (2012)*

protein synthesis pathway at an excitatory synapse. Disruptions in gene expression of the genes coloured in red are known to cause neurodevelopmental disorders with an increased prevalence of ASD (Zoghbi., et al, 2012). Epileptic seizures are also a common feature of these disorders, some of which, due to their connection with protein synthesis, are discussed further below:

Tuberous sclerosis complex and Fragile X disease are both conditions caused by single genes involved in regulating protein synthesis, and both diseases are characterised by intellectual disability and autism. Synaptic function in mouse models of the two conditions were shown to lie at opposite ends of a spectrum of metabotropic glutamate receptor (mGluR)- mediated protein synthesis (Auerbach et al., 2011). *Tsc2*$^{+/-}$ mice, which model Tuberous Sclerosis, have a deficit in mGluR-LTD, whereas mice that

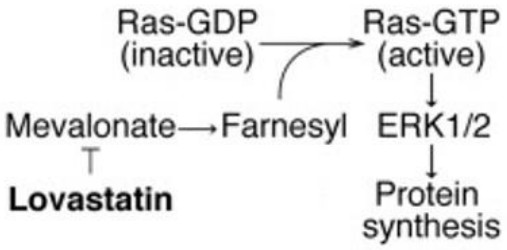

Figure 1.7 Lovastatin mildly inhibits ERK1/2 signalling *by reducing conversion of the inactive GDP-bound form of Ras to the active, GTP-bound form. Adapted from Osterweil et al., (2013).*

model Fragile X, *Fmr1*$^{-/y}$ suffer from excessive mGluR-LTD (Osterweil et al., 2010). The aberrant LTD levels in both models can be corrected by modulating mGluR5 signalling, and even more strikingly, offspring of the two mouse models that carry both mutations have LTD levels indistinguishable from wildtype. In behavioural tests, both *Fmr1*$^{-/y}$ and *Tsc2*$^{+/-}$ mice suffer deficiencies in context discrimination, but this defect is erased in the double mutant mice (Osterweil et al., 2010).

If misregulation of protein synthesis at the synapse is a common pathway across different neurological conditions, then the possibility for common therapies arises. The upstream events controlling protein synthesis at the synapse involve the extracellular signal-regulated kinase (ERK1/2) pathway. Pathological changes observed in FXS are believed to stem in part from an elevation of basal protein synthesis downstream of an extracellular signal-regulated kinase (ERK1/2) signalling pathway (Bhakar et al., 2012). ERK1/2 is part of the MAPK pathway, at the head of which lies Ras, the modulation of which may prove a viable therapeutic target in Fragile X disease, amongst others. Lovastatin, a drug widely used to treat high cholesterol is able to mildly inhibit ERK1/2 signalling through a reduction in the active, GTP-bound form

of Ras as shown in Figure 1.7 . This reduction in ERK1/2 signalling resulted in a normalisation of protein synthesis levels and prevented mGluR-induced epileptogenesis in *Fmr1* KO hippocampal slices. Furthermore it corrects the audiogenic seizure phenotype found in *Fmr1* KO mice (Osterweil et al., 2013).

Sufferers of Angelman Syndrome, characterised by ID, developmental delay, seizures and various behavioural problems (Angelman, 1965) have mutations that affect expression of ubiquitin E3 ligase (UBE3A) (See figure 1.6). UBE3A is necessary for proteolysis at the synapse, and it is believed that increases in proteins usually targeted for degradation by UBE3A may be the cause of synaptic deficiencies in Angelman patients. Activity-regulated cytoskeletal protein (Arc) is one such substrate, and is overexpressed in Ube3a-null mice (Greer et al., 2010). Translation of Arc occurs downstream of GluR5 signalling and is regulated by FMRP, illustrating another disorder in which disruption of protein synthesis at the synapse plays a contributing role.

As well as affecting protein synthesis and degradation at the synapse, ASD/ID/epilepsy-causing mutations can affect synaptic function in other ways. Neuroligins such as NLGN3/4 and neuroexins such as NRXN1 (see figure 1.6) are synaptic cell adhesion molecules essential for synaptic transmission, mutations in which can cause autism spectrum disorders (Jamain et al., 2003; Lawson-Yuen et al., 2008).

SHANK proteins are scaffold proteins that connect ion channels and neurotransmitter receptors to the actin cytoskeleton (Boeckers et al., 2002). Shank3 mutations can cause a range of neurological phenotypes dependent on the exact nature of the mutations and their effects on protein function, with haploinsufficiency of SHANK3 known to cause Phelan-McDermid syndrome (see figure 1.6) (Phelan et al., 2012), characterised by global developmental delay, neonatal hypotonia, aggressive behaviour and seizures. *De novo* mutations of *SHANK3* were also found in patients with schizophrenia (Gauthier et al., 2010).

The commonly overlapping phenotypes of intellectual disability, autism and epilepsy are certainly linked by pathways that in many cases converge on synaptic form and function.

1.5 Cilostazol and eEF1A1

A 2011 paper (Hashimoto and Ishima, 2011) reported that a drug, cilostazol, enhances neurite outgrowth in PC12 cells in an eEF1A-dependent manner. Cilostazol is a type-3 phosphodiesterase (PDE3) inhibitor that inhibits platelet aggregation and is vasodilatory. It raises intracellular cAMP levels by selectively inhibiting the degradation of cAMP by phosphodiesterase. It is specific for PDE type 3A, present in heart, platelet and vascular smooth muscle and so is used in the treatment of intermittent claudication (the major symptom of patients with peripheral arterial disease) and to reduce the risk of recurrence of ischaemic stroke (reviewed in (Goto, 2005).

Several studies have shown that cilostazol may have beneficial activity in the treatment of neuropsychiatric diseases. A study in mice showed that cilostazol treatment had a protective effect against cognitive deficits in an Alzheimer's disease mouse model (Park et al., 2011) and Alzheimer's disease sufferers showed less severe cognitive deficits in patients co-treated with cilostazol (though this report was not available to be read) (Arai and Takahashi, 2009). A recent report also showed that treatment augmented with cilostazol reduced depressive symptoms in two patients with geriatric depression (Takahashi and Mikuni, 2012).

Hashimoto and Ishima (2011) found that cilostazol has a potentiating effect on neurite outgrowth in PC12 cells. This cell line is derived from rat pheochromocytoma cells. When treated with nerve growth factor (NGF), or one of several other factors, they stop proliferating and develop neurites. PC12 has been used extensively to study neuronal development. Hashimoto found that cilostazol treatment on its own had no

effect on PC12 cells, however when used simultaneously with NGF a higher percentage of PC12 cells developed neurites than under NGF treatment alone.

Hashimoto performed a proteomics analysis to discover potential molecular targets of cilostazol's action. eEF1A1 was found to have a significantly higher protein level in cells treated with cilostazol than with two other PDE3 inhibitors. An RNAi experiment showed that knockdown of eEF1A1 antagonised the effects of cilostazol on neurite outgrowth, but did not antagonise the effects of NGF alone on neurite outgrowth.

Cilostazol potentiated neurite outgrowth but two other PDE3 inhibitors tested by Hashimoto, cilostamide and milrinone, had no such effect. Hashimoto suggests that cilostazol's neurogenic effects are therefore not due to inhibition of PDE3 but some other, as yet unidentified action of the drug.

1.6 Main Project Aims

The emerging findings that *de novo* heterozygous missense mutations in eEF1A2 cause epilepsy and intellectual disability, together with the evidence showing changes in eEF1A levels in Fragile X Syndrome, Alzheimer's disease, Parkinson's disease and schizophrenia make eEF1A a gene worthy of investigation, both in terms of the different isoforms' contributions to neural development and maintenance, and the possibility of eEF1A as a therapeutic target. With this in mind, the aims of my PhD are:

1. **Confirm and extend the finding that cilostazol potentiates neurite outgrowth in an eEF1A-dependent manner**
2. **Model the newly identified epilepsy-causing eEF1A2 mutations in neuronal cell lines, with the intention of developing a phenotypic assay to screen for drugs capable of correcting any observed phenotype.**
3. **Model the epilepsy-causing eEF1A2 mutations in mouse to better understand the mechanisms behind the human phenotype.**

Chapter 2 Materials and Methods

2.1 Materials

2.1.1 Solutions

Solutions used in this project are listed in the following table. Unless otherwise specified, all dilutions are in distilled water.

Table 2.1 Table of solutions

Solution	Component	Volume/weight/ concentration
Bradley lysis buffer	1M Tris-Hcl (pH7.5) 0.5M EDTA 20% SDS (w/v) 5M Sodium chloride	20mM 10mM 0.5% (v/v) 10mM
DNA loading buffer (48x) **Dilute to 6x working soln**	Glycerol Bromophenol Blue Xylene cyanol	30% (v/v) 0.2% (w/v) 0.2% (w/v)
PBS-T (10x)	Tween-20 in 10x PBS	0.2% (v/v)
RIPA buffer **1 Complete Protease inhibitor tablet (Roche) added to 10ml RIPA buffer just before use**	Sodium chloride NP-40 Sodium deoxycholate SDS Tris-HCl (pH8.0)	150mM 1% (v/v) 0.5% (w/v) 0.1% (v/v) 50mM
20x TBE	Tris base Boric acid 0.5M EDTA (pH 8.0)	1.78 M 1.78 M 40 mM
Western Transfer Buffer	10x TGS (Bio-rad) Methanol	10% (v/v) 20% (v/v)

2.1.2 siRNAs used in RNAi

siRNAs were designed manually and ordered from Sigma Aldrich

siRNA name	Species	Sequence
eEF1A1 siRNA 1	rat	AUGGAAAGUCACCCGCAAAGA[dT][dT]
eEF1A1 siRNA 2	rat	CACCAUACAGUCAGAAGAGAU[dT][dT]
eEF1A2 siRNA	Rat	CUGGAAGGUAGAGCGUAAG[dT][dT]
Negative siRNA	rat	MISSION(R) siRNA Universal Negative Control #1 (Sigma Aldrich)

2.1.3 Oligonucleotides for CRISPR

Oligonucleotides used to make gRNAs used for CRISPR experiments are listed in the following table in the form in which they were ordered from Sigma Aldrich. Subheadings indicate the particular experiments they were used for:

Table 2.2 Oligonucleotides used to make gRNAs for use in CRISPR genome editing

gRNA oligonucleotides used to incorporate G70S mutation in SHSY5Y cells	
eEF1A2 h 103/134 A top	CACCGGATGGTGATGTAGTACTTGG
eEF1A2 h 103/134 A bottom	AAACCCAAGTACTACATCACCATCC
eEF1A2 h 103/134 B top	CACCGATCACCATCATCGATGCCCC
eEF1A2 h 103/134 B bottom	AAACGGGGCATCGATGATGGTGATC
eEF1A2 h 28/62 A top	CACCGCTTCAGCTTGTCCAGCACCC
eEF1A2 h 28/62 A bottom	AAACGGGTGCTGGACAAGCTGAAGC
eEF1A2 h 28/62 B top	CACCGCTGAAGGCGGAGCGTGAGCG
eEF1A2 h 28/62 B bottom	AAACCGCTCACGCTCCGCCTTCAGC
gRNA oligos used to incorporate D252H mutation in LUHMES cells	
H D252H sgRNA 18A	CACCGGCTTGTCCGTGGGGCGCGTG
H D252H gRNA 18B	AAACCACGCGCCCCACGGACAAGCC
H D252H gRNA 75A	CACCGCAGGACGTGTACAAGATTGG
H D252H gRNA 75B	AAACCCAATCTTGTACACGTCCTGC

2.1.4 PCR and Sequencing Primers

Primers used in PCR and sequencing applications are listed in the following table, subheadings indicate the experiments they were used for:

Table 2.3 PCR and Sequencing Primers

Colony PCR insert check primers for human gRNAs targeting G70S	
H ins chk 28/62A F	CACCGCTTCAGCTTGTCCAGCA
H ins chk 28/62B F	TGAAGGCGGAGCGTGAGCG
H ins chk 103/134A F	GGATGGTGATGTAGTACTTGG
H ins chk 103/134B H	ACCGATCACCATCATCGATG
BbsI BbsI ins chk F	ACGAAACACCGGGTCTTCG
Ins Chk R	ACGAAACACCGGGTCTTCG
PCR and Sequencing primers for SHSY5Y G70S colonies	
F Mut chk5 (PCR)	TGGTTGAGGAAGGGATCTGG
R Mut chk5 (PCR)	TGTGTCCACGTCCCCATC
F Mut chk2 (sequencing)	GTTTATCCCATCTGGCGGCT
R Mut chk4 (sequencing)	ACTCTGACACTGGCTGGAT
PCR and sequencing primers for LUHMES D252H colonies	
hD252H 1F (PCR)	TTCCTCATCTCAAAGGGCACG
hD252H 1R (PCR)	CAAGTTTAGCCTGAACAGCAGTA
hD252H 2F (sequencing)	CCCACAGAAGTGTGTGGTAAG
hD252H 2R (sequencing)	TTGGAGACAGCCAGTCTTG
PCR and sequencing primers for G70S mouse genotyping	
mG70S short F: (PCR 2nd round)	TGAGTTGTGCCTCTACCCTT
mG70S short R: (PCR 2nd round)	ACACCTGGGATGTGCCTGTA
mG70S long F: (PCR 2nd round)	ATCAACACCAGAGAGATGGGAC
mG70S long R: (PCR 2nd round)	TCTTGAGGGACTCTATGCCCAAC
mG70S seq F (Sequencing)	GGACAGAGGTCTTCAGTTC
mG70S seq R (Sequencing)	GATGGAGAGGACATGGAGA
Allele specific Sequencing Primers used in G70S mouse samples	
mG70S single allele 1F	CTCTACCCTTCCAGATGGGG
mG70S single allele 2F	TCCAGATGGGGAAGGCT
mG70S single allele 3F	ATATGCCTGGGTGCTGGA

2.2 Methods

2.2.1 Tissue Culture

A number of cell lines were used throughout the course of this project. HEK293FT cells are derived from human embryonic kidney, and have been transformed with the SV40 large T antigen, meaning they are able to produce high levels of protein from vectors containing the SV40 origin. HCT116 cells are isolated from human colorectal carcinoma. LUHMES and SHSY5Y are both human neuronal cell lines, and Neuroscreen-1 is a rat neuronal cell line, a PC12 subclone, derived from a rat pheochromocytoma. The cell lines used and their growth conditions are shown in the table below:

Table 2.4 Growth conditions for Cell Lines

Cell-line	Species	Cell type	Growth medium	eEF1A isoform expression
HEK-293FT	Human	Embryonic Kidney	DMEM + 10% FBS (v/v)	eEF1A1
HCT116	Human	Colorectal carcinoma	Advanced DMEM/F12 +10% FCS (v/v) +1% 200mM L-Glutamine (v/v)	eEF1A1 eEF1A2
LUHMES	Human	Fetal mesence-phalon	Advanced DMEM/F12 + 1% N2 supplement (v/v) (Gibco) + 40ng/ml b-FGF (w/v) + 1% 200mM L-Glutamine (v/v) Plate coating Poly-l-ornithine + fibronectin	eEF1A1 eEF1A2
Neuroscreen-1 (NS1)	Rat	Pheochro-mocytoma	RPMI 1640 + 10% Horse serum (v/v) + 5% FBS (v/v) +1% 200mM L-Glutamine (v/v) Plate coating 0.01% Poly-l-lysine (PLL)	eEF1A1 eEF1A2
SHSY5Y	Human	Neuroblasto ma	DMEM + 10% FBS (v/v)	

LUHMES cells were obtained by kind gift from the laboratory of Professor Adrian Bird, NS1 cells were purchased from Cellomics.

Cell lines were maintained at 37°C, 5% CO_2 in growth medium specific to the cell line, shown in the table above. Unless otherwise specified in the following sections, cells were passaged by washing with prewarmed calcium- and magnesium-free DPBS (Life Technologies), then detaching using TryplE Express (Life Technologies). Detached cells were collected by centrifugation at 1200 rpm for 5 minutes, counted using a Cellometer Vision (Nexcelom) and reseeded as required.

Cells to be cryopreserved were detached as above, counted, and $1x10^6$ cells resuspended in freezing medium comprising the normal growth medium supplemented with 10% DMSO (v/v).

2.2.1.1 Cell Culture of NS1 Cells

All plates used for NS1 cells were precoated with 0.01% poly-l-lysine (PLL) solution, molecular weight 70 000-150 000 (Sigma Aldrich). Sufficient PLL was added to the flask to coat the bottom of the plate, and allowed to incubate at 37°C for 5 minutes. It was then washed off with distilled water, and the plate allowed to dry in sterile conditions. Cells were then grown as per the general cell line culture protocol given above and the growth medium specified above.

In neurite outgrowth experiments cells were plated at 7000 cells per cm^2 in normal growth medium, which after 24 hours was replaced with a reduced-serum medium comprising RPMI 1640 supplemented with 1% horse serum (Gibco), 0.5% FBS (Gibco), 1% L-glutamine and 50ng/ml nerve growth factor (NGF) -7S from murine submaxillary gland, (Sigma Aldrich).

In experiments involving cilostazol, variable concentrations (2.5ng/ml-50ng/ml) of NGF were used, alongside 10μM cilostazol (Sigma Aldrich) or 10μM cilostamide (Sigma Aldrich). Cilostazol or cilostamide treatments were applied at the same time

as reduced serum medium and NGF.

2.2.1.2 LUHMES cells

2.2.1.2.1 Maintenance as Proliferating Cells

Flasks were coated with 50µg/ml poly-L-ornithine (Sigma Aldrich) and 1µg/ml human fibronectin (Sigma Aldrich). Flasks with coating were incubated at 37°C for between 2 and 16 hours. Flasks were then rinsed three times with sterile distilled water and allowed to air dry in a biological cabinet.

Cells were generally maintained in T75 Nunclon™ cell culture flasks. They were passaged by washing gently with calcium- and magnesium-free DPBS (Gibco), before addition of enough trypLE to cover the bottom of the flask (7ml for a T75 flask). Cells were then incubated at room temperature for up to 2 minutes. The flask was tapped to detach the cells and 12ml prewarmed Advanced DMEM/F12 (Gibco) without supplements added. The cell suspension was immediately centrifuged at 300g for 5 minutes. Supernatant was removed and cells reseeded as desired in freshly prepared, filter-sterilised growth medium.

2.2.1.2.2 Differentiation

Cells were differentiated according to the protocol outlined by Scholtz et al (2011). $3x10^6$ cells were seeded in a precoated T75 cell culture flask containing growth medium. After 24 hours, growth medium was exchanged for differentiation medium comprising advanced DMEM/F12 (Gibco) , 1% 200mM L-Glutamine, 1% N2 supplement (life technologies), 1mM cAMP (Sigma), 1µg/ml tetracyclin (Sigma) and 20ng/ml GDNF (R&D). After 48 hours, cells were trypsinised, counted and replated at $1.2x10^5$ cells/cm². Differentiation is complete three days later. Differentiating cells were fed every 2-3 days by replacing half the medium with freshly prepared differentiation medium.

2.2.1.2.3 Thawing and Freezing Down

LUHMES cells were thawed as follows: A T25 Nunclon™ culture flask was coated with PLO/fibronectin (see separate protocol) and a cryovial containing LUHMES cells warmed in a water bath set at 37°C. The contents of the cryovial were pipetted into 19ml of additive-free advanced DMEM, and centrifuged at 300g for 5 minutes. The

supernatant was then aspirated, cells resuspended in 10ml proliferation medium and transferred to the pre-coated culture flask.

LUHMES cells were frozen down as follows: Cells were washed with warmed PBS, and 7ml trypLE™ added to each T75 flask of cells. Volume of trypLE was scaled up or down according to flask size. After three minutes the flask was tapped to detach cells, and contents transferred to a 50ml falcon tube. The flask was rinsed with advanced DMEM/F12 without supplements, and the rinse added to the falcon tube, which was centrifuged at 300g for five minutes. The supernatant was aspirated and cells resuspended in 10ml of advanced DMEM/F12 without supplements. Cells were counted and 1ml of Bambanker™ (Anachem) freezing medium prepared for every $2x10^6$ cells. Cells were again centrifuged at 300g for five minutes and resuspended in the appropriate volume of Bambanker, which was then quickly aliquoted into precooled cryovials. Cells were transferred into a Mr Frosty™ and left for at least 48hours at -80°C before transferral to storage in liquid nitrogen

2.2.2 RNAi in NS1 Cells

siRNAs 21 bp in length were manually designed to optimise the differences between rat eEF1A1 and eEF1A2, have a GC content of between 40 and 60%, and avoid long stretches (>3nt) of one base. A BLAST search was performed at the blast.ncbi.nlm.nih.gov website using the relevant species' refseq database to ensure specificity to the RNA they were designed to silence. siRNAs were ordered from Sigma-Aldrich using their custom siRNA order tool. dTdT overhangs were included on 3' ends of the siRNAs. Negative siRNA used was MISSION® Universal Negative Control siRNA (Sigma-Aldrich), an siRNA tested extensively in human, mouse and rat cells and shown to have no homology to any known gene sequences.

siRNAs were diluted to 20µM using nuclease-free water and stored at -20°C. RNAi experiments were generally carried out in 6-well plates using siLentFect™ lipid reagent (Bio-Rad). NS1 cells were counted, and 10 000 cells per cm^2 (95 000 per well) were seeded in 1250µl full medium per well. After 24 hours, for each well (A) 123.5µl serum-free medium and 1.5µl siLentFect, and (B) 124.25µl serum-free medium and

0.75µl of the desired 20µM siRNA were made. Master mixes could be used. (A) and (B) were then mixed and incubated at room temperature for 20 minutes. The siRNA/siLentFect mixtures were then added to wells (250µl per well) and rocked to mix.

2.2.3 Neurite Outgrowth Assays in NS1 cells

To measure neurite outgrowth of NS1 cells, phase-contrast pictures were taken using an inverted microscope with a differential interference contrast (DIC) setting and a 10x objective. Blinding to condition was achieved by a colleague renaming image files by number. Each image was then analysed using FIJI (1), an image processing package. The number of neurites on each cell was counted and labelled using the FIJI cell counter plug-in, to provide an automatic tally. A neurite was defined as any projection longer than a cell body diameter in length.

Neurite length was measured using the line tool in FIJI. The longest neurite of each cell was traced from edge of cell body to tip of neurite. Pressing 't' added the trace to the ROI manager, and after all cells in view were measured, the 'measure' command gave lengths of all neurites traced. These were transferred to Microsoft Excel, and neurite length normalised to the number of cells counted.

2.2.4 Alamar Blue Viability Assay

NS1 cells were plated at 7000 cells/cm^2 into a poly-l-lysine- coated 96 well plate, in 100µl per well of full medium (RPMI containing 10% horse serum, 5% FBS) containing 10% alamar blue (Invitrogen). After 24 hours the fluorescence of cells was measured in a FLUOstar OMEGA plate reader using an excitation wavelength of 540-570nm, and an emission wavelength of 580-610nm. Medium was replaced with 50µl per well full medium containing 10% alamar blue, and incubated at 37°C for one hour whilst siRNA complexes prepared (see separate RNAi protocol). The prepared siRNA complexes were added to cells and plate rocked to mix.

After a further 24 hours full medium was replaced with differentiation medium containing 10% alamar blue. Fluorescence was measured every day until results were saturated.

2.2.4.1 Transfection methods

Transient transfection of mutant eEF1A2 cDNA constructs was performed using Lipofectamine 2000 (Invitrogen). Cells were seeded into 12-well plates 24 hour hours prior to transfection. NS1 and HEK293FT cells were seeded at 62 500 cells per cm^2, HCT116 cells were seeded at 50 000 cells per cm^2. 1µg DNA per well was mixed with 3µl lipofectamine in 95µl Optimem and allowed to incubate at room temperature for 15 minutes before application to the cells, which were harvested after 24 to 48 hours.

2.2.4.2 eEF1A2 cDNA construct preparation

Justyna Janikiewicz (2011) originally prepared the wildtype eEF1A2 cDNA constructs on a pcDNA3.1 backbone, which were then mutated by Shannon Clark, an MSc student of this laboratory, to include the epilepsy-causing point mutations used and discussed in this thesis. The point mutations were made using the Q5® site directed mutagenesis kit (New England Biolabs) according to the manufacturer's instructions. Correct inclusion of mutations was confirmed by Sanger sequencing analysis by Shannon Clark.

2.2.5 Click-IT AHA Protein Assay

The Click-IT AHA protein assay requires cells to be grown in a medium lacking methionine. Methionine- and cysteine-free DMEM (Life Technologies) was used and 0.063mg/ml L-cysteine dihydrochloride (Sigma-Aldrich) added, along with 10% FBS to give methionine-free growth medium.

The required wells of a black-sided clear-bottom 96-well plate were coated with 0.01% poly-l-lysine for 5 mins, before washing with water and allowing to dry in tissue culture hood.

20 000 HEK293FT cells per well were then seeded in 100µl/well normal DMEM supplemented with 10% FCS. 24 hours later, cells were transfected with the required

DNA using lipofectamine. 0.2µl/ per well of 0.5µg/µl DNA was added to 25µl per well of Optimem (Gibco). 0.4µl per well of Lipofectamine 2000 (Invitrogen) was added to the DNA and mixed. The DNA/lipofectamine mixture was incubated at room temperature for 15 minutes, then 25µl added to each well of cells as required.

After 24 hours 50µl per well of AHA working solution was made by diluting it 1:1000 in methionine-free medium, then 100µl methionine-free medium added to give 150µl AHA solution per well.

Medium was aspirated very gently from cells, they were washed once with DPBS and the prepared AHA-containing medium added. Cells were then incubated for 30 minutes at 37°C, 5% CO_2.

After this, cells were fixed for 5 minutes in ice-cold 50:50 acetone:methanol, then washed twice with 3% BSA in PBS. Cells were then permeabilised by adding 100µl per well of 0.5% Triton-X in PBS and incubating 20 minutes at room temperature. Meanwhile, the Click-iT reaction cocktail was prepared as follows: the AHA buffer additive was diluted 1:10 by adding 120µl of additive to 1.08ml of water in a 15ml falcon tube. To this, 10ml of Click-iT supermix was added.

Cells were washed twice with 3% BSA in PBS and 100µl per well of Click-iT reaction cocktail applied. They were then incubated in the dark for 30 minutes. The cocktail was removed and wells washed once with 3% BSA in PBS. Hoescht was applied and incubated at room temperature for 30 minutes in the dark. Each plate was washed twice with PBS and then scanned in a FLUOstar plate reader using the following excitation/emission maxima:

Protein synthesis measurement: 495/519
Hoescht measurement (normalisation factor): 350/461

2.2.6 General Sequencing Protocol

Where Sanger sequencing was required, the following protocol was followed. The target locus was amplified by PCR, then unincorporated primers and dNTPs were

eliminated by treatment of PCR products with exoSAP-IT (Affymetrix). 5µl of each PCR product was mixed with 2µl exoSAP-IT and incubated at 37°C for 15 minutes, followed by 80°C for 15 minutes. The big dye reaction, using Big dye V3.1 (Thermo Fisher) was set up as follows:

Component	Volume (µl)
Primer (3.2µM)	1.5 (45ng)
Big Dye	1.0
BD Buffer	1.5
H_20	4

2µl of PCR product was added to each reaction, which was mixed by vortexing before being run on the following program in a Bio-Rad C1000 Touch Thermal Cycler:

Initial activation: 1 min at 96 °C
Then 30 cycles:-
10 seconds at 98°C
5 seconds at 50°C
4 minutes at 60°C

The sequencing reaction was cleaned up by adding 1µl of 125mM EDTA to each well, followed by 1µl 3M sodium acetate, and 25µl 100% absolute ethanol. The reactions were mixed by inverting 4 times and incubated at room temperature for 15 minutes. They were then centrifuged in a Jouan centrifuge with plate adaptor at 3000 rpm for 30 minutes. The ethanol was removed, and 30µl 70% ethanol added to each well. The plate was then centrifuged at 3000 rpm for 15 minutes, and ethanol again removed. The plate was then left to dry at room temperature for 10 minutes, and then stored at -20°C prior to processing on a 3130 or 3730 Genetic Analyser (Applied Biosystems).

2.2.7 Mutant Cell line generation using CRISPR

2.2.7.1 Performing a puromycin killing curve

A Poly-L-ornithine/fibronectin-coated 12-well plate was seeded with $3x10^5$ cells per well in 2ml proliferation medium. After 24 hours, varying volumes of 1mg/ml puromycin was added to each well to give a range of final concentrations of between 0.5µg/ml and 9µg/ml puromycin. Cells were examined under phase-contrast

microscopy conditions every day for the next three days, and the lowest dose required to kill the cells was chosen as the appropriate dose.

2.2.7.2 Cas9n plasmids

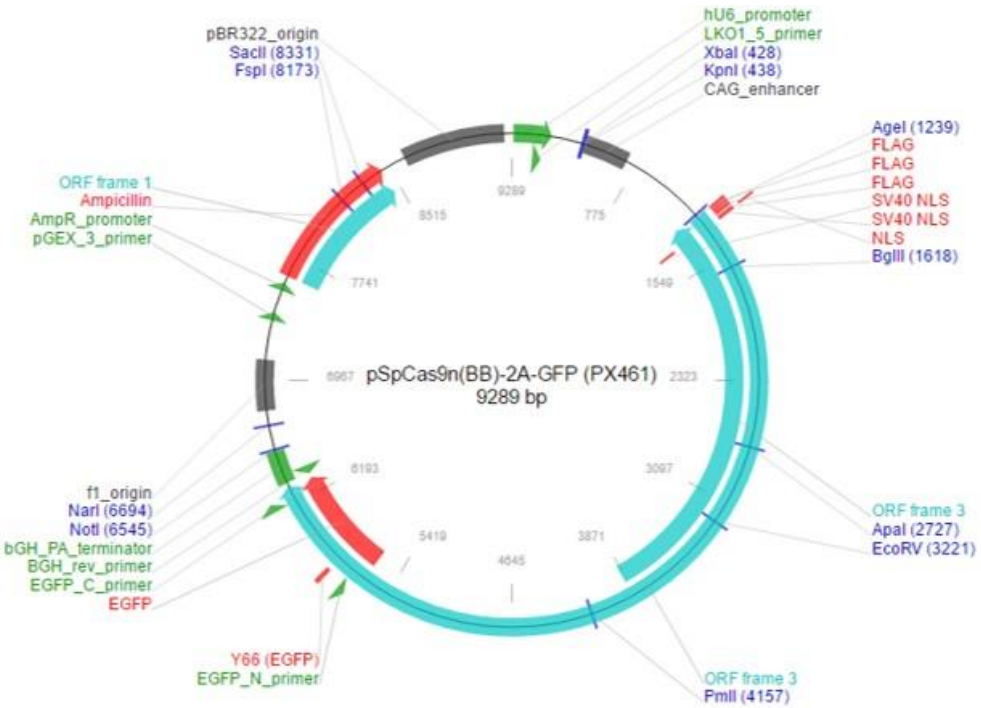

***Figure 2.1 Map of pSpCas9n(BB)-2A-GFP plasmid** used to deliver Cas9n and gRNAs into the cell. Px462, also used in some experiments, differs only in the presence of a puromycin resistance gene in place of EGFP. Map supplied by Addgene*

pSpCas9n(BB)-2A-Puro (px462) and pSpCas9n(BB)-2A-GFP (px461) (see Figure 2.1) were kind gifts from Feng Zhang.

2.2.7.3 Cloning of gRNA oligonucleotide into a Cas9n vector

The following mixture was prepared for each guide oligonucleotide:

Component	Volume (ul)
sgRNA top (100µM)	1
sgRNA bottom (100µM)	1
T4 ligation buffer, 10x	1
T4 polynucleotide kinase	1
dd$\boldsymbol{H_2O}$	6

The oligonucleotides were then phosphorylated and annealed in a Bio-Rad C1000 Termal Cyclerat 37°C for 30 minutes, 95°C for 5 mins, then ramp down to 25°C at 5°C per minute.

Some oligonucleotides did not clone on the first attempt. The protocol was adapted for these oligos, so that the ramp down phase was performed in a heat block, which was removed from the machine after the 5 minutes at 95°C step and allowed to cool to room temperature over a number of hours

Phosphorylated and annealed oligonucleotides were diluted 1:200 by adding 1µl of oligo to 199µl room temp ddH_2O A ligation reaction was set up for each gRNA to clone it into the pSpCas9n(BB)-2A-GFP (px461) or pSpCas9n(BB)-2A-PURO (px462) plasmid as follows:

Component	Vol (µl)
Diluted oligo duplex	2
pSpCas9n(BB)-2A-GFP, 100ng	1
T4 DNA ligase HC (NEB)	0.5
Tango buffer 10x	2
ATP 10mM	1
DTT 10mM	1
Fastdigest Bbs1	1
ddH_2O	11.5

The ligation reactions were then incubated at 37°C for 5 minutes and then 21°C for 5 minutes, with this cycle repeated six times. The ligation reactions were treated with PlasmidSafe ATP-dependent DNase (Epicentre) to digest any residual linearized DNA:

Component	Vol (µl)
Ligation reaction	11
PlasmidSafe Buffer	1.5
ATP, 10mM	1.5
PlasmidSafe endonuclease	1

The PlasmidSafe reactions were incubated at 37°C for 30 min, followed by 70°C for 30 mins. The reaction was then stored at -20°C until transformation.

2.2.7.4 Transformation of gRNAs

50µl per sample of DH5α competent cells (Life Technologies) were thawed on ice. 1.5ml microcentrifuge tubes were cooled on ice. 50µl of the DH5α cells were aliquoted into each tube. 2µl of the PlasmidSafe reaction product was added to the cells, stirred to mix, then the cell-DNA mixture was incubated on ice for 30 minutes. It was then heat-shocked at 42°C for 20 seconds before a further incubation on ice for two minutes. 950µl SOC medium was added to each tube, and they were then incubated at 37°C for 1 hour at 225rpm.

For each transformation two LB plates containing ampicillin were prepared and either 50µl or 150µl added to each and spread. Plates were then incubated at 37°C overnight. At this point a colony PCR was performed to check for correct insertion of the gRNA oligonucleotides into the Cas9n vector (see separate protocol below). Colonies were then individually picked into 2ml L-broth containing 100µg/ml ampicillin, and after 8 hours incubation at 37°C with shaking at 220 rpm, transferred to 200ml L-broth containing 100µg/ml ampicillin and left to incubate at 37°C overnight with shaking at 220 rpm.

500µl of each culture was mixed with 500µl of 50% glycerol and frozen at -80°C to provide a glycerol stock, then the plasmid DNA from the remainder of the cultures

was isolated using a Qiagen Endo-free Maxiprep kit, following the manufacturer's instructions.

2.2.7.5 Colony PCR to check correct insertion of gRNA oligonucleotides into Cas9n vector

Two colony PCRs were performed per colony picked, one to check for insertion of the gRNA oligonucleotide, and the other to ensure that no BbsI sites remained. The forward primers for each reaction were specific to each gRNA and are listed in Table 2.3, as are the BbsI forward primer used and the reverse primer, named 'Reverse Insert Check', which was used in all colony PCRs of this type.

PCR reactions were set up on ice as follows, with mastermixes made up when possible depending on the number of colonies picked:

Component	Vol (µl)
10x PCR buffer	2.5
10mM dNTP mixture	1
50mM $MgCl_2$	1.5
Taq	0.2
Primer F (10 µM)	1
Primer R (10 µM)	1
Water to 25ul	17.8

Colonies were then picked into each PCR reaction using a small pipette tip, thoroughly vortexed and run through a thermocycler as follows:

Step	Temperature (°C)	Time
Initial denaturation	98	10 minutes
8 cycles	98	5 seconds
	68, -1 each cycle	10 seconds
	72	10 seconds
22 cycles	98	5 seconds
	60	10 seconds
	72	10 seconds
Final extension	72	5 minutes

Products were then run out and visualised on a 2% agarose gel containing SYBR safe DNA gel stain.

2.2.7.6 Transfection of gRNAs into SHSY5Y and LUHMES cells

Nucleofection (using a Lonza Nucleofector™ II) was used to deliver DNA into the cells for both cell lines. Cell line Nucleofector kit V (Lonza) was used for SHSY5Y cells, and the basic primary neuron kit (Lonza) for LUHMES cells.

Cells were harvested, counted and $1x10^6$ cells per condition aliquoted into separate transfection tubes. These were then centrifuged at 90g for 10 minutes, and all medium carefully aspirated. Cells were resuspended in 100µl freshly made-up Nucleofector solution, and the required DNA added. In general, 2µg of plasmid DNA was transfected for each condition, this made up of 1µg of each gRNA. The plasmids were all diluted to approximately 0.5µg/µl to keep volumes to a minimum. In addition, where a single-stranded oligonucleotide repair template was to be supplied, 2µl of 10µM template was applied as well as the 2µg of plasmid DNA.

Each suspension was transferred to Nucleofector cuvettes and Nucleofected using program D-33 for LUHMES, A-23 for SHSY5Y. In the case of LUHMES cells, 650µl prewarmed RPMI 1640 was immediately added to each cuvette and the cells incubated at 37°C for 5 minutes. Cells were then very gently transferred to prepared plates.

2.2.7.7 Isolation and expansion of clonal lines

If the puromycin resistance plasmid was used (px462) then cells were allowed to recover for 48 hours and then diluted to $2x10^4$ cells/ml. 96-well plates were prepared with 100µl prewarmed growth medium in each well, and 200µl of cell suspension added to well A1 using a normal pipette. 100µl from this well was then transferred down to B1 using the same pipette tip, and so on down the first column. An 8-well multipipette was then used to transfer 100µl from the wells of the column 1 into column 2 and mixed by pipetting up and down several times. This was repeated with

each column, and the final volume of each well brought to 200µl by adding 100µl medium to each well.

If the GFP-expressing plasmid was used (px461) then cells were allowed to recover for 48-72 hours after transfection, and then GFP-positive cells were sorted into individual wells of a pre-prepared 96-well plate using a FACSJazz cell sorter (BD Biosciences).

After approximately 7 days, each well was examined under an inverted microscope, and any wells seen to contain just one colony of cells were marked. These wells had medium topped up as required, and colonies transferred to larger vessels when necessary.

2.2.8 Mutant mouse generation using CRISPR

The gRNAs, Cas9n plasmid and repair template to generate G70S mutant mice had been previously prepared and the DNA was converted to RNA using *in vitro* transcription by Dr Hemant Bengani, and micro-injected into C57BL/6J single-cell embryos by staff at the Evans Transgenic unit, Western General Hospital. Embryos were then implanted in a pseudopregnant female mouse, and the pups born were closely monitored by staff at the facility, with ear clips taken at 12 days old for genotyping and identification purposes.

2.2.9 Genotypic analysis of CRISPR *in vitro* experiments

2.2.9.1 Isolation of DNA from 96-well plate of CRISPR colonies using Bradley Lysis buffer

Proteinase K was added to Bradley lysis buffer just before use to give a final concentration of 1mg/ml proteinase K. Media was removed from 96-well plate and cells were washed with 150µl/well of PBS before the addition of 50µl per well of Bradley lysis buffer containing proteinase K. The 96-well plate was then sealed in a plastic bag containing a moistened paper towel and incubated overnight at 60°C. The plate was then allowed to cool to room temperature and 100µl of ice cold ethanol/sodium chloride (75µl 5M sodium chloride in 5ml absolute ethanol) added to

each well to precipitate DNA. After a 30 minute incubation at room temperature the plate was centrifuged at 3000 rpm for 20 minutes and then inverted to remove supernatant. 150µl per well of ice cold ethanol was added and the plate centrifuged again at 3000 rpm for 10 minutes to rinse the pellet before removal of the supernatant. This pellet washing step was repeated once more and the plate was then air dried. DNA was resuspended in 30µl per well of warmed TE buffer pH8.

2.2.9.2 PAGE-based mutation analysis of indel efficiency

The area around the mutation locus was amplified using the mutation check primers (see Table 2.3) 50µl reactions were set up on ice as follows:

Component	Volume (µl)
Nuclease-free water	20.8
5x Phusion GC buffer	8
10mM dNTPs	0.8
10µM Forward primer	2
10µM R Reverse primer	2
DNA 50 – 200ng	1
DMSO	4
Phusion polymerase	0.4

The desired locus was amplified using the following conditions in a Bio-Rad C1000 Thermal Cycler:

Step	Temperature (°C)	Time
Initial denaturation	98	3 minutes
8 cycles	98	5 seconds
	68, -1 each cycle	10 seconds
	72	10 seconds
22 cycles	98	5 seconds
	60	10 seconds
	72	10 seconds
Final extension	72	5 minutes
Final denaturation	95	5 minutes
Ramp down, 0.1° per second	25	∞

The reaction was then removed from the Thermal Cycler and incubated at room temperature for 5 minutes to allow time for annealing. Meanwhile a 15% acrylamide gel was made by mixing the following and pouring between two Western blot mini-PROTEAN pouring plates (Bio-Rad),

Component	For 2 gels
TBE 10x	1.5ml
30% 29:1 acrylamide	7.5ml
water	5.9ml
25% APS	50µl
TEMED	6µl

Gel was assembled in a mini-PROTEAN electrophoresis tank (Bio-Rad) filled with 1x TBE as a running buffer. 6x DNA loading buffer was mixed with each sample and loaded onto the gel. Tank was run at 150V for two hours. The gel was then carefully floated into 50ml TBE containing 5µl SYBR-safe. This was incubated on a Whirlimix for 10 minutes and bands visualised under a UV transilluminator (uvitec).

2.2.9.3 T7 endonuclease mutation analysis of indel efficiency

The desired locus was amplified using the same reaction components and cycling conditions as for the PAGE-based mutation assay described above, except without the ramping down step at the end. PCR products were then removed from the Thermal Cycler, and 10µl of each product was added to 6µl distilled water and 2µl NEBuffer 2 (NEB). Reactions were placed back in the Thermal Cycler for an extended denature/anneal step as follows:

95°c for 10 minutes
Ramp down at 0.1°C/second to 85°C
85°C for 2 minutes
Ramp down at 0.1°C/second to 75°C
75°C for 3 minutes
Ramp down at 0.1°C/second to 65°C
65°C for 3 minutes
Ramp down at 0.1°C/second to 55°C
55°C for 3 minutes
Ramp down at 0.1°C/second to 45°C
45°C for 3 minutes
Ramp down at 0.1°C/second to 35°C
35°C for 3 minutes
Ramp down at 0.1°C/second to 25°C
25°C for 3 minutes
Hold at 4°C

After this, to each reaction 1.3µl water, 0.2µl NEBuffer 2 and 0.5µl T7 endonuclease I (NEB) was added and mixed by vortexing, then incubated at 37°C for 60 minutes, heated lid off. At the end of this time the reactions were removed immediately, centrifuged briefly and quenched with 2µl 0.25M EDTA. They were loaded immediately onto a 2% agarose gel containing SYBRsafe, and subsequently visualised using a UV-transilluminator.

2.2.9.4 Sanger Sequencing of Clonal Lines

The following PCR mix was set up for each DNA sample to amplify around the locus of interest. For both SHSY5Y and LUHMES cells the ‘Mut chk’ primers were used. The sequences of these primers are listed in Table 2.3

Component	Volume (µl)
Nuclease-free water	10.4
5x Phusion GC buffer	4
10mM dNTPs	0.4
10µM F Mut chk	1
10µM R Mut chk	1
DNA 50ng – 200ng	1µl
DMSO	2
Phusion polymerase	0.2

The reactions were run in a PCR machine using the following conditions:

Step	Temperature (°C)	Time
Initial denaturation	98°C	3min
8 cycles	98°C	5s
	68°C	10s
	-1°each cycle	
	72°C	10s
22 cycles	98°C	5s
	60°C	10s
	72°C	10s
Final extension	72°C	5min
Hold	4°C	∞

PCR products were then sequenced using the primers listed in section 2.1.4 and the general sequencing method found in section 2.2.66.

2.2.9.5 TOPO® cloning of Clonal Lines

TOPO cloning of mouse DNA made use of the same Phusion PCR protocol used in the Sanger sequencing of clonal lines section above. TOPO cloning requires PCR products to have an overhanging deoxyadenosine (A) at the 3'-end. Phusion polymerase leaves PCR products with a blunt end, so to add the overhanging 'A', 1 unit (0.2µl) Taq (Invitrogen) was added to each sample and incubated for 10 minutes

at 72°C. The samples were then placed on ice and used immediately in the TOPO reaction.

2µl of PCR product was mixed with 2µl water, 1µl of salt solution and 1µl TOPO vector provided with the TOPO TA cloning kit (Life Technologies). This was mixed and incubated for 30 minutes at room temperature, before being placed on ice and transformed into DH5α cells as per the transformation protocol in section 2.2.7.4. 10 colonies were picked per DNA sample, miniprepped using the Qiagen miniprep kit and sequenced using primers provided in the TOPO TA cloning kit.

2.2.10 Genotypic analysis of CRISPR *in vivo* experiments

2.2.10.1 Purification of mouse ear-notch DNA

300µl of 15mM sodium hydroxide was added to ear notches, which were then boiled for 10 minutes. These were vortexed and 25µl 1M TRIS at pH8 added to the ear clips, which were then shaken to mix.

2.2.10.2 PCR and Sanger Sequencing of mouse DNA

A nested PCR, optimised by Francis Nuñez, was used to amplify the region around the G70S mutation site in mouse eEF1A2 due to difficulties amplifying the region. The PCRs were set up as follows, with mG70S Long primers used for the first round of PCR, and mG70S Short primers used for the second round.

Reaction component	**Volume (µl)**
10x buffer	2.5
50 mM $MgCl_2$	1
5 mM dNTPs	1
10 µM forward primer	1
10 µM reverse primer	1
5x Q solution (Qiagen)	5
Taq (Invitrogen)	0.5
Ear notch DNA	1
dH_20	12

The reaction was placed in a PCR machine and amplified using the following cycling program:

Initial activation: 5 min at 98 °C
Then 20 cycles:-
Denaturation: 10 s at 98 °C
Annealing: 30 s at 61.5 °C
Extension: 30 s at 72 °C
Final extension: 5 min at 72 °C

The PCR products were diluted 1:10 with distilled water, and then 2.5µl of each product added to a new PCR reaction using mG70S short primers, which were designed to be 'nested' within the mG70S Long primer set. This was then subject to the same cycling program as above, but with an annealing temperature of 58°C.
Sequencing was performed twice for each mouse DNA sample, using the general sequencing protocol, once using a forward primer (mG70S seq F) across the G70S locus, once using a backwards primer (mG70S seq R).

2.2.10.3 Allele specific sequencing

Allele specific sequencing made use of the same nested PCR and sequencing protocol as basic Sanger sequencing above, but used allele-specific sequencing primers, these are listed in Table 2.3.

2.2.10.4 TOPO cloning of mouse DNA

TOPO cloning of mouse DNA made use of the same nested PCR protocol as used in the basic Sanger sequencing of mouse DNA section above and then followed the TOPO reaction protocol as given in section 2.2.9.5

2.2.11 Reverse transcriptase PCR of LUHMES clonal lines

Cell pellets from the LUHMES clonal lines were resuspended in buffer RLT from the Qiagen RNeasy kit and frozen at -80°C until required. RNA was then isolated from each sample using the Qiagen RNeasy kit, following manufacturer's instructions.

Quality and concentration of RNA was checked by running a small sample of each through the Agilent Bioanalyzer.

cDNA was made from RNA using the AffinityScript Multiple Temperature cDNA Synthesis Kit, following manufacturer's instructions. Controls utilised were a minus RNA control in which all components were added except RNA, and a minus RT control to detect genomic contamination in which 1µl of each sample was mixed and used to make cDNA without addition of the Affinityscript RT. cDNA was then stored at -20°C until required.

The following PCR reaction was set up for each gene (eEF1A2 and APP5B). Prevalidated primers (PrimerDesign) were used, a kind gift from Dr Peter Tennant.

Component	Vol (µl)
Nuclease-free water	14.5
10x PCR buffer	2.5
10mM dNTPs	1
Primerdesign primer mix	1
MgCl2	1
DMSO	2
Taq (Invitrogen)	0.2
cDNA	1

A two-step PCR was performed using the following cycling conditions:

Initial activation: 3 minutes at 95 °C
Then 28 cycles:-
Denaturation: 10 seconds at 95 °C
Anneal/extend: 60 seconds at 60 °C
Final extension: 5 minutes at 70 °C

Products were run out on a 2% TBE agarose gel containing SYBRsafe and visualised on a transilluminator.

2.2.12 Western blot

Table 2.5 Table of antibodies used for Western Blot Note that exact antigens used to generate antibodies are not given by the supplying companies, except in the case of eEF1A, which was raised against residues 439-452 of mammalian eEF1A1

Name	Source	Species	Conditions Used
eEF1A2 (1°) (Monoclonal)	Genetex (Gtx326)	Rabbit	1:2000 1 hr room temperature
eEF1A1-1 (1°) (Polyclonal)	Helen Newbery (Newbery, 2003)	Sheep	1:2000 1hr room temperature
V5 (1°) (Monoclonal)	Invitrogen (46 0705)	Mouse	1:2500 2 hr room temperature
eEF1A (1°) (Polyclonal)	Upstate (05-235)	Mouse	1:1000 2 hr room temperature
IRDye 800CW Anti-mouse (2°)	LI-COR 926-32212	Donkey	1:10000 1 hr room temperature
IR Dye 800CW Anti-goat (2°)	LI-COR 926-32214	Donkey	1:10000 1 hr room temperature
IRDye 680RD Anti-rabbit (2°)	LI-COR 926-68071	Goat	1:10000 1 hr room temperature
Polyclonal anti-goat immunoglobulins/HRP (2°)	DAKO P0449	Rabbit	1:2000 1 hr room temperature
Polyclonal anti-rabbit immunoglobulins/HRP (2°)	DAKO P0448	Goat	1:2000 1 hr room temperature

2.2.12.1 Protein extraction

Protein lysates from cultured cells were normally prepared from six-well plates. After aspiration of cell medium, cells were washed once with DPBS (Life Technologies), then a small volume, between 30-100µl depending on the confluency of the cells, of ice cold RIPA buffer containing one EDTA-free protease inhibitor tablet per 10ml

RIPA buffer, was added to each well. A cell scraper was used to collect all the cells at one edge of the well. The RIPA/cell mixture was removed to a microcentrifuge tube and vortexed for 30 seconds to lyse the cells before being stored at -20°C. When required, lysates were defrosted on ice and then thoroughly mixed on a tube rotator at 4°C for 30 minutes, before centrifugation at 12 000g at 4°C for 15 minutes. Lysates were transferred to a new tube and the pellet discarded.

Protein lysates from tissues were prepared by adding 10µl per 10mg tissue of ice cold 0.32M sucrose with protease inhibitors (1 mini-complete tablet in 10ml sucrose solution). Samples were then homogenised using the Precellys®24 homogeniser for 2 x 1 minute, putting samples straight back onto ice afterwards. Steel-kit balls were used for muscle tissue, ceramic balls for other tissues. Samples were subsequently centrifuged at 10 0000g for 15 minutes at 4°C and the pellet discarded.

2.2.12.2 Quantification of protein lysate concentration

The Pierce BCA protein assay kit (Pierce) was used to quantify protein levels in cell lysate samples. A range of protein standards were made up by serially diluting a known concentration of bovine serum albumin, provided with the kit, with RIPA buffer as diluent. 10µl of each known concentration was pipetted in triplicate into a 96 well plate. 10µl of each cell lysate was also pipetted into the plate, in duplicate or triplicate if there was sufficient volume.

The BCA working reagent was made up by mixing reagents A and B in the ratio 50:1. 200µl of working reagent was added to each well of the 96-well plate, and the plate was mixed by rocking before incubation at 37°C for 30 minutes.

After this time, the plate was allowed to re-equilibrate to room temperature before measuring absorbance at 562nm using a FLUOstar Omega plate reader. Concentrations of cell lysates were determined using a standard curve generated from the albumin standards.

2.2.12.3 Preparation of samples for electrophoresis

Using the results of the BCA protein assay, samples were diluted with RIPA buffer (for cell lysates) or 0.32M sucrose (for tissue lysates) to give an equal concentration of protein across each set of samples. Laemmli sample buffer (Bio-Rad) was added in a 1:1 ratio, and then the samples were incubated for 7 minutes in a heat block set to 100°C before addition of 10% (v/v) 1M dithiothreitol (DTT). Samples were stored at -20°C before use.

2.2.12.4 SDS-PAGE electrophoresis

10% mini-PROTEAN TGX precast gels were purchased from Bio-Rad, however homemade gels were sometimes prepared, in which case the following protocol was used:

Bio-Rad mini-PROTEAN plates were cleaned using 70% ethanol and assembled in a casting frame. A 10% separating gel was prepared using the chemicals and volumes listed below:

Components for 4 Separating gels	**Vol (µl)**
dH_2O	13.4 ml
1.5 M Tris pH8.8	8 ml
30% Acrylamide/bis (Bio-Rad)	10.4 ml
20% SDS (w/v)	160 µl
TEMED	20 µl
25% AMPS	80 µl

. The gel was poured between the plates and dH_2O layered on top to stop the gel drying out whilst polymerizing. When separating gel was fully polymerised the dH_2O was removed from the top of the separating gel and a 4.3% stacking gel, prepared as shown below was poured on top.

Component for 4 stacking gels	Vol (µl)
dH_2O	11.9 ml
0.5 M Tris pH6.8	5 ml
30% Acrylamide/bis (Bio-Rad)	2.9 ml
20% SDS (w/v)	100 µl
TEMED	10 µl
25% AMPS	100 µl

A 10- or 15-well comb was added to the top and the gel left to set. Prepared gels could be stored for several days wrapped in cling film and stored at 4°C.

Combs were removed and the mini-PROTEAN tank assembled. About 500ml TGS running buffer was added, and then up to 15µl of each of the required samples were carefully pipetted into the wells. A protein ladder (High-Range Rainbow ladder, RPN756E, GE Healthcare) was always added to one well. Separation was performed at 250V when using a precast gel, or 120V when using a homemade gel. Gels were run until the blue dye front reached the bottom of the gel.

2.2.12.5 Western Blot Transfer

After SDS-PAGE, tanks were disassembled and gels equilibrated in transfer buffer for 5 minutes, along with, per gel, 2 sponges and 2 pieces of Whatman filter paper cut to the size of the sponges. 1 piece of Hybond-P PVDF membrane (GE Healthcare), cut to the size of the gel, was wet in methanol for a few seconds and then equilibrated in transfer buffer for 5 minutes.

The transfer sandwich was assembled as follows: On top of the black side of the cassette were placed the sponge, filter paper, gel, membrane, filter paper, sponge. The gel and membrane were carefully rolled using a plastic stripette to ensure no bubbles were trapped between them. The tank was filled with transfer buffer and cassettes loaded. Transfer occurred at 100V for 60 minutes at 4°C.

After this time, blots were removed and marked with pencil to indicate the side of the membrane that had faced the gel during transfer (this side gives the strongest signal

after immunostaining). Blots were dried by leaving out on the bench overnight, or hung in a hybridisation oven set to 40°C for 20 minutes. Dried blots were stored at 4°C.

2.2.12.6 Quantification of Equal Loading by Measuring Total Protein

The success of this protocol relies upon using blots that have not yet been blocked, nor probed using antibodies.

Blots were re-wet by immersion in methanol for a few seconds, and then incubated with rocking in 7% acetic acid, 10% methanol for 15 minutes. They were washed four times in dH_2O for 5 minutes each wash, and incubated with rocking in Sypro Ruby Protein Blot Stain (Invitrogen) in darkness (using a box with an opaque lid) for 20 minutes. After this blots were washed twice in dH_2O, 1 minute per wash, to remove excess dye, and the protein bands visualised immediately using a transilluminator. The staining pattern can be easily destroyed, so blots were transferred to the transilluminator very carefully, using forceps.

Blots could then be used straight away for immunostaining, or dried and stored. Dried blots were always rewet in methanol before further use.

2.2.12.7 Immunostaining using HRT-conjugate secondary antibodies

If dry, blots were rewet briefly in methanol, then incubated in 20ml Western blocking buffer (5% Dried skimmed milk in PBS with 0.2% Tween-20) in a darkened box with rocking for either 90 minutes at room temperature or overnight at 4°C.

They could then be incubated in primary antibody diluted in Western blocking buffer (for specific times and conditions see Table 2.5), washed 4 times in PBS-T for 5 minutes per wash, then incubated in the appropriate HRP-conjugated secondary antibody. After further 4 washes in PBS-T, blots were visualised by spraying with Rapidstep ECL Reagent (Merck-Millipore) and leaving for one minute before wrapping in cling-film and exposing using autoradiography film.

2.2.12.8 Immunostaining using LICOR

If dry, blots were rewet briefly in methanol, then incubated in 20ml Li-cor Odyssey Blocking buffer (Li-cor) in a 50ml centrifuge tube with rocking on a benchtop roller for either 90 minutes at room temperature or overnight at 4°C. All antibodies were diluted in Li-cor Odyssey blocking buffer, (for specific times and conditions see Table 2.5). After primary antibody incubation, blots were washed 4 times in PBS-T for 5 minutes per wash with rocking. Li-cor secondary antibodies were used, always incubated in the dark, then blots were again washed in PBS-T as before. Membranes were maintained in the dark in PBS-T until ready to image in Li-cor Odyssey Fc Imaging system.

2.2.12.9 Densitometry

Relative protein levels were determined using densitometric analysis of Western blots. Blots that had been exposed to film were digitised and analysed using FIJI (1). Blots imaged using the Odyssey Fc Imaging system were analysed using Image Studio Lite Version 4.0.

2.2.13 Statistical Tests

GraphPad Prism V7.0 was used throughout to draw graphs and perform statistical analyses. To test for significance unpaired Student's T-Tests with Welch's correction were used, or 1-way ANOVA with Sidak's Multiple Comparison tests where appropriate.

Chapter 3 eEF1A and Neuritogenesis

3.1 Introduction

Total loss of eEF1A2 in mouse causes motor neuron degeneration and death at around four weeks of age, but there are growing lines of evidence that eEF1A dysregulation plays a role in a range of different neurological diseases. Downregulation of eEF1A has been identified in various brain regions in Alzheimer's and Parkinson's disease cases (Beckelman et al., 2016; Garcia-Esparcia et al., 2015), and increased levels of ribosomal and translation factors, including both eEF1A1 and eEF1A2 have been identified in induced stem cell-derived neural progenitor cells from four schizophrenia patients (Topol et al., 2015). Furthermore, mutations in *EEF1A2* are now known to cause epilepsy and intellectual disability (see section 1.2.2)

These findings, along with the study showing eEF1A is upregulated as a result of mGluR5-mediated LTD (Antion et al., 2008) raise the possibility that eEF1A could be a relevant therapeutic target in the range of neurological diseases linked to protein synthesis misregulation and alterations in mGluR LTD.

There could even be a case for upregulating eEF1A1 in neurons to mitigate the loss of eEF1A2, especially given the key regulatory role that eEF1A1 plays in the stress response (see section 1.1.2.1), a role not shared with eEF1A2, the predominant eEF1A isoform expressed in mature neurons. Identifying modulators of eEF1A expression in neurons would therefore be of interest.

I aimed to confirm and extend the investigation of Hashimoto and Ishima (2011) investigation, in which they showed that cilostazol, a phosphodiesterase type-3 (PDE3) inhibitor, potentiated NGF-induced neurite outgrowth in PC12 cells in an eEF1A1-dependent manner.

Hashimoto's RNAi experiment showed that knocking down eEF1A1 in PC12 cells had no effect on the number of cells differentiated upon treatment with NGF, however

the RNAi experiment graph showed that the knockdown of eEF1A1 achieved was very inefficient. Comparing the negative RNAi experiment to the eEF1A1 RNAi, the level of knockdown achieved was insignificant. The statistics on the paper compared eEF1A1 RNAi to no RNAi, whereas a reliable conclusion could only really be drawn by comparing eEF1A1 RNAi to negative RNAi.

I therefore repeated the RNAi experiment from this paper, aiming for a much more efficient knockdown of eEF1A1. Hashimoto used the percentage of cells displaying one or more neurites as a measure of PC12 cell differentiation. A neurite was counted if it was at least as long as the cell body it grew from. This is a measure of likelihood of differentiation. I also planned to knockdown eEF1A2, separately, to confirm that it really is the eEF1A1 isoform that provides the potentiation effect.

There is a possibility that eEF1A1 itself may have an effect on neuritogenesis, since it has been linked to the mechanisms by which both heat shock (Vera et al., 2014) affects neurite outgrowth in PC12 cells, and eEF1A1 expression is preferentially upregulated (compared to eEF1A2) in response to NGF treatment of PC12 cells (Petroulakis and Wang, 2002). Although knocking down eEF1A1 in PC12 cells was shown to have no effect on neurite outgrowth by Hashimoto (Hashimoto and Ishima, 2011), the RNAi experiment, as mentioned above, was not effective in knocking down basal levels of eEF1A1. As part of my experiments using PC12 cells and cilostazol treatments I aimed to examine the effect of eEF1A1 knockdown on neuritogenesis to test the hypothesis that eEF1A1 is directly involved in the regulation of neuritogenesis.

3.1.1 Aims:

- **Confirm and extend Hashimoto's experiments by examining whether one or both of the isoforms of eEF1A are involved in the potentiation of neurite outgrowth in PC12 cells by cilostazol**
- **Examine the direct effects of knocking down eEF1A1 and separately eEF1A2 on neuritogenesis in PC12 cells.**

3.1.1 Transient knockdown of eEF1A1 and eEF1A2 achieved in NS1 cells

Given that eEF1A1 and eEF1A2 mRNA sequences share 73% identity it was important to maximise sequence differences when designing siRNAs in order to knockdown only the desired isoform. With this in mind I identified sequences within the mRNA of eEF1A1 or eEF1A2 that were 19-21 bp in length, with at least 4 bp or difference between the two isoforms.

Although Hashimoto used PC12 cells, initial experiments in these cells showed them to be prone to forming large clumps, making any sort of neurite outgrowth analysis tricky. I therefore started using a PC12 subclone called Neuroscreen-1 (NS1) developed by Cellomics®. The advantage of this subclone is that cell aggregation is much reduced whilst maintaining the cell line's responsiveness to NGF. siRNAs were validated by transfection into NS1 cells. After two days cells were harvested and levels of eEF1A1 and eEF1A2 protein tested by Western blot. Results showed all three of the designed siRNAs to be selective for the specified isoforms, and active in silencing the desired isoform by 80±2.0%, 45 ±11.6% and 66 ±2.5% respectively for each of siRNA eEF1A1.1, eEF1A1.2 and eEF1A2. (Figure 3.1A). Furthermore the silencing activity of 1A1.1, the best performing siRNA lasts at least six days (Figure 3.1B) and is active in both proliferating and differentiating NS1 cells (Figure 3.1C)

3.1.2 Transient knockdown of eEF1A1 but not eEF1A2 reduces neurite outgrowth in differentiating NS1 cells

I next developed neurite outgrowth assays to measure the proportion of cells to develop neurites, and the length of those neurites (see section 2.1.2) I was able to show that in differentiating NS1 cells, knockdown of eEF1A1 but not eEF1A2 caused a reduction in both proportion of cells to develop neurites (Figure 3.2A), and the length of those neurites (Figure 3.2B). Because the neurite outgrowth assay I had developed used phase contrast pictures of living cells, I was able to directly measure

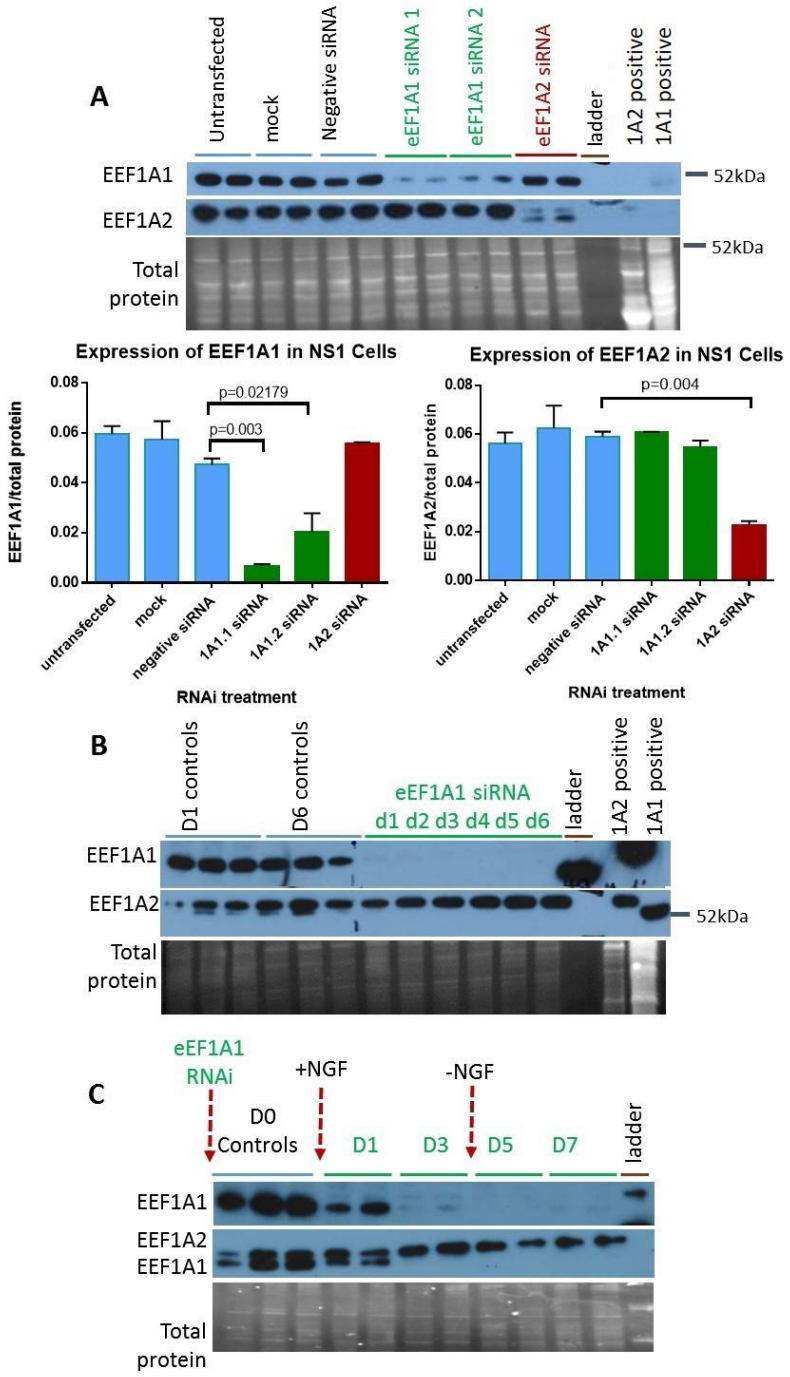

Figure 3.1 Silencing of eEF1A1 and, separately, eEF1A2 in Neuroscreen1 (NS1) cells, *a PC-12 subclone. (A) Two siRNAs against eEF1A1 (1A1.1 and 1A1.2) and one siRNA against eEF1A2 (1A2) were transfected into NS1 cells. 48 hours later, the cell lysates were extracted and probed using either an eEF1A1 or eEF1A2 antibody. (B) eEF1A1 expression was knocked down using siRNA 1A1.1, as in (A), and cells tested over six subsequent six days for eEF1A1 and eEF1A2 expression. (C) eEF1A1 knocked down using siRNA 1A1.1 in differentiating NS1 cells and eEF1A1 and eEF1A2 protein levels tested across seven days. The eEF1A2 antibody used here began to pick up both eEF1A isoforms from this point, but eEF1A2 is still identifiable by size, being slightly larger than eEF1A1. Controls for each isoform are shown in (B). (B) and (C) are single experiments*

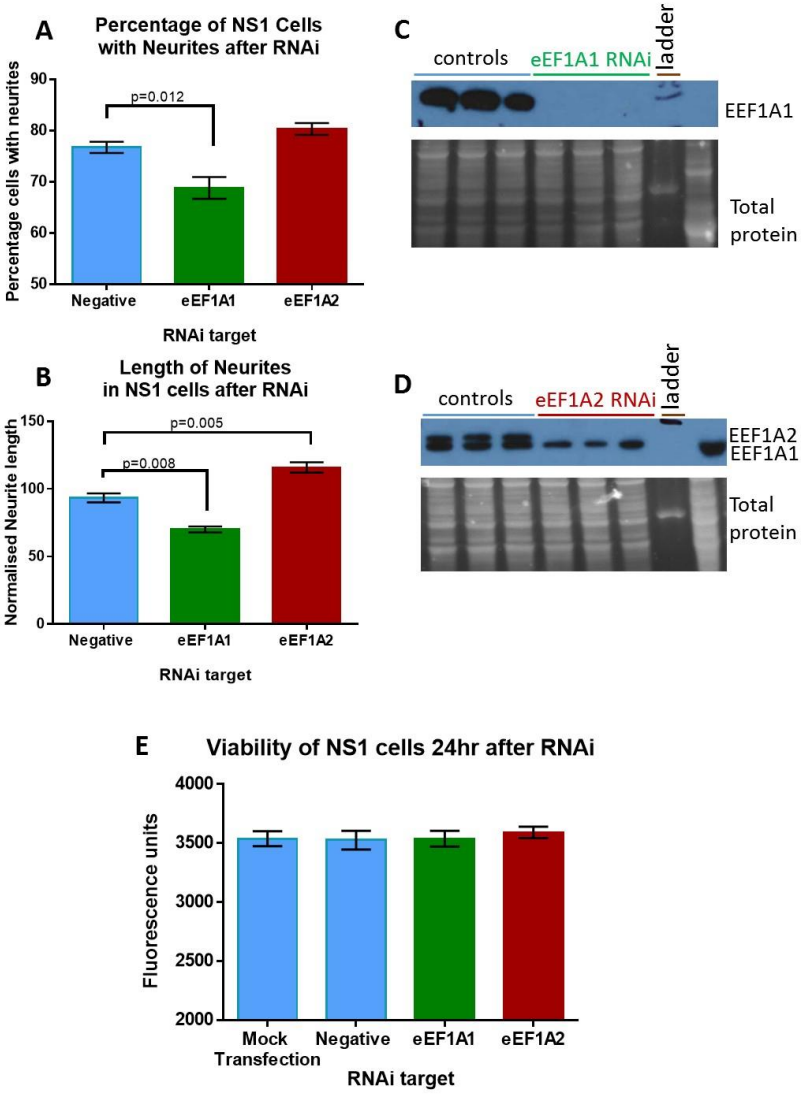

Figure 3.2 ***Neurite outgrowth response to silencing of eEF1A1 or eEF1A2*** *A) The percentage of NS1 cells with neurites 72 hours after RNAi and 48 hours after treatment with differentiating medium. Mean +/- SEM calculated by counting 600 to 800 cells and averaging across wells. B) Length of neurites in NS1 cells 72 hours after RNAi, 48 hours after treatment with differentiating medium. Lengths calculated by adding up the lengths of the longest neurite growing from each of between 600 to 800 cells, divided by the number of cells counted, averaged across three different wells of cells. C) Western blot showing silencing of eEF1A1 in the cells used in (A and B). D) Western blot showing the silencing of eEF1A2 in the cells used in (A and B). E) Viability of cells as measured using alamar blue 48 hours after RNAi treatment.*

eEF1A1 (Figure 3.2C) and eEF1A2 (Figure 3.2D) protein levels in the actual cell populations used for neurite analysis. This is an advantage over neurite analysis systems based on immunofluorescence, where the cell populations used for counting cannot also be used for protein analysis, having been stained and fixed as part of the

immunofluorescence protocol. I also showed that the reduction in eEF1A expression in each case had no effect on the cells' viability (Figure 3.2E).

3.1.2 Cilostazol had no effect on proportion of NS1 cells differentiated, or on expression of eEF1A isoforms

Hashimoto and Ishima (2011) found that cilostazol treatment of differentiating PC12 cells tripled the number of cells that developed neurites, but that treatment of cells with another PDE3 inhibitor, cilostamide, did not have this potentiating effect. In attempting to replicate this finding I tested several concentrations of NGF in a small initial experiment counting around 200 cells per condition, as I had noted that Hashimoto uses a very low (2.5ng/ml) dose of NGF compared to the typical (25-50ng/ml) dose used in PC12 differentiation experiments (Chung et al., 2010; Das et al., 2004; Greene, 1978; Read et al., 2008). This experiment showed that at the 2.5ng/ml dose of NGF, cilostazol did seem to have a significant potentiating effect on the number of cells developing neurites, with twice as many cells developing neurites under treatment with cilostazol (Figure 3.3A), however three further experiments in which significantly more cells were counted did not show any such effect (Figure 3.3B). Across these experiments neither cilostazol nor cilostamide had any effect on neurite outgrowth.

Hashimoto also found that eEF1A1 protein levels were significantly increased in cells treated with cilostazol, but not in cells treated with cilostamide. I probed for levels of eEF1A1 and eEF1A2 in cells treated with cilostazol or cilostamide and found no significant difference in the levels of either isoform (Figure 3.3C and 3.3D).

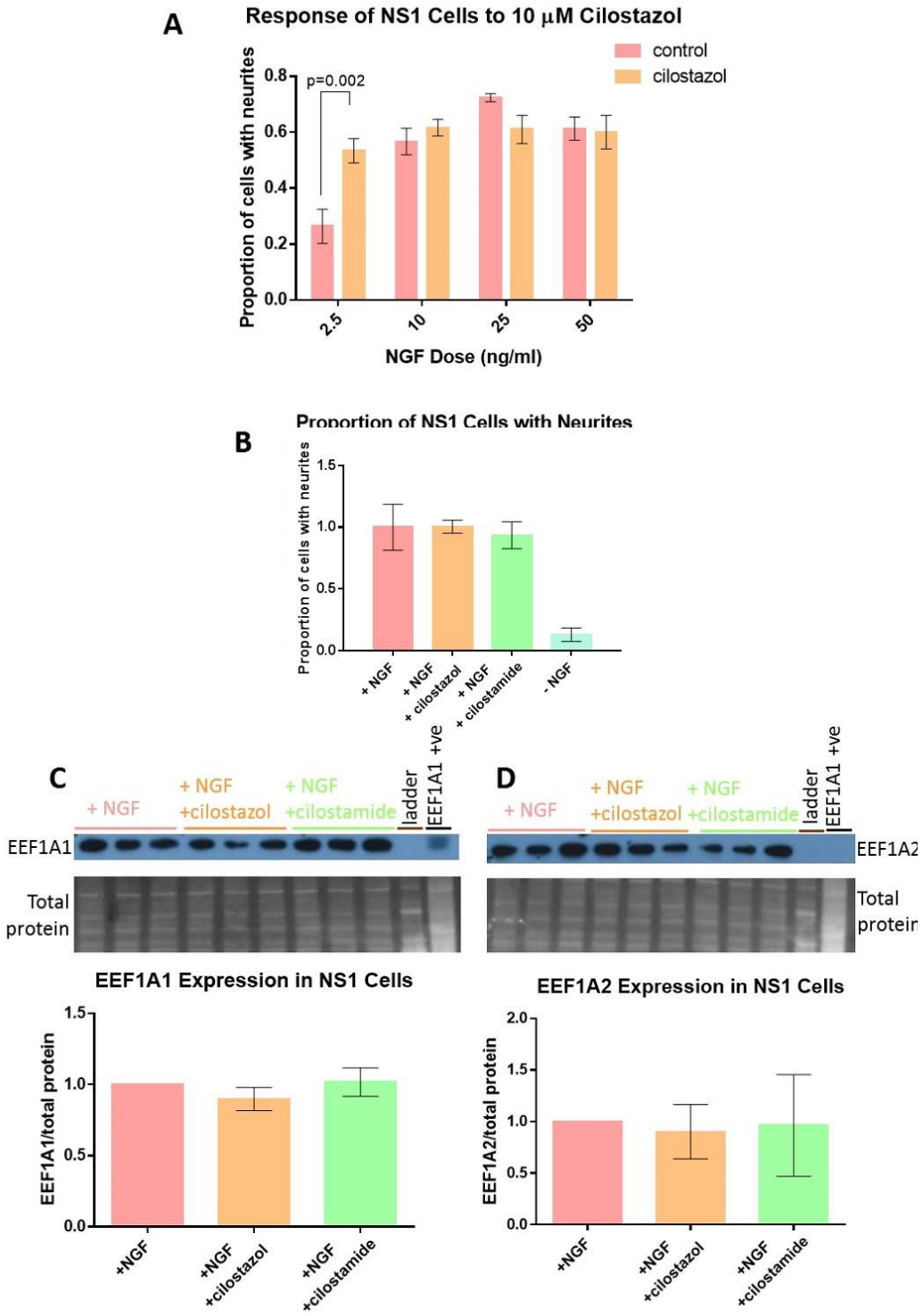

Figure 3.3 The neurite outgrowth response to cilostazol treatment. *(A) One pilot experiment showed that at the lowest levels of NGF treatment, cilostazol cotreatment induced a significant increase in the proportion of cells with neurites. (B) Averaging three repeated experiments using the same low dose of NGF (2.5ng/ml) found no significant difference between cilostazol and non-cilostazol treated cells. Results normalised to NGF treated cells. Cilostazol did not vary either (C) eEF1A1 protein levels, or (D) eEF1A2 protein levels as measured by Western blot of cell lysates. Blots shown are representative images, graphs are the mean of three separate experiments.*

3.2 Discussion

eEF1A isoforms, cilostazol and neuritogenesis

In this chapter I have validated the use of isoform-specific siRNAs to knockdown eEF1A2 or eEF1A1 expression in a NS1 cells, a PC12 subclone. The knockdown achieved was of at least 50%, and was shown to be robust across at least six days, and in both proliferative and differentiating conditions. Cells knocked down for each isoform were differentiated and the number of cells with neurites was shown in to be fewer in cells depleted of eEF1A1. Likewise the length of neurites was lower in eEF1A1-depleted cells. Conversely, knocking down eEF1A2 caused the lengths of neurites to significantly increase, although had no effect on the proportion of cells that developed neurites. Viability of the cells was not affected by RNAi targets.

eEF1A1 knockdown affecting neurite outgrowth fits with the idea that eEF1A1 is important in neuronal development – eEF1A1 being the only isoform found in neurons in early mouse development. Furthermore it is interesting to see that the eEF1A2 endogenously expressed in this cell line does not appear able to take over this role when eEF1A1 is absent, pointing to a difference in function between the two isoforms. That eEF1A2 knockdown actually increased the length of neurites does not seem to be due to an upregulation of eEF1A1, as no such increase was detected in RNAi testing (Figure 3.1A), but could be due to the change in ratio of the two isoforms, or some antagonistic effect related to the differences in non-canonical function of the two isoforms. To further investigate the role of eEF1A isoforms in neuritogenesis, engineering a mutant NS1 line null for one or other isoform would be most informative, and would add weight to the RNAi results reported here. A protein synthesis assay in proliferating and differentiating cells, with and without RNAi against eEF1A isoforms would also give more information as to the mechanism by which eEF1A knockdown effects neuritogenesis.

Hashimoto and Ishima (2011) did not find any difference in neurite outgrowth when they performed RNAi against eEF1A1 in PC12 cells, though the paper concedes that the RNAi did not reduce basal levels of eEF1A1, only prevented the cilostazol-induced

rise in eEF1A1. This difference in knockdown efficiency may explain why eEF1A1 RNAi antagonised the cilostazol-induced potentiation of neurite outgrowth, but had no effect on neurite outgrowth alone.

Apart from one small pilot experiment, I was unable to find any change in NGF-dependent neurite outgrowth from treatment with cilostazol, contrary to the results in Hashimoto and Ishima, (2011). This could be due to differences in experimental procedure, since I used a subclone of PC12 which could well have a different response to applied treatments. The use of such a low dose of NGF appeared to be necessary to give a sub-maximal level of neurite outgrowth which could then be potentiated by drug treatment. A limitation of my experimental design was not including a 'cilostazol only' control, or some sort of positive control to check that the cilostazol I was using was active.

In my hands at least, cilostazol treatment does not appear to modulate eEF1A levels or neurite outgrowth of NS1 cells, but in researching this result I have been able to set up and optimise neurite outgrowth assays which would be amenable to conversion to high throughput assay using a system such as the IncuCyte, a system capable of analysing phase-contrast images, making it possible to perform expression analysis of the counted cells themselves, something not possible with immunofluorescence-based neurite outgrowth assays. Since eEF1A isoforms are a possible therapeutic target in several neurological disorders, a neurite outgrowth assay that could function as a high-throughput drug screen could be useful in finding drugs able to modulate eEF1A's function in neurons. However, in order to use the IncuCyte system to its full potential, measurements must be made over a period of weeks. This precludes the use of RNAi to knock down gene expression but would lend itself to analysis of cell lines in which expression of either eEF1A1 or eEF1A2 had been permanently ablated by genome editing.

Chapter 4 Modelling disease-causing mutations of eEF1A2 *in vitro*

4.1 Introduction and previous work

Previous work in this laboratory studying the epilepsy-causing mutations focused on characterising their expression *in vitro.* A pcDNA 3.1 vector expressing eEF1A2 with a V5 tag was mutated using site-directed mutagenesis to create four constructs, each expressing eEF1A2 with one of the epilepsy-causing mutations, D252H, E122K, G70S and R423C (site-directed mutagenesis performed by Shannon Clark). The mutant eEF1A2 constructs were then separately transfected into HEK293FT cells, a cell line which does not express eEF1A2 endogenously, and the expression of the constructs measured by reverse transcriptase PCR and western blot, probing protein lysates for V5. Results of this experiment, performed by Jennifer Doig, show that although mutant eEF1A2 mRNA is expressed at an even higher level than wild type eEF1A2, at the protein level it is expressed at significantly lower levels than wild type. This low expression can be restored if the transfected cells are treated with a proteasomal inhibitor, indicating that the mutations cause instability of the protein, but that mutant eEF1A2 is still expressed in the cell to some degree.

Whether or not the mutant eEF1A2 proteins are functional is not known, though SIFT, an algorithm which predicts the effect of amino-acid substitution on protein function, predicts protein function to be affected for G70S, D252H and R423C, while PolyPhen, which likewise predicts the effects of mutations on structure and function of proteins, predicts G70S, E122K and D252H to be probably damaging. Mapping the mutations onto a 3D structure of the protein reveals them all to be situated at or near key areas of the protein, either the eEF1Bα binding site, the GDP/GTP binding site, or inter-domain contacts as shown in figure 1.4.

Since all the identified epilepsy-causing mutations in eEF1A2 have been heterozygous mutations, it is important to consider potential interactions between wildtype and mutant eEF1A2, given that several lines of evidence indicate that eEF1A2 can homodimerise (Sanges et al., 2012), or even heterodimerise with eEF1A1 (see section 1.1.2.2).

4.1.1 *In vitro* Experiment Aims

My *in vitro* experiments seek to explore the effects that the epilepsy-causing mutations have on the expression and function of eEF1A2 in immortalised cell lines, building on previous work done in our lab. To achieve this I use two complementary approaches:

1) Exogenous expression of mutant constructs in immortalised cell lines to investigate the effect of mutations on stability of eEF1A2 itself, and the effects on protein synthesis within the cell.
2) Generation of mutant neuronal cell lines which have been engineered such that the endogenous eEF1A2 carries an epilepsy-causing mutation to investigate functional effects of the mutations. Lines carrying such mutations would be tested for differences in phenotype compared to wildtype, and if such phenotypes can be found then cell lines could be used to develop a high-throughput drug screen.

4.2 eEF1A2 carrying the R423C mutation is expressed at lower levels than wildtype eEF1A2 but is rescued by cotransfection with wildtype eEF1A2

To investigate expression of mutant eEF1A2 *in vitro*, I initially focussed on one mutation, R423C, one of the mutants with the lowest expression level in HEK293FT cells (see section 4.1) Since the human mutation is heterozygous, and HEK cells do not express endogenous eEF1A2, I cotransfected several cell lines with wildtype and R423C eEF1A2 constructs to model the human condition transiently. I extended this analysis to three different cell lines including one that does express eEF1A2, Neuroscreen-1 (NS1) a PC-12 subclone, in order to assess whether the presence or absence of endogenous eEF1A2 affected the results

Figure 4.1 shows transfections of HCT116 (Figure 4.1A), HEK293FT (Figure 4.1B) and NS1 (Figure 4.1C) with either wildtype eEF1A2 tagged with V5 (WT-V5), R423C

eEF1A2 tagged with V5 (R423C-V5), or R423C-V5 plus wildtype eEF1A2 tagged with mCherry (WT-mCherry). The mCherry construct contains a T2A peptide sequence between eEF1A2 and mCherry, so the two proteins are cleaved after translation.

Expression of mutant or wildtype eEF1A2 was measured in all cases by probing a western blot of protein lysates for V5. Probing for V5 rather than eEF1A2 avoided the possibility of antibody cross-reaction with endogenous eEF1A1, and, in the case of NS1 cells which express it endogenously, eEF1A2. Use of the different protein tags also allowed me to tease out the effects of wildtype eEF1A2 on mutant eEF1A2: in coexpression conditions, the mutant eEF1A2 was tagged with V5, and the wild type eEF1A2 with mCherry, so that the expression data shown is known to relate to the V5-tagged mutant eEF1A2, not the cotransfected wildtype.

Expression of the R423C construct is significantly lower than that of the wildtype construct in both NS1 (Figure 4.1C) and HEK293FT (Figure 4.1B) cells with P-values of 0.009 and 0.019 respectively, and follows the same trend, though falls short of significance, in HCT116 cells (Figure 4.1A), confirming the initial experiments on R423C mutant expression (see section 4.1). This low expression is restored to wildtype levels or above in all three cell lines by coexpression of the wildtype eEF1A2 (mCherry-tagged) construct. Expression of the R423C mutant when coexpressed with wildtype eEF1A2 is five times higher than R423C mutant expression alone in HCT116 cells, and seven times higher in HEK293FT and NS1 cells.

The mCherry-tagged eEF1A2 construct does not cause a similar increase in expression when cotransfected with the wildtype V5 construct, showing that the rescue of the R423C mutant expression is not artefactual.

These data demonstrate that the presence of wildtype eEF1A2 influences the expression level of the mutant form of the protein in that the instability of the mutant protein is reduced by the presence of the wildtype.

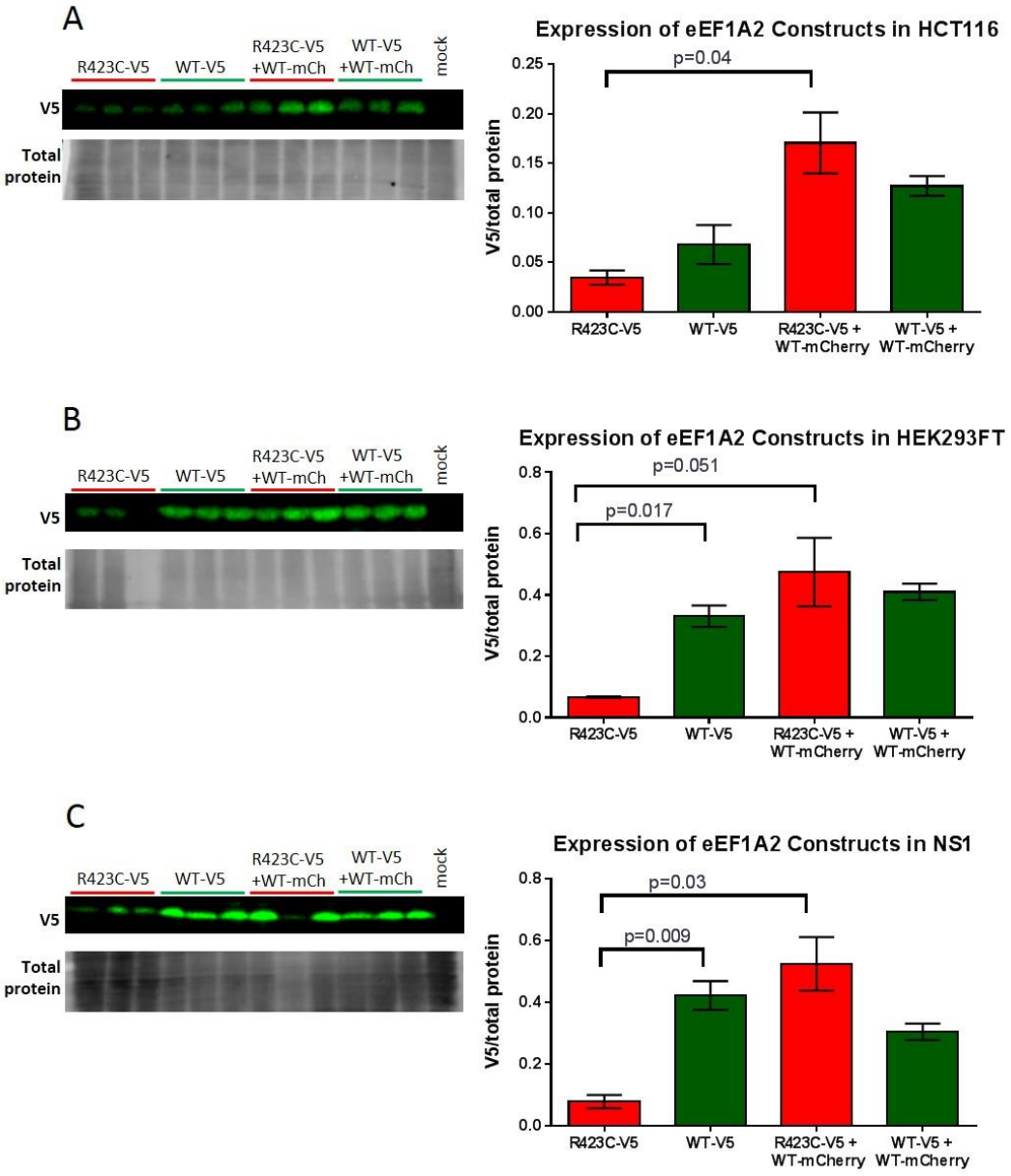

Figure 4.1 Expression of eEF1A2 construct containing the R423C mutation in three different cell lines *eEF1A2 constructs tagged with V5 were transfected into three cell lines, and their expression determined by semi-quantitative analysis of western blot probed for the V5 tag, so as to be sure of no accidental cross-reaction of antibodies with endogenous eEF1A1, or in the case of NS1, with endogenous eEF1A2. Fold changes above R423C-V5 expression alone are indicated in R423C-V5 + WT-mCherry conditions. Significance as determined by Students t-test is indicated by a line above bars, with corresponding P-value.*

.

4.3 Protein synthesis is not affected by exogenous application of mutant eEF1A2 constructs to HEK293FT cells, indicating the mutations do not exert a dominant negative effect on eEF1A1

Since the epilepsy-causing eEF1A2 mutations are predicted to have a deleterious effect on eEF1Bα- and/or GTP/GDP binding, I tested whether global protein synthesis in cells expressing these mutant proteins is disrupted. Whether the mutations disrupt cell function through loss of function of the mutant protein itself, or a dominant negative effect in which wildtype protein is adversely affected by the presence of the mutant, is not known.

The click-iT AHA protein synthesis assay used here involves incorporation of an amino acid analogue into newly synthesised proteins in the cell. This azido-modified amino acid is then detected with an Alexa Fluor 488 alkyne (the 'click' reaction).

Mutant and/or wildtype eEF1A2 constructs were transfected into HEK293FT cells, and 24 hours later, nascent protein synthesis levels determined. HEK293FT was chosen because it does not express eEF1A2 endogenously, although, as is the case in all immortalised cell lines, it does express eEF1A1. This adds complexity to analysis of the experiment, given that any changes in protein synthesis due to the exogenous eEF1A2 constructs have to be analysed against a backdrop of endogenous eEF1A1-mediated translation.

pMaxGFP, a GFP-expressing construct was also transfected into wells and imaged after 24 hours to give an indication of transfection efficiency. Figure 4.2A shows representative images of wells expressing GFP. The mat-like appearance of HEK cell growth makes individual cell counts a challenge, but transfection rates were estimated at 40% by counting the number of GFP-positive cells and dividing by total number of cells.

Wildtype and mutant eEF1A2 constructs were transfected in HEK293FT cells on three separate occasions and protein synthesis measured each time in triplicate per condition, after 24 hours. Cyclohexamide treatment of one set of wells provided a negative control. The results of each experiment were normalised to the mock signal, then the mean ± SEM reported in Figure 4.2A. One-way ANOVA of the different treatment groups (not including the negative control cyclohexamide treatment) showed the differences among the means to be statistically significant ($p=0.0016$). Post-hoc tests (Sidak's multiple comparison test) showed that the only treatment group significantly different from wildtype was D252H, however protein synthesis within the cells treated with the D252H mutant eEF1A2 construct was higher than wild type, an unexpected result given that D252H is overlaps with the eEF1Bα binding site and is predicted to have a deleterious effect on protein function (see figure 1.4).

A further experiment was performed in which the mutant constructs were cotransfected with a wildtype eEF1A2 construct (Figure 4.2C). Given the stabilising effect that wild type eEF1A2 had on expression of R423C in three different cell lines (see section 4.2), a difference in function of eEF1A2 (as measured by protein synthesis rate) might be expected here, although since the rate of protein expression in cells transfected with mutant constructs is no lower than that seen in cells transfected with wild type eEF1A2, it is unsurprising that the differences seen were modest and inconsistent.

A drop in protein synthesis in cells transfected with mutant eEF1A2 would have been evidence of a dominant negative effect, the action of the mutant eEF1A2 interfering with the endogenous translation elongation function of eEF1A1. However there was no evidence for this using this model system.

In order to clarify the results obtained through exogenous application of mutant constructs, I decided to continue investigating the action of epilepsy-causing eEF1A2 mutations through endogenous expression of the mutants, in the hope that this would avoid some of the confounding factors that exogenous protein experiments often present (though not the presence of eEF1A1).

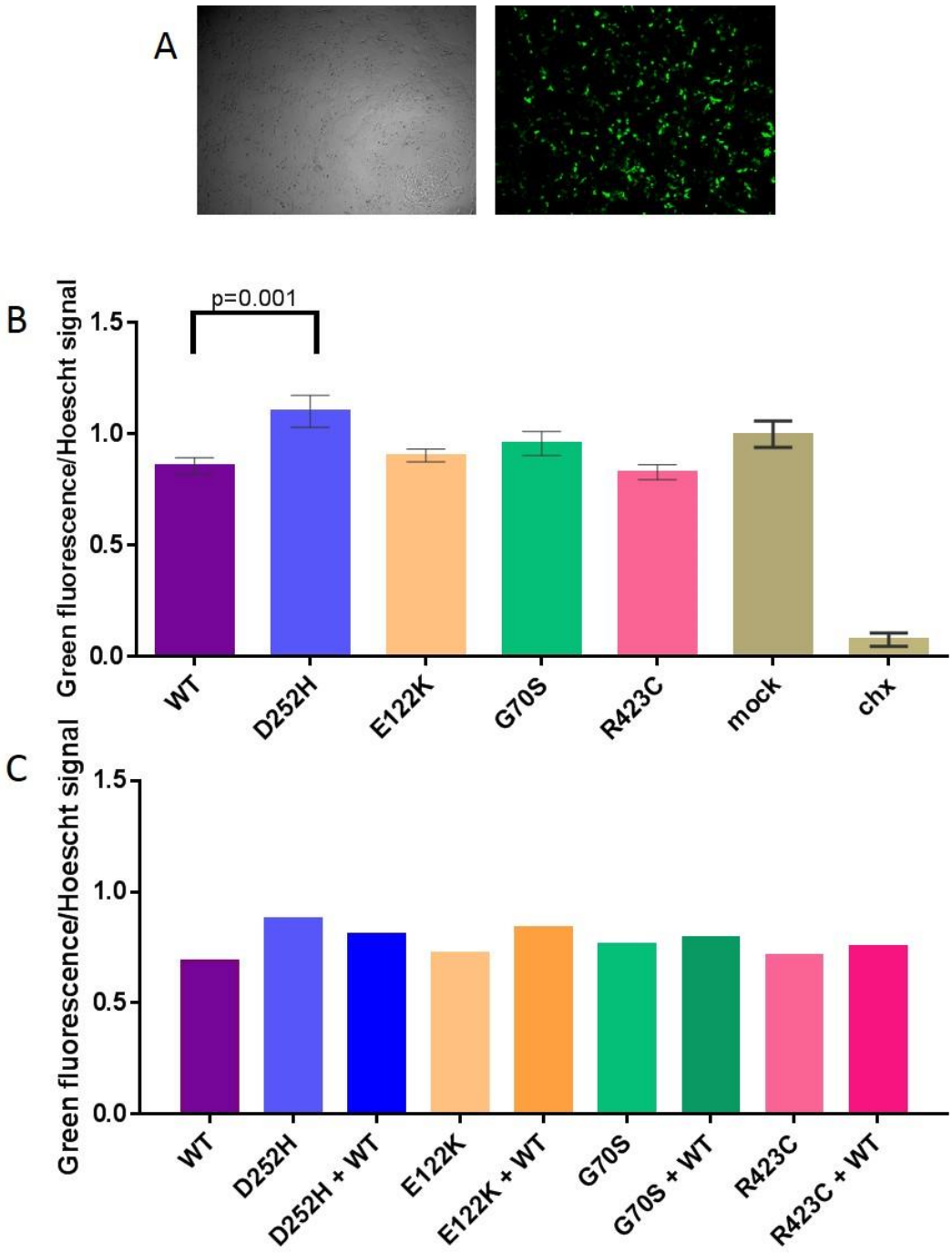

Figure 4.2 Nascent protein synthesis is not affected by exogenous transfection of HEK293FT cells with mutant eEF1A2 constructs. *(A) Bright field and fluorescent images of representative well of HEK293FT cells transfected with pMaxGFP. (B) Protein synthesis as determined by Click-IT AHA protein synthesis assay in cells transfected with either wildtype (WT) eEF1A2 or a mutant version of the protein. Mock cells were lipofectamine only, Cyclohexamide (chx) treatment was used as a negative control. Bars represent mean±SEM across three repeat experiments, three wells of a 96-well plate per condition. Significance measured using Sidak's multiple comparison test indicated above bar with corresponding P-value. (C) Experiment conducted as in (B) but using cotransfected wildtype eEF1A2 in indicated wells, results show one experiment only.*

4.4 Initial Attempts to mutate the eEF1A2 gene in SHSY5Y Cells

Although my ultimate aim was to model the eEF1A2 mutations in LUHMES, a human dopaminergic neuronal cell line that can differentiate into post-mitotic neurons, I chose to conduct an initial experiment in a cell line that was easier to culture and transfect than LUHMES. SHSY5Y is a human neuroblastoma line with a neuronal phenotype, in that it can be differentiated using retinoic acid, or various other reagents, to produce neurites. It is also straightforward to culture and transfect, so ideal for a preliminary CRISPR experiment, the aim of which was to test the CRISPR system and ensure the gRNAs I designed were functional.

CRISPR makes use of an RNA-targeted DNA endonuclease enzyme, Cas9, to cause a double stranded break in a DNA region of interest. I made use of a Cas9 mutant, Cas9n, in which a pair of guide RNAs (gRNAs) is used to make two nicks on complementary DNA strands at the desired locus (Ran et al., 2013b), in this case, the G70S epilepsy-causing mutation in *EEF1A2*. The two nicks are healed by the cell in the same manner as a double-stranded break, using one of two different pathways: Homology directed repair (HDR), and non-homologous end joining (NHEJ) (Figure 4.3B). By supplying a repair template along with the targeted DNA-cutting enzyme (Cas9n), precise gene editing can be achieved using HDR (Ran et al., 2013a). In the absence of a repair template NHEJ will repair a double-stranded DNA break, but this pathway being error-prone, indels are very often introduced at the site of the break.

Frameshift mutations would likely disrupt the protein by causing a premature stop codon which are detected and degraded by the nonsense-mediated decay pathway as long as the premature stop codon is located at least 50 nt 5' of an exon-exon boundary (Popp et al. 2013). Given that the mutation is found near the 5' end of the gene, in exon 3 of 8 (Figure 4.3A), mutant transcripts would in all likelihood be degraded. Any truncated proteins that were not subject to nonsense-mediated decay would be unlikely

to be functional but could nevertheless exert dominant negative or toxic effects if they were to be stably produced.

The human epilepsy-causing mutations have all been found on one allele of the affected patient, with the other allele being wildtype, so cell lines heterozygous for the mutation are likewise the aim here. An experiment in which CRISPR/Cas9 is used to mutate endogenous genes in cell lines from beginning to end has multiple stages. My planned workflow for the initial CRISPR experiment using SHSY5Y cells is shown in

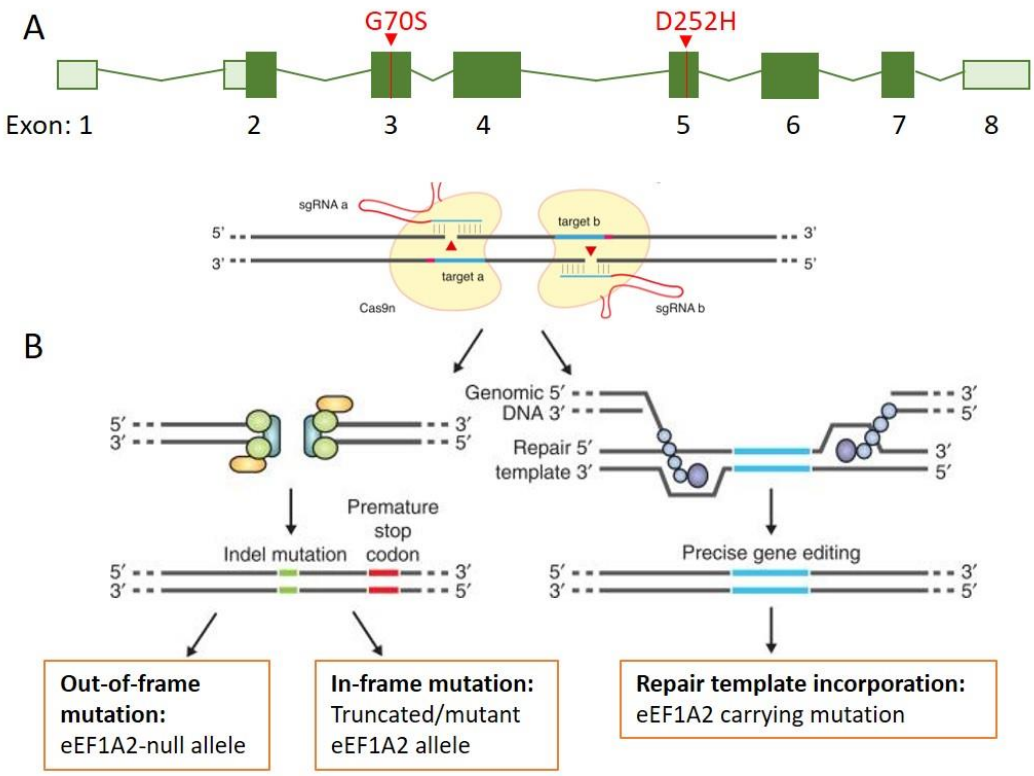

Figure 4.3 (A) Location of the two CRISPR-modelled epilepsy-causing mutations within EEF1A2 *(B) EEF1A2 can be targeted using the CRISPR/Cas9n system to create either indel mutations giving null alleles or a truncated protein, or correct insertion of the G70S mutation. Adapted from Ran et al., (2013).*

Figure 4.4. The following sections describe the implementation and optimisation of the CRISPR workflow in SHSY5Y cells.

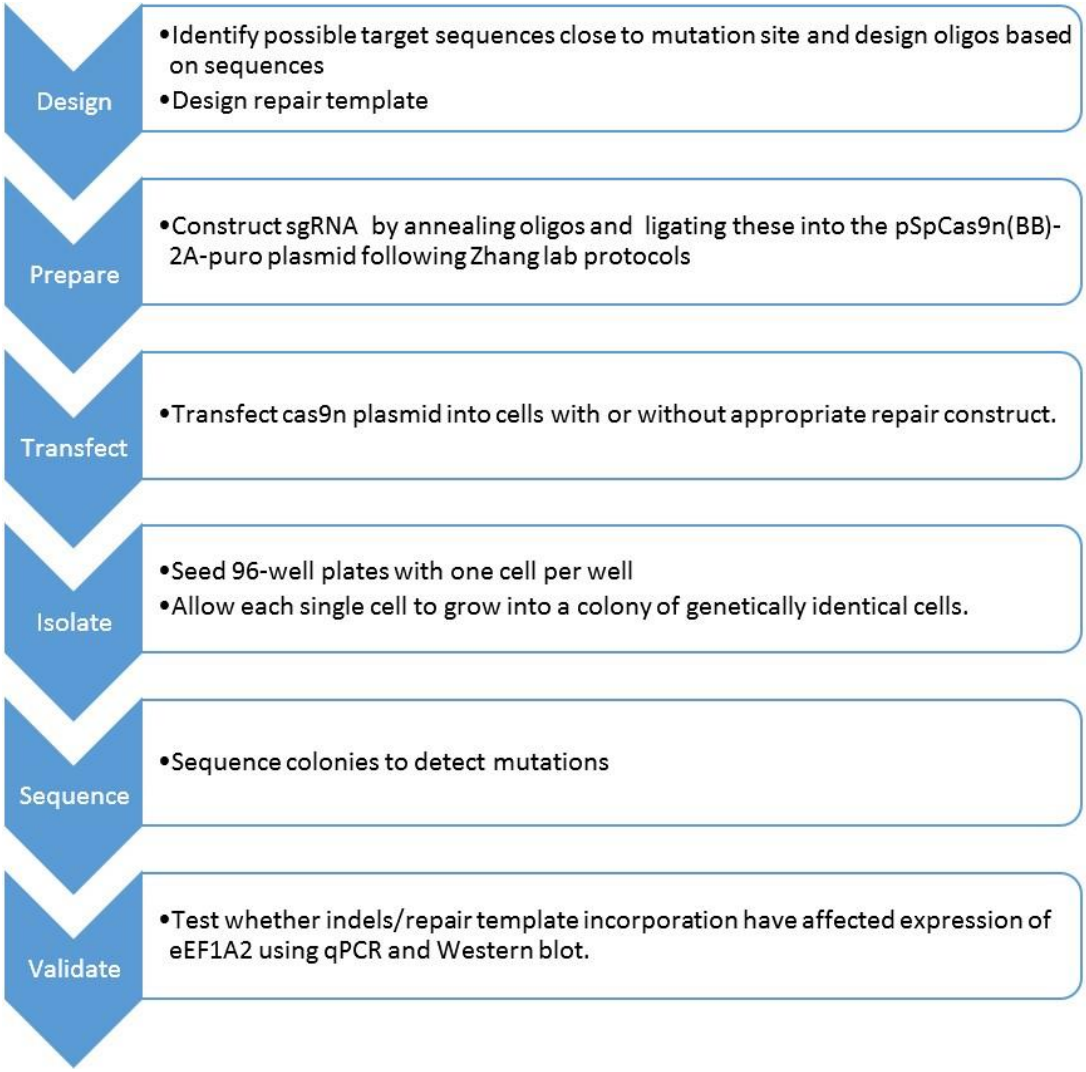

Figure 4.4 Basic workflow for genome engineering experiments using CRISPR/Cas9

4.4.1 Suitable gRNAs and a repair construct designed to introduce the G70S mutation into a human mammalian cell line

Use of Cas9n required a pair of gRNAs designed to target Cas9n to two adjacent sites on opposite strands of DNA. Specifically I chose to use the pSpCas9n(BB)-2A-puro plasmid, which contains the Cas9n enzyme, a double Bbs1 restriction site (adjacent Bbs1 sites on opposite strands) which allowed for straightforward ligation of gRNAs

in the correct orientation, and a puromycin selection cassette (map of plasmid shown in section 2.1.6.2).

The gRNA sequences were designed using the CRISPR design tool maintained at the website CRISPR.mit.edu, which takes a region of interest, identifies possible gRNAs within the region and ranks them according to target specificity and number off genic off targets. The input was exon 3 of human eEF1A2, this being the exon surrounding the location of the G70S mutation. I used two of the top three ranked gRNA pairs, discarding the pair furthest from the G70S site as distance between cut-site and site of mutation has been shown to be a factor in the efficiency of repair template incorporation (Inui et al., 2014).

4.4.1.1 An excel spreadsheet for designing gRNAs to clone

The gRNA target sites given by the design tool at CRISPR.mit.edu had to be modified to allow for cloning into the plasmids used by Ran et al (Ran et al., 2013). Specifically, a 'G' should be added to the 5' end of the sequence to facilitate transcription by the hU6 upstream promotor on the pSpCas9n(BB)-2A-puro plasmid. Further bases are added to each end of the guide to complement the overhangs provided by the two Bbs1 restriction sites. To facilitate this modification process I designed an excel spreadsheet which takes any gRNA offered by the crispr.mit.edu website and offers as an output the two oligonucleotide sequences (top and bottom) required to construct each gRNA. (see Figure 4.5) These can then be ordered as two simple single-stranded oligonucleotides per gRNA, an invaluable timesaver.

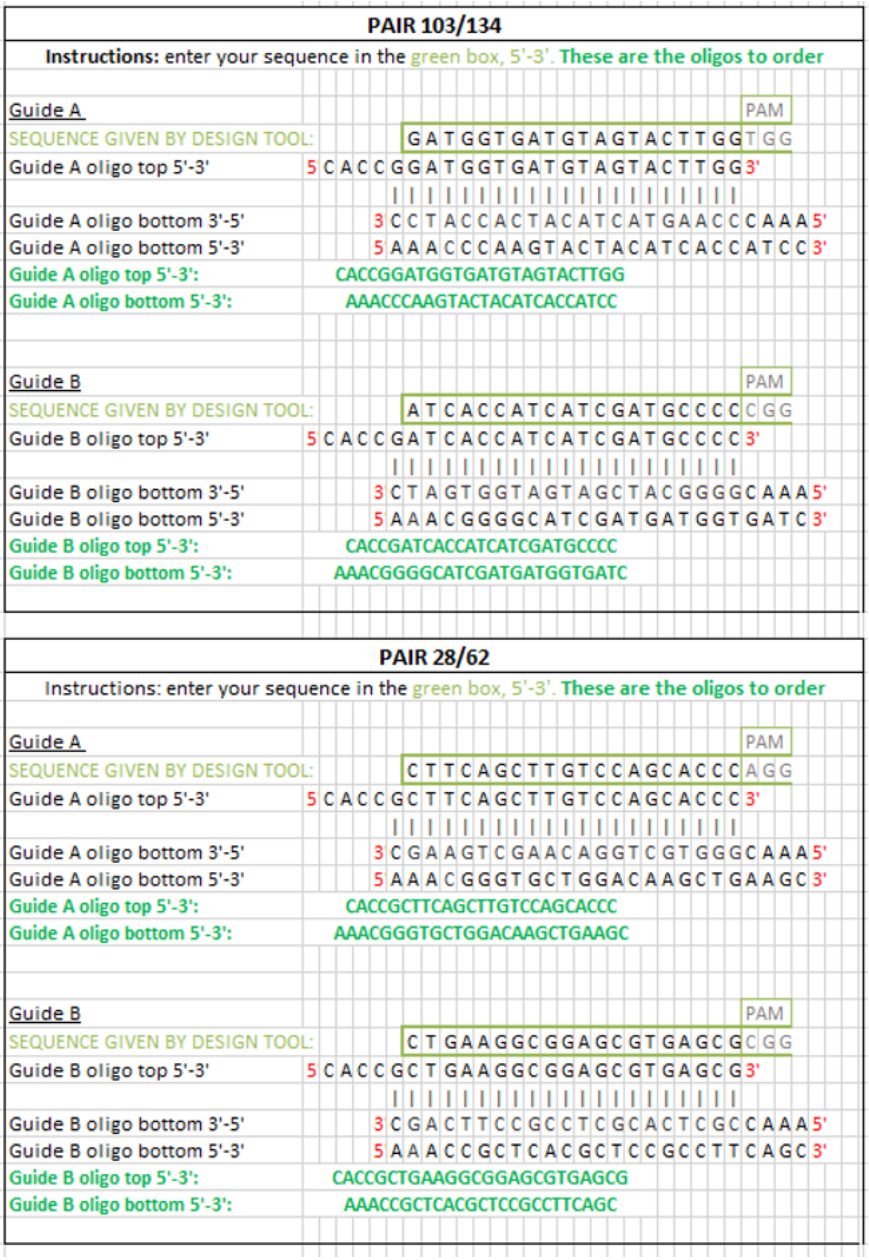

PAIR 103/134

Instructions: enter your sequence in the green box, 5'-3'. **These are the oligos to order**

Guide A	PAM
SEQUENCE GIVEN BY DESIGN TOOL:	GATGGTGATGTAGTACTTGGTGG
Guide A oligo top 5'-3'	5CACCGGATGGTGATGTAGTACTTGG3'
Guide A oligo bottom 3'-5'	3CCTACCACTACATCATGAACCCAAA5'
Guide A oligo bottom 5'-3'	5AAACCCAAGTACTACATCACCATCC3'
Guide A oligo top 5'-3':	CACCGGATGGTGATGTAGTACTTGG
Guide A oligo bottom 5'-3':	AAACCCAAGTACTACATCACCATCC
Guide B	PAM
SEQUENCE GIVEN BY DESIGN TOOL:	ATCACCATCATCGATGCCCCCGG
Guide B oligo top 5'-3'	5CACCGATCACCATCATCGATGCCCC3'
Guide B oligo bottom 3'-5'	3CTAGTGGTAGTAGCTACGGGGCAAA5'
Guide B oligo bottom 5'-3'	5AAACGGGGCATCGATGATGGTGATC3'
Guide B oligo top 5'-3':	CACCGATCACCATCATCGATGCCCC
Guide B oligo bottom 5'-3':	AAACGGGGCATCGATGATGGTGATC

PAIR 28/62

Instructions: enter your sequence in the green box, 5'-3'. **These are the oligos to order**

Guide A	PAM
SEQUENCE GIVEN BY DESIGN TOOL:	CTTCAGCTTGTCCAGCACCCAGG
Guide A oligo top 5'-3'	5CACCGCTTCAGCTTGTCCAGCACCC3'
Guide A oligo bottom 3'-5'	3CGAAGTCGAACAGGTCGTGGGCAAA5'
Guide A oligo bottom 5'-3'	5AAACGGGTGCTGGACAAGCTGAAGC3'
Guide A oligo top 5'-3':	CACCGCTTCAGCTTGTCCAGCACCC
Guide A oligo bottom 5'-3':	AAACGGGTGCTGGACAAGCTGAAGC
Guide B	PAM
SEQUENCE GIVEN BY DESIGN TOOL:	CTGAAGGCGGAGCGTGAGCGCGG
Guide B oligo top 5'-3'	5CACCGCTGAAGGCGGAGCGTGAGCG3'
Guide B oligo bottom 3'-5'	3CGACTTCCGCCTCGCACTCGCCAAA5'
Guide B oligo bottom 5'-3'	5AAACCGCTCACGCTCCGCCTTCAGC3'
Guide B oligo top 5'-3':	CACCGCTGAAGGCGGAGCGTGAGCG
Guide B oligo bottom 5'-3':	AAACCGCTCACGCTCCGCCTTCAGC

Figure 4.5 Screenshot of an excel spreadsheet designed to automate the conversion of gRNA sequences given by the design tool at CRISPR.mit.edu to the oligonucleotides to order. *The gRNAs displayed are those I chose to order to cut near the G70S mutation site in eEF1A2.*

4.4.2 Designing a suitable repair construct to include the G70S mutation

In designing the repair template, I centred the repair template around the G70S mutation site and used 100 bp upstream and downstream of this point to give a 200 bp repair template (Figure 4.6) which was then synthesised as a single stranded oligonucleotide (ssODN). This repair template only differed from the human wildtype sequence at the point at which the G70S mutation was encoded.

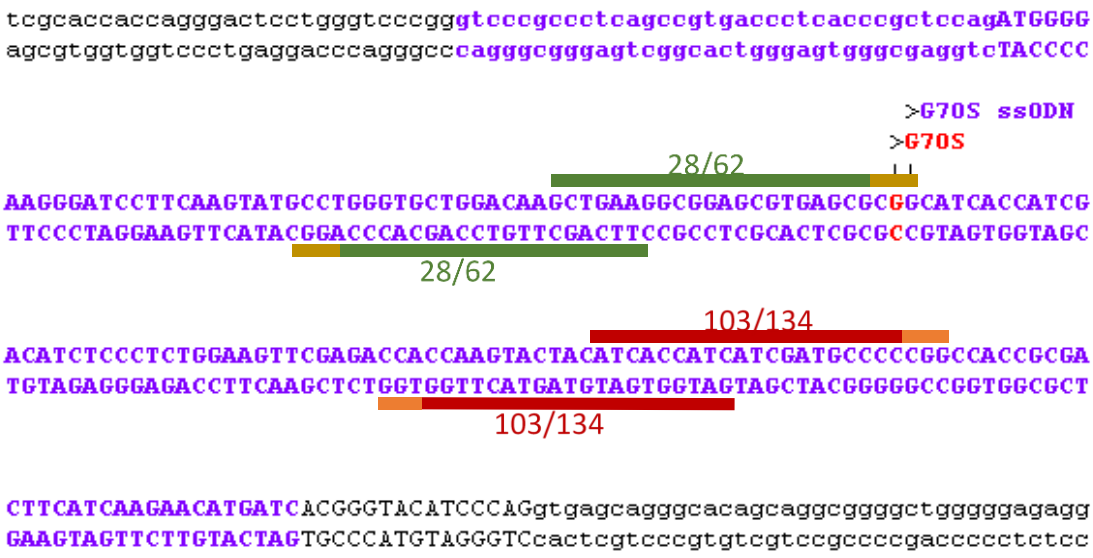

Figure 4.6 G70S CRISPR design *Both strands of human eEF1A2 exon 3 shown in upper case, surrounding introns in lower case. Location of repair template shown in purple, and gRNA pairs (28/62 in green and 103/134 in red) also shown, with corresponding PAM sites (light green and orange)*

Protospacer adjacent motif (PAM) sites are three base pair sequences immediately 3' of the DNA sequence targeted by the cas9 nuclease. Cas9n will not successfully bind to and cleave DNA if the PAM site is not present. The PAM site using the CRISPR system employed here must be of the form NGG (Jinek et al., 2012), where the first nucleotide of the PAM, which can be any nucleotide, is followed by two guanines. In order to prevent re-cutting of DNA after incorporation of the repair template, the PAM sites on the repair template itself can be mutated so that Cas9n nuclease will not recognise them. Such mutations must be carefully designed so as not to change the amino acids for which they code.

I did not mutate any of the PAM sites on the repair template as the actual G70S mutation destroyed the PAM site of one gRNA in guide pair 28/62, and no silent mutations were possible for PAM sites of the other guide pair, 103/134. (see Figure 4.6)

4.4.3 gRNAs cloned into the Cas9n Plasmid and verified

The two gRNA pairs specified above were cloned into pSpCas9n(BB)-2A-puro plasmid. To check correct insertion of gRNA sequences, after ligation and transformation, three colonies for each gRNA were picked and colony PCR performed using gRNA-specific forward primers and a common reverse primer named Reverse Insert Check. Each colony was also separately amplified using primers designed against the double Bbs1 site present on pSpCas9n(BB)-2A-puro. Absence of a band using the Bbs1 forward primer confirmed the colonies to be pure for each of the four gRNAs. (Figure 4.6B). One colony of each gRNA was maxiprepped and then sequenced to double check correct insertion of gRNA into the plasmid. (Figure 4.6 C)

4.4.4 Transfection of plasmids containing gRNAs into SHSY5Y cells and clone isolation

Transfection condition	Number of Clones to analyse
gRNA pair 28/62	5
gRNA pair 28/62 + repair template	10
gRNA pair 103/134	3
Empty Cas9n plasmid (control)	4

Table 4.1 Clonal SHSY5Y lines obtained from preliminary G70S CRISPR experiment

Both pairs of plasmids containing gRNAs were transfected separately into SHSY5Y cells using nucleofection, gRNA pair 28/62 was also separately cotransfected in with the repair template. Single cell isolation of transfected cells was performed using the

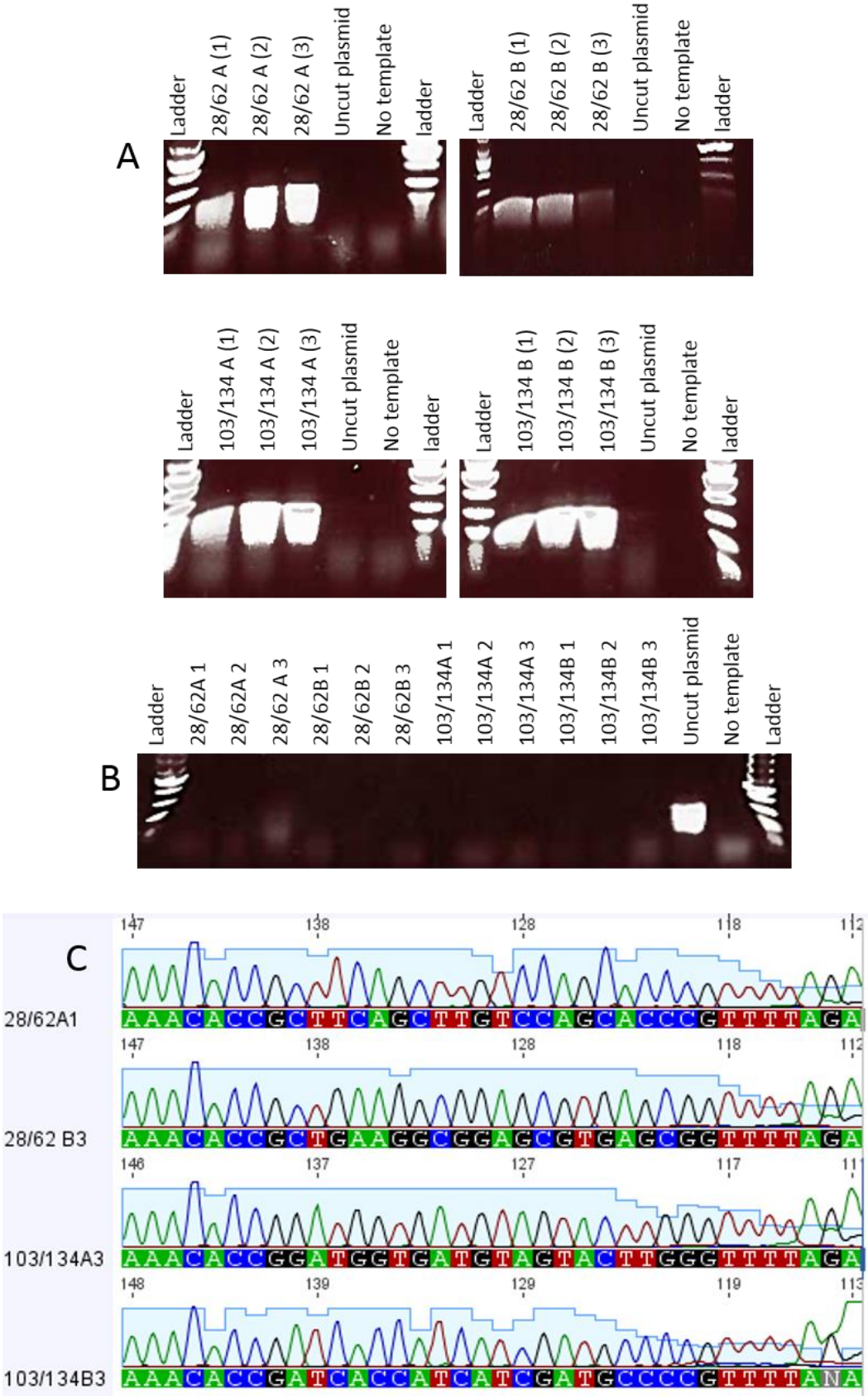

Figure 4.7 Cloning of two gRNA pairs into pSpCas9n(BB)-2A-puro. *Three colonies of each gRNA were picked. Colony PCR using gRNA-specific forward primers (A) to confirm insertion, and Bbs1Bbs1-specific forward primers (B) to confirm purity of colony. One colony for each gRNA was miniprepped, then sequenced (C) to confirm correct sequence.*

dilution method. For each transfection condition I plated out four 96-well plates. I allowed cells to proliferate within wells that only contained one cell, until they reached the T25 flask stage. Clonal lines were then frozen down and DNA taken for mutation analysis. Table 4.1 shows the number of clones obtained from each transfection condition.

4.4.5 One of seventeen clonal lines sequenced contained indels, and none had integrated the repair template

DNA was isolated from each of the clonal lines and a PCR product amplified around the region of the G70S mutation. Initially, standard PCR conditions using Phusion polymerase and HF buffer gave no products, using two different primer pairs. I attempted to optimise the PCR using three different polymerases (Figure 4.8A). The PCR product was GC-rich (66% GC) so the Phusion GC enhancer was tested, along with OneTaq and Q5 polymerases. Phusion plus GC enhancer gave the best results, method, meaning the annealing temperature is 5°C higher than the melting temperature (Tm) in the first cycle, then is reduced by 1°C per cycle until it reaches a point 2°C below the Tm. The program then continues as normal. This combination of changes produced much better results (Figure 4.8B), with all six test samples amplified. I then repeated the PCR using all samples and still found three samples that had not amplified Figure 4.7C. A further repeat left just two samples unamplified. Although there was a possibility that these samples were not amplifying because a large indel had ablated the PCR priming sites, this seemed unlikely since the PCR product was 540 bp long.

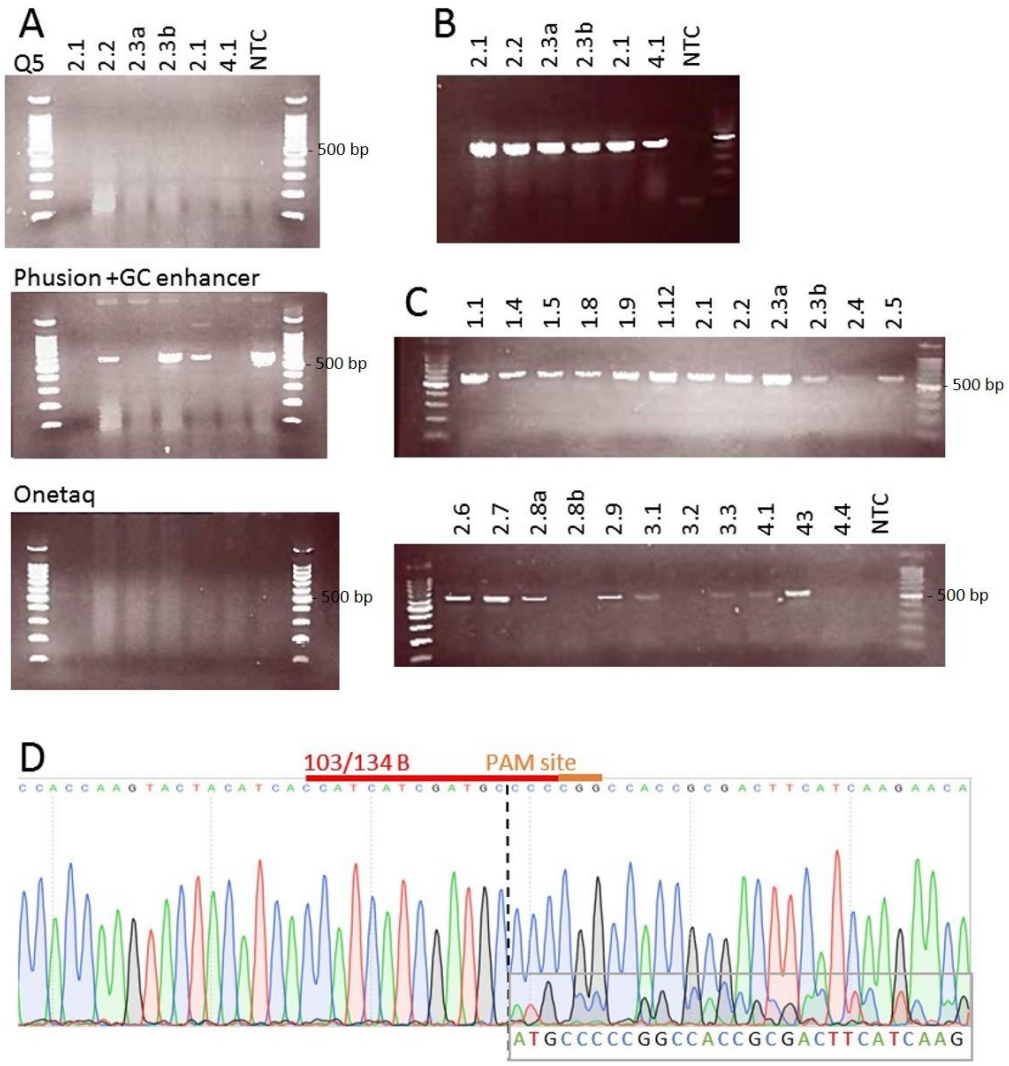

Figure 4.8. Identifying mutations in Clonal SHSY5Y lines by sequencing*. (A) shows the PCR results on a subset of clonal lines using three different polymerases. Ladders indicate 100 bp increments, 500 bp marker given as reference. (B) shows an optimised version of the PCR with 10% DMSO and a touchdown cycling protocol. (C) shows the PCR products of all clonal lines. (D) shows the sequencing chromatogram of the one mutated line, 2.5. It was found to have a 4 bp insertion on one allele at the site of the 103/134B PAM.* ***c***

I then sequenced the PCR product from each of the 17 SHSY5Y clonal lines successfully amplified in the PCR described above. Of the 17 lines, one contained an indel: cell line 2.5 had a 4 base pair insertion on one allele, located at the PAM site of the gRNA103/134, based on interpreting the sub peaks from the sequencing chromatogram (Figure 4.8D). None of the clonal lines from the 'repair' transfection condition had incorporated the repair construct.

I next began an experiment to clone the PCR products from the mutated clonal line into the pGEM-T vector. Subsequent sequencing of multiple colonies should allow visualisation of each individual allele present, and confirm the interpretation of the whole-product sequencing I first used. Unfortunately, whilst optimising the pGEM-T procedure, I attempted to defrost the mutant line 2.5 with the intention of proliferating the line and checking for expression levels of eEF1A2. It had not survived. Upon investigating the other clonal lines, I found that most had not survived the freezing-down and defrost procedures. I had used a standard freezing down procedure which had not caused any problems previously with SHSY5Y cells. Loss of the lines effectively terminated the initial CRISPR experiment, though I was left with useful data in the form of DNA from a confirmed mutated SHSY5Y line, 2.5, as well as the knowledge that at least one of my pairs of gRNAs (103/134) displayed DNA cutting activity at the desired locus.

4.4.6 Refinement of CRISPR workflow based on initial experiment

Reviewing the workflow of the initial CRISPR experiment, a number of developments and changes were required to the workflow.

1) Growing up multiple potential mutant lines from single cells to the T25 flask point was a bottleneck in the process, taking up a great deal of time. For the next round of CRISPR experiments I wanted to find and optimise a method of screening cells at the earliest possible time-point so that only cell lines with a mutation are grown up, thus reducing time pressures.
2) In the initial CRISPR experiment I did not make use of the puromycin cassette in the pSpCas9n(BB)-2a-puro plasmid. Having only obtained one mutant line from 16 sequenced, I decided to enrich the transfected population using puromycin to kill untransfected cells.
3) A screen at an early time point, just after puromycin selection, that indicates whether the gRNA pairs have worked would save much time and effort. If no cutting activity was identified then there would be no need to continue on to the single-cell isolation stage

The above changes are represented in Figure 4.8, with the changes from the initial CRISPR experiment highlighted.

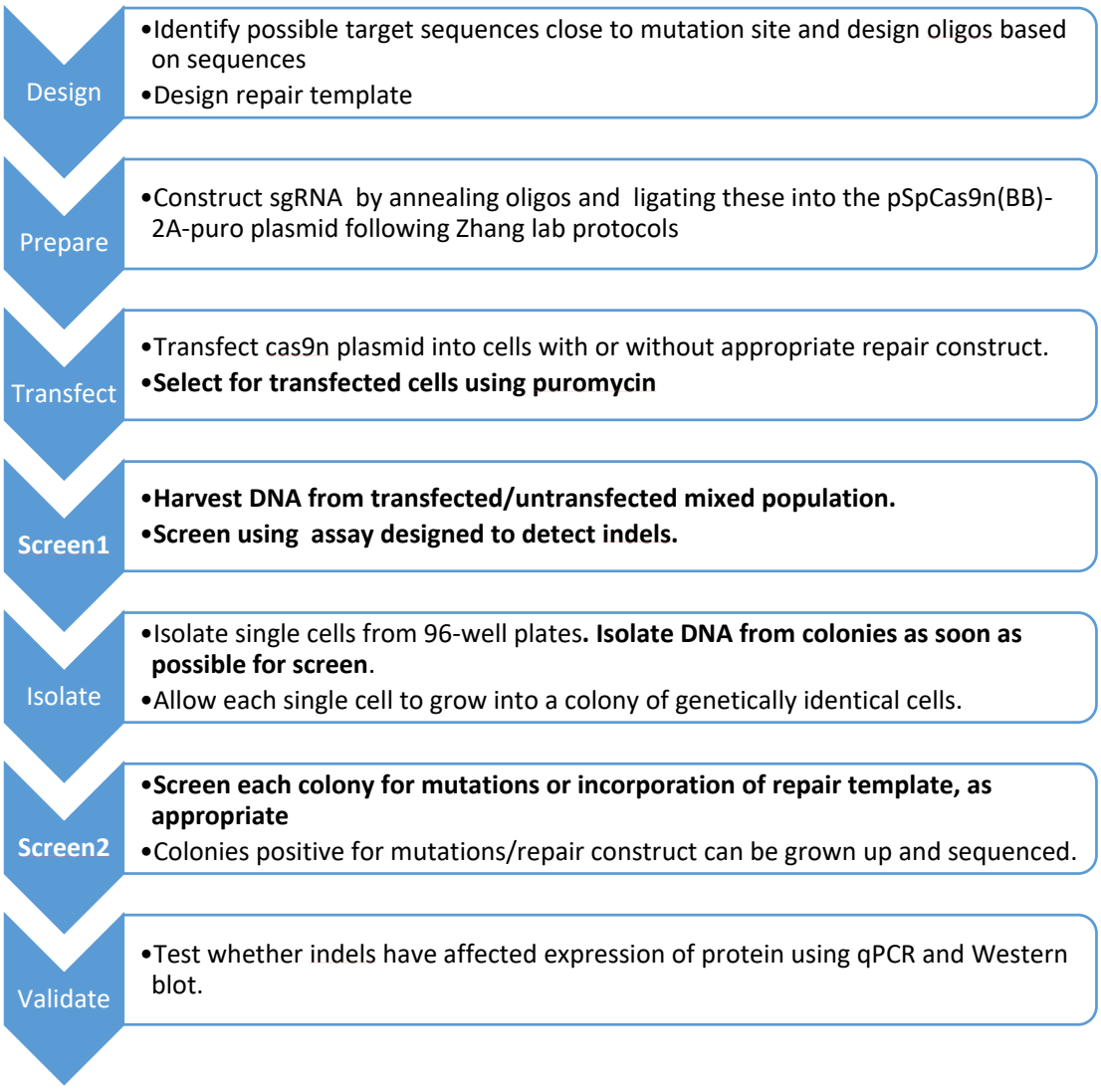

***Figure 4.9 CRISPR experiment workflow**, modified after initial CRISPR experiment (modifications shown in bold) to include two screening steps, designed to minimise tissue culture workload by only growing up clonal lines that have been shown to have a mutation in the screen.*

4.4.6.1 A Comparison of Two Mutation Detection Strategies

An ideal mutation detection assay would be able to detect mutations in a mixed population of cells just after puromycin (screen 1). A negative result at the screen 1 checkpoint would mean mutations are found at such a low frequency that the

experiment should be discontinued. The mutation detection assay would also be used in screen 2, to detect whether individual colonies have mutations. To these ends, I tested two different mutation detection strategies, the T7 endonuclease assay and the PAGE-based mutation assay, these are tested and compared in section 4.4.6.1.2.

Both assays are based on DNA heteroduplex mismatch. A PCR is performed around the target locus, then the DNA is denatured, and slowly allowed to anneal. Some mutated DNA strands anneal to unmutated strands, forming a heteroduplex. T7 endonuclease 1 then selectively cleaves DNA strands that have a mismatch. The products of this enzyme reaction are run out on an agarose gel, and any bands smaller than the original PCR product indicate presence of a mutation. The PAGE-based mutation assay runs out the DNA heteroduplexes on a TBE acrylamide gel. DNA heteroduplexes form a kink at the site of the mismatch, and so run significantly slower than homoduplexes through the TBE acrylamide gel, indicating presence of a mutation.

4.4.6.1.1 Optimisation of DNA Extraction for Screen 2.

In order to screen single-cell isolates at the earliest possible time point, I tested two different methods of extracting DNA from cell colonies in 96-well plates: QuickExtract (Epibio) and cell lysis using Bradley Lysis buffer followed by ethanol precipitation (Table 4.2). I found that Quickextract, a proprietary one-step DNA extraction reagent, was the most sensitive method of harvesting sufficient DNA from one well of a 96-well plate, yielding detectable levels of DNA even when the cells in the well were subconfluent, giving me more flexibility around when I screen individual clonal lines for mutations.

Type of DNA extraction	Confluency of Cells in one well of 96-well plate		
	High	Medium	Low
		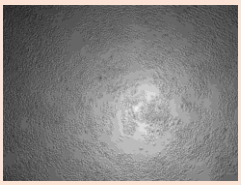	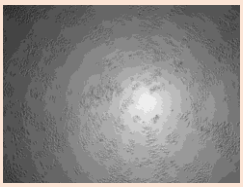
Bradley lysis buffer and ethanol precipitation	350 ng/µl	0 ng/µl	0 ng/µl
Quickextract (epicentre)	340 ng/µl	113 ng/µl	38 ng/µl

Table 4.4 An experiment to test two different methods of DNA extraction from small numbers of cells in a 96-well plate. *Representative images of well confluency are given, followed by the concentration of DNA obtained after extraction of all the cells in one well of a 96-well plate*.

4.4.6.1.2 Both the T7 Endonuclease and PAGE-based Assays Can Detect Mutations in SHSY5Y Cell Lines

Both assays were first tested to ensure they could differentiate between a mutant and a wildtype cell line. DNA from the mutated SHSY5Y line 2.5, generated during the initial CRISPR experiment, was used as a positive control. Sequenced wild type lines from the same experiment were used as a negative control. Both the T7EI, (Figure 4.10B) and the PAGE-based assay (Figure 4.10D) could detect the mutant cell line, so either would be suitable for use in screen 2, however I chose to continue with the PAGE-based assay for two reasons: firstly, the PAGE-based assay is easier to perform and takes less time than the T7EI. Secondly, the T7EI assay shows three bands apart from those representing the PCR product and the known mutation. (Figure 4.10A and B). These extra bands are present in all control line samples, so the T7EI assay would need to be used carefully, always comparing unknown samples with confirmed wild type cell line samples to distinguish mutations from background.

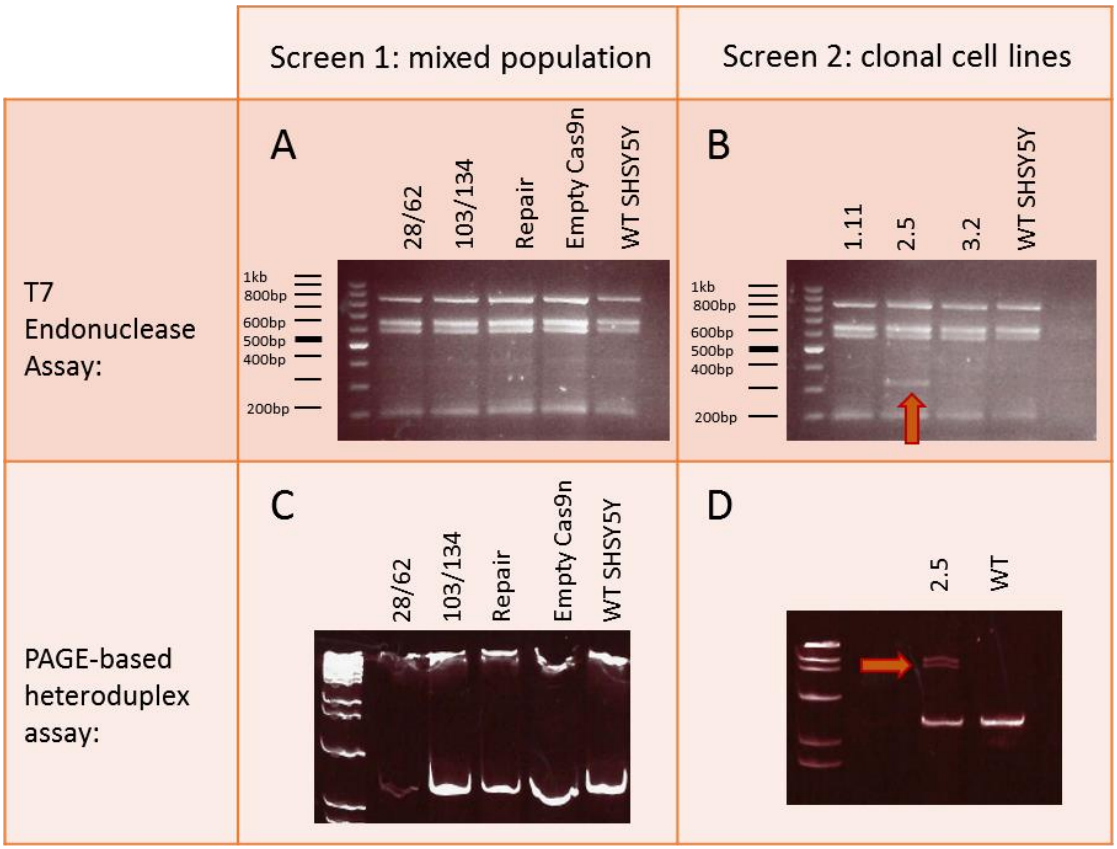

Figure 4.10 Two different mutation-detection assays *were tested for their sensitivity in picking up low frequencies of mutations (screen 1). (A) and (C) 103/134 was a transfection condition known to have produced mutations, so is effectively a positive control. Neither assay detected mutations, showing they are not sensitive enough to detect mutations in a population at this frequency. (B) and (D) Both assays successfully detected the Screen 2 mutation in SHSY5Y line 2.5, as indicated by the arrows. The T7 endonuclease assay had a number of cleavage products apart from the known positive control, so the assay would always have to be used with confirmed negative controls.*

4.4.6.1.3 Neither Mutation Assay is Sensitive Enough to Detect Mutations in Mixed Populations of SHSY5Y Cells

Having shown that both assays functioned well to detect mutations in pure clonal lines, I sought to test their sensitivity using cell populations from the initial CRISPR experiment, using surplus cells left over from the single-cell isolation step. The cells transfected using gRNA pair 103/134 were used as a positive control, as the one mutant line produced in the initial CRISPR experiment came from this cell population, so it was highly likely that more mutations were present, if at a low frequency. One out of 16 cell lines sequenced contained a mutation, so an estimated mutation frequency of around 6% was present in this sample. Neither assay was sensitive enough to detect

mutations using these samples, however I hoped, in my next CRISPR experiment, to significantly enrich mutant cell populations using puromycin selection, so screen 1 could still prove to be useful in subsequent experiments.

4.4.7 Optimisation of a Restriction Digest Assay to Detect Repair Template Incorporation

An assay that specifically detects repair template incorporation would be very useful at both screening points. I used the sequence mapping function of 'Serial Cloner v2.5', to identify restriction site changes that occur in the DNA sequence when the G70S mutation is incorporated. I found that a BstUI site is deleted, and a BbvI site introduced

Using a PCR product of 437 bp around the site of the G70S mutation, I performed two separate restriction digests using BstUI and BbvI. Samples used were the mixed populations of cells used previously in Figure 4.9 A and C. In the absence of a positive control this would at least demonstrate that the assay performs correctly with DNA extracted from cells under identical experimental conditions.

Figure 4.11 shows no evidence of repair template incorporation in the 'repair' transfection condition using either restriction enzyme. However, as the sensitivity of this assay is not known, it was possible that repair template incorporation had occurred but below the detection efficiency of this assay.

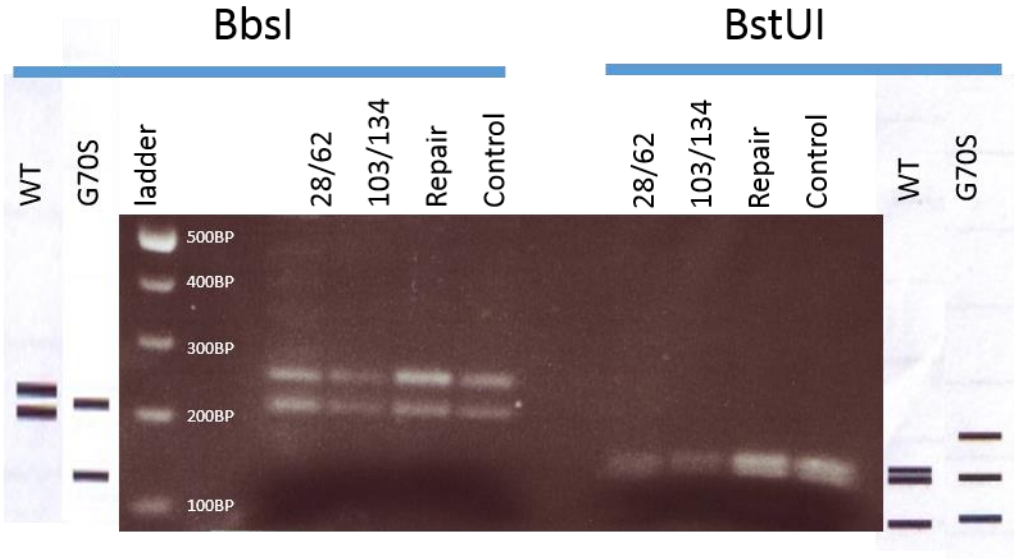

Figure 4.11 Populations of transfected cells were used to attempt to detect repair template incorporation. *DNA was extracted and a PCR product of 437 bp around the G70S mutation site amplified. Restriction digests were performed on this PCR product. Predicted bands are given to the sides of the actual results. There is no evidence here of repair template incorporation.*

4.5 Use of CRISPR to Mutate the eEF1A2 Gene in LUHMES Cells

Having optimised my CRISPR experimental design using SHSY5Y cells, I went on to attempt to mutate NS1 cells, a rat neuronal cell line which display marked differentiation upon neural growth factor treatment characterised by development of neurites. Having worked previously with this cell line and optimised neurite outgrowth assays, a mutant NS1 line containing an epilepsy-causing mutation would have been advantageous. The CRISPR experiments using this line were ultimately not successful, yielding no clonal lines, but have been included in appendix A

I then focused on mutating LUHMES cells. LUHMES is a human dopaminergic neuron cell line, originally isolated from foetal mesencephalon (Scholz et al., 2011). It is karyotypically normal, and proliferates well until the myc transgene used to

immortalise the line is switched off with tetracyclin, and certain neuronal growth factors are added. Over several days the cells sprout long neurites and by day five are uniformly post mitotic. They can form synapses and display increasing levels of spontaneous electrical activity as they differentiate (Scholtz et al., 2011). LUHMES is an ideal cell line for study of the effect of epilepsy- and AD-causing eEF1A2 mutations, as they have a strong differentiated phenotype.

The LUHMES line is particularly useful as a model, given that it can be differentiated into post-mitotic neuronal-type cells. It could also be suitable for use in a high-throughput drug screen if the mutations incorporated provide a clear phenotype amenable to detection by such a screen.

4.5.1 CRISPR Protocols Modified for LUHMES Experiment

4.5.1.1 A New Cas9n Plasmid

The pSpCas9n(BB)-2A-puro plasmid used up until now did not provide very high levels of puromycin resistance to cells, (see section A1.4), so I decided to change selection methods. I began using a slightly different form of the Cas9n plasmid, with a GFP cassette instead of puromycin resistance: pSpCas9n(BB)-2A-GFP. The advantages of using GFP expression as a selection mechanism over puromycin selection are that it can be used directly as a test of transfection efficiency, and it can also reduce hands-on time in the experiment, as GFP-positive cells can be FAC-sorted directly into individual wells of a 96-well plate, eliminating the need for making single-cell dilutions.

4.5.1.2 Design of gRNAs and Repair Template to Incorporate the D252H Mutation in Human Cells

The gRNAs and repair template against human G70S I designed for the initial SHSY5Y experiment could be reused here in LUHMES, but new gRNAs and repair template were needed to attempt to incorporate the D252H mutation in a human cell line. A pair of gRNAs (18/75) was chosen as previously described in section 4.4.1. The repair template was designed to incorporate the D252H mutation, silently mutate the PAM site of gRNA 18, and silently mutate a section of DNA recognised by gRNA 75. The PAM site for gRNA 75 cannot be silently mutated, but four mutations were introduced along the 20 bp length recognised by the gRNA to attempt to prevent gRNA

Figure 4.12 (A) Both strands of human eEF1A2 exon 5 (capitals) with surrounding introns *(lower case). Site of the D252H repair template shown in purple, the D252H base change in red. gRNA pair 18/75 indicated by red line, the PAM recognition sites with a blue line. (B) The D252H repair template with site of gRNAs in red and blue. Bases that differ from wildtype are underlined, the D252H mutation is given in green.*

recognition. Two of these silent mutations introduce a new restriction enzyme recognition site, PsiI. The placement of the gRNAs and repair template is summarised in Figure 4.11A, and the sequence of the repair template itself is given in Figure 4.12B. gRNA 18 was cloned into pSpCas9n(BB)-2A-GFP, and gRNA 75 was cloned into pSpCas9n(BB)-2A-puro so that either selection method, or both, could be used to enrich the transfected cell population.

4.5.1.3 Optimisation of LUHMES Transfection and GFP Selection

Commonly used transfection reagents are not suitable for use with LUHMES. Published methods for transfecting this cell line are use of lentivirus, or Amaxa nucleofection. In this case, nucleofection was chosen and the method described by Schildknicht et al. (2013), used.

An experiment was performed to ascertain:

1) The best Amaxa Nucleofection program for LUHMES cells

2) The response of LUHMES cells to FACS

3) The performance of LUHMES when cells are isolated singly and left to proliferate

Two different Amaxa nucleofection programs were tested, A-33 and D-33. These programs were used to transfect pMaxGFP into LUHMES cells. Both transfections worked well and GFP-positive cells were visible using fluorescence microscopy when checked after 24 hours. The cells were allowed to recover for 48 hours and then sorted using a BD FACSJAZZ to sort GFP-positive cells into 96-well plates, one cell per well. 30% of cells were reported to be GFP-positive. The LUHMES cells reacted well to the sorting procedure, and grew nicely from single cells. Nine days after sorting, the number of wells containing single colonies was counted for each transfection condition. The D-33 plate contained sixteen colonies, and the A-33 plate contained nine. I decided to use program D-33 in future LUHMES CRISPR experiments.

4.5.2 Transfection of gRNAs and Repair Templates in LUHMES Led to Isolation of Three Clonal Lines

The D252H mutation was targeted in the first LUHMES CRISPR experiment. pSpCas9n(gRNA18)-2A-GFP and pSpCas9n(gRNA75)-2A-puro were transfected into LUHMES along with the human D252H repair template. The FACSJAZZ cell sorter was not available 48 hours after transfection, so the cells were sorted into 96-well plates 72 hours after transfection, by which time GFP expression appeared to be past its peak. As a result only three 96-well plates could be filled with GFP-positive cells, and there were no cells left over for Screen 1. Two weeks after transfection, 22 colonies expanded from single cells were transferred to 48-well plates. Between this point and the point of freezing down confluent T25 flasks of cells, all but three clonal lines died. Then when defrosting lines for propagation, a further two of these lines died. LUHMES cells can be tricky to grow, they require very specific growth conditions, so some deaths may have been due to the stress of the experiment. Alternatively, the deaths could have been due to the effect of mutations on the cells' ability to live, though if this were the case I would have expected cells to die soon after transfection, not several weeks afterwards.

Although I only had three living clonal lines frozen down, I had DNA samples from seven clonal lines. Because of the relatively low number of clonal lines to deal with, I abandoned Screen 2, the advantage of which was ease of screening large numbers of clonal lines together. Instead I simply PCR amplified the region around the D252H mutation and then sequenced across the mutation site, both forwards and backwards.

4.5.2.1 PCR and Sequencing Show Mutations in Six out of Seven Clonal Lines

The PCR of the region around the D252H mutation alone showed evidence of mutation in the clonal lines (Figure 4.13A), with one mutant line, 1.2, showing two alleles of different sizes, and one mutant line, 1.13, showing three alleles. This may indicate that it is not a true clonal line, but instead is derived from two (or more) cells rather than one.

The sequencing results shown in Figure 4.13B and Figure 4.14 show one mutant line with no mutations (1.15), five lines with indels around the cut sites of the gRNAs, and one line (1.11) with incorporation of the repair template.

Mutant line 1.2 shows a homozygous deletion of around 14 bp across the D252H mutation site, and two indels, indicated with red arrows, shown by the sequencing chromatogram splitting into double peaks. They are most likely on different alleles given the two differently sized PCR products seen in Figure 4.11A. Mutant line 1.4 shows no incorporation of D252H, but a homozygous 20 bp deletion upstream of the site.

By utilising both forward and backwards traces, and reading the sub-peaks of each double trace, I was able to unpick the complex indels shown in the chromatogram for mutant line 1.5. Reading the sub-peaks of the forward trace, I found a 32 bp deletion from 12 bp to 43 bp upstream of the D252H mutation site, with no integration of the mutation. Reading the reverse trace I could find a 33 bp deletion on the other allele, from 19 bp upstream to 6 bp downstream of the D252H site.

Both the forward and backwards sequencing chromatograms for mutant line 1.11 (Figure 4.14) showed a clean integration of the repair template. Interestingly, not all the template was incorporated – the silent mutation 17 bp downstream of the D252H

mutation (indicated by a red arrow) was not incorporated, though the other three silent mutations between this point and the D252H mutation were.

1.13 has indels on both alleles, and no incorporation of the repair template (Figure 4.14). On one allele the D252H site has been ablated, on the other allele it shows the wildtype sequence. The indels are too complex to unpick on a single chromatogram. Since this cell line had not survived, I did not pursue the identification of the mutation. 1.15 was a wildtype line, confirmed by both the forwards and backwards sequencing trace, 200 bp up and downstream of the D252H mutation site (Figure 4.14)The sequencing for mutant line 1.16 shows either a homozygous mutation, or that one of the alleles has not been amplified due to a very large mutation erasing the primer sites. Between the two red arrows in Figure 4.14 *1.16*, there is a 3 bp deletion and a 25 bp substitution. The 25 bp substitution matches a region of the reverse strand of exon 5, 20 bp downstream of the D252H mutation site. The mutations identified have been summarised below in table 4.3:

***Table 4.3 Table summarising mutations in LUHMES clonal lines around the site of the potential D252H mutation in exon 5 of* eEF1A2.**

Clonal line	Nature of mutation identified
1.2	Allele 1: 8 bp insertion, 22 bp deletion spanning D252H mutation site Allele 2: 17 bp deletion, 2 bp insertion spanning D252H mutation site
1.4	Biallelic 20 bp deletion upstream of D252H mutation site.
1.5	Allele 1: 32 bp deletion upstream of D252H mutation site Allele 2: 33 bp deletion spanning D252H mutation site
1.11	Perfect incorporation of D252H mutation. No indels.
1.13	Allele 1: Unidentified indel spanning D252H mutation site Allele 2: Unidentified indel upstream of D252H mutation site
1.15	Wildtype
1.16	Biallelic 25bp substitution, 3 bp deletion upstream of D252H mutation site.

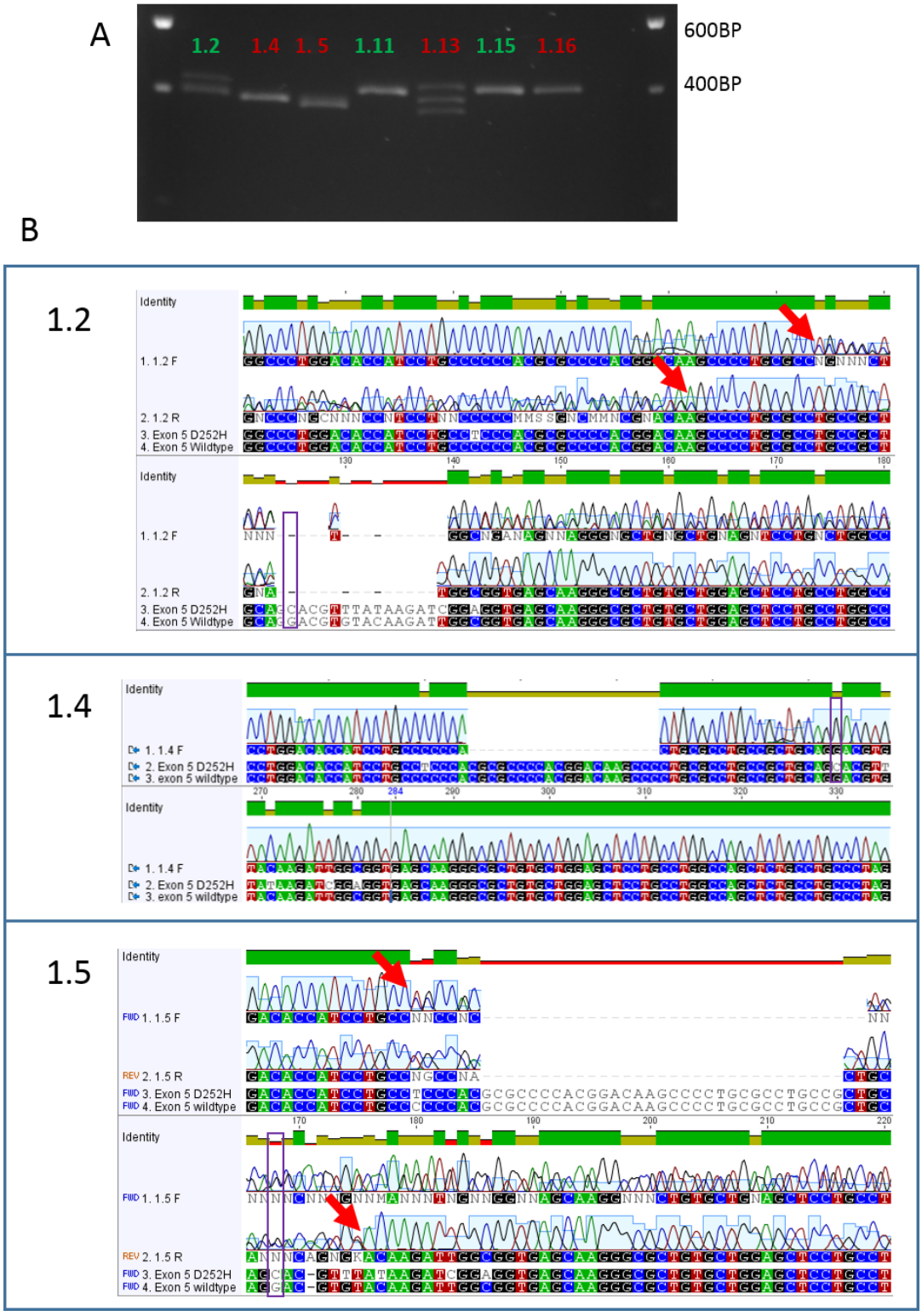

Figure 4.13 PCR and sequencing of three LUHMES mutant cell lines. *(A) LUHMES clonal line PCR products of D252H locus separated on a 2% agarose gel. Clonal line ID given in red for lines lost during the expansion and freezing down process, in green for lines successfully expanded and cryopreserved. (B) Sanger sequencing of three LUHMES clonal lines. A purple box outlines the site of the D252H mutation. Red arrows indicate splitting of the sequence into two superimposed peaks, indicating an indel on one allele.*

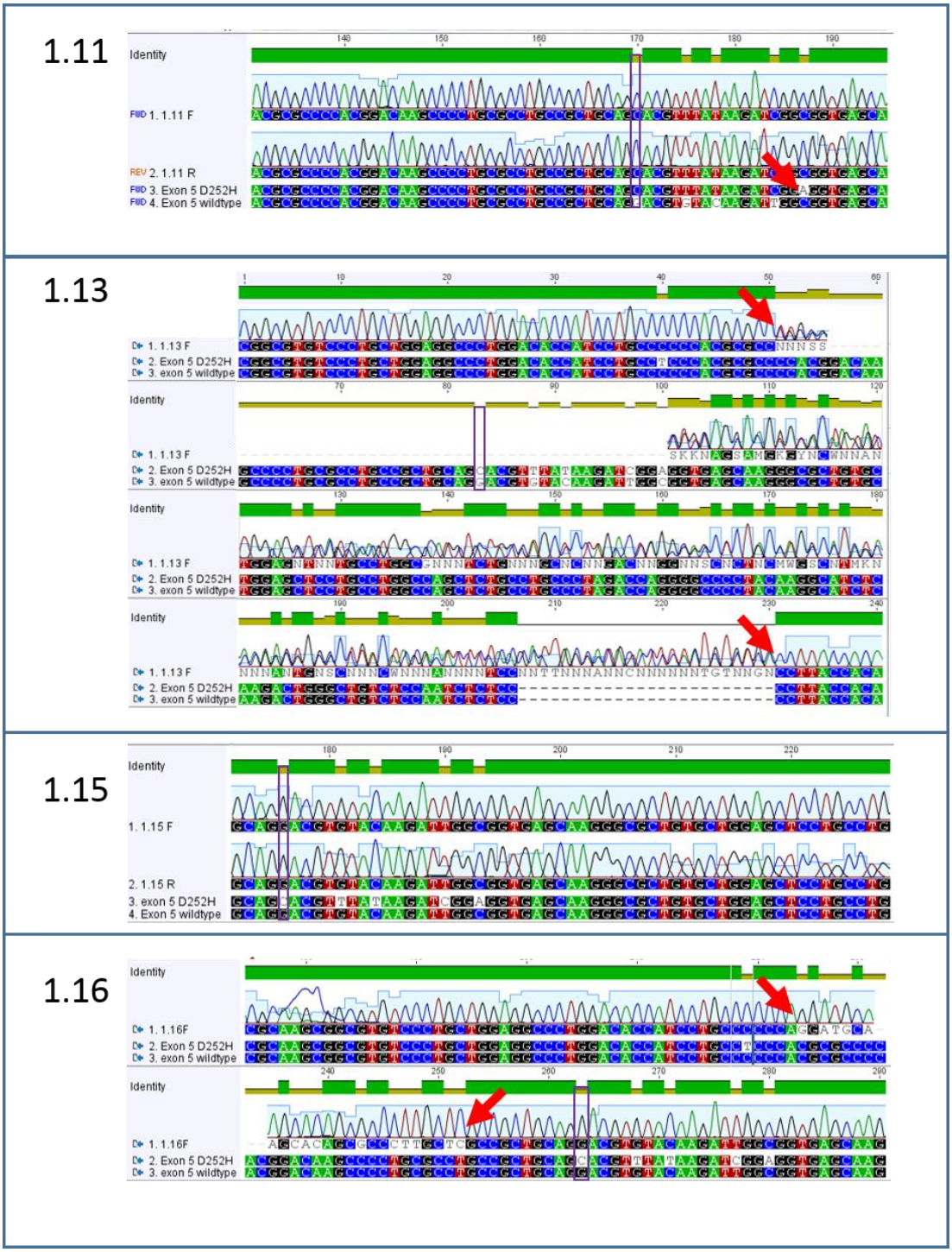

Figure 4.14 Sequencing of four LUHMES mutant lines after CRISPR. *All lines were sequenced forwards and backwards and then aligned to both wildtype and mutated eEF1A2. A purple box outlines the site of the D252H mutation. Red arrows indicate splitting of the sequence into two superimposed peaks, indicating an indel on one allele.*

4.5.2.2 TOPO Cloning Of Selected Clonal Lines Confirms the Results of Initial Sequencing

Two of the three surviving mutant lines, 1.2 and 1.11, were TOPO cloned to enable visualisation of the sequence of each allele separately. (Figure 4.15) 1.15 was not TOPO cloned as the sequencing had showed it to be wildtype.

The TOPO cloning of mutant line 1.2 produced five sequenced PCR products. Four showed one allele, one showed the other. Allele 1 has an 8 bp insertion 22 bp upstream of the D252H mutation site, and also a 15 bp deletion across the mutation site itself. Allele 2 has a 17 bp deletion across the site of the D252H mutation, and also a 2 bp insertion. This gives a 15 bp in-frame deletion overall, deleting 5 amino acids, AA 252-256, and substituting one further amino acid, Q251H.

Two sequenced PCR products were obtained from TOPO cloning mutant line 1.11. Both showed incorporation of the repair template, and so supported the analysis of basic sequencing that the repair template incorporation is homozygous.

Figure 4.15 TOPO cloning and subsequent sequencing of mutant LUHMES lines 1.2 and 1.11 *shows each allele separately, aligned to the reference sequence which contains the D252H mutation.. Purple box indicates D252H site.*

4.5.3 The mutations introduced into LUHMES cell line 1.2 are likely to be deleterious to protein function.

The frameshift mutation in allele 1 of LUHMES mutant line 1.2 causes formation of a premature termination codon in exon 5 of 8 of eEF1A2 at the site of the 15 bp deletion. Although it is impossible to be certain without experimental proof, it is highly likely that the mRNA transcribed from this allele would be subject to nonsense mediated decay, which is generally activated when a premature stop codon is located at least 50-55 nucleotides upstream of any exon-exon boundary (Popp and Maquat, 2013), as is the case here.

The mutation in allele 2 of LUHMES line 1.2 maintains the sequence in frame. The mutant allele was submitted to Provean, an online tool designed to predict the effects of amino acid substitutions, insertions and deletions on protein function (Choi et al., 2012). The mutation is assigned a Provean score. Anything under -2.5 is considered deleterious. LUHMES 1.2 Allele 2 was given a Provean score of -30.5, so was considered deleterious using this algorithm.

4.5.4 Functional Validation and Analysis of LUHMES Mutant Lines

Having generated two mutant lines, 1.2 and 1.11, I checked expression of eEF1A2 using reverse transcriptase PCR to look for mRNA expression, and western blotting to examine expression of the protein.

4.5.4.1 Differentiated mutant line 1.2, but not 1.11, the D252H homozygous line, expresses eEF1A2 mRNA at a lower level than wildtype LUHMES.

Reverse transcriptase PCR (RTPCR) was performed to detect whether or not eFE1A2 was expressed in the mutant lines at an RNA level. RNA was extracted from differentiated mutant and wildtype LUHMES cells (three repeats of each, separately differentiated). cDNA was made and eEF1A1, eEF1A2 and a housekeeping gene, APP5B, amplified using PCR. The results of this reverse transcription PCR reaction can be seen in Figure 4.16A, and semi quantitative analysis (Figure 4.16B) indicates that in mutant line 1.2, eEF1A2 mRNA is expressed at a significantly lower level

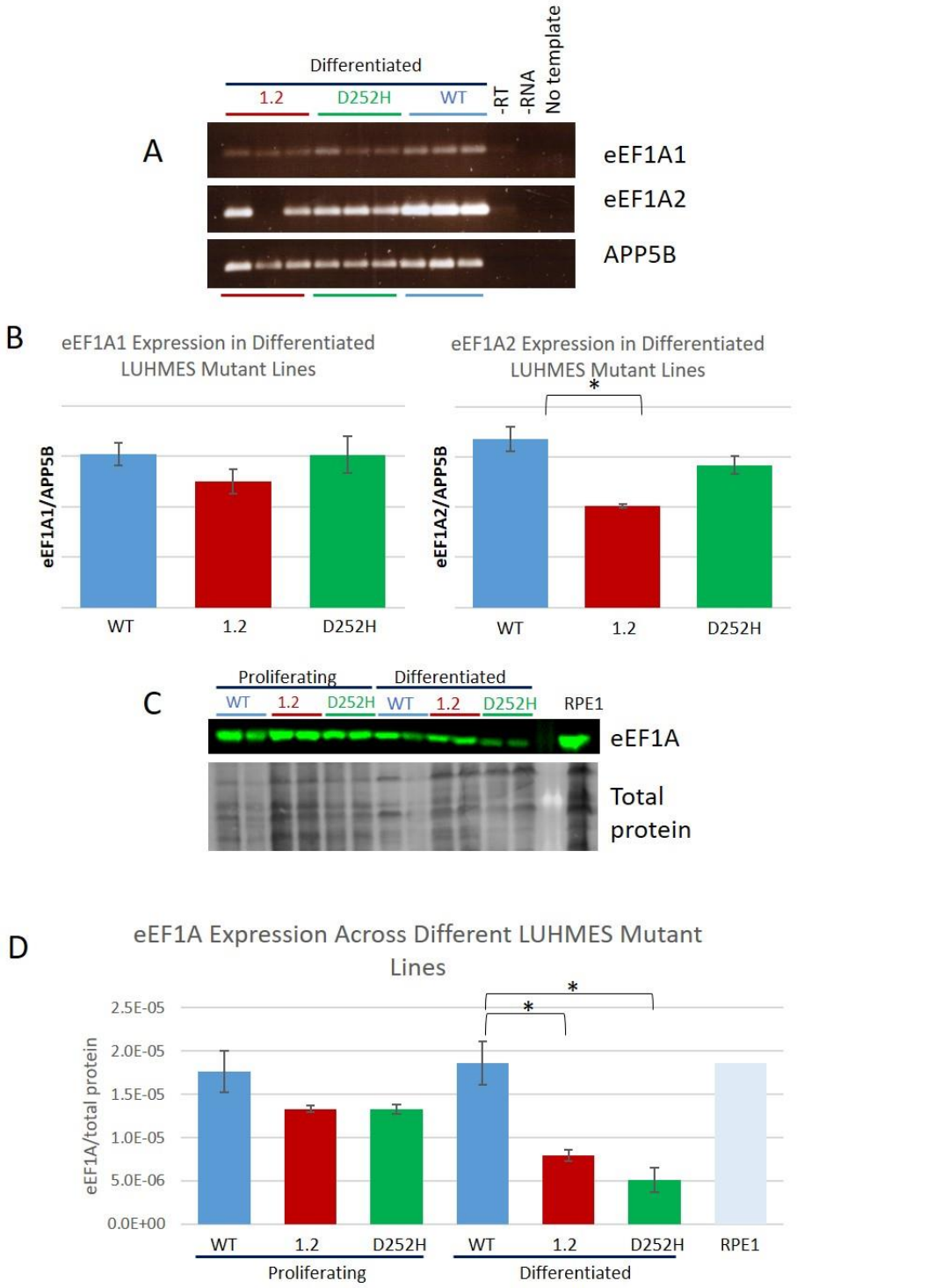

Figure 4.16 The mRNA and Protein Expression of eEF1A isoforms in LUHMES mutant cell lines. *(A) RT-PCR of three LUHMES mutant lines for eEF1A1, eEF1A2 and a housekeeping gene, APP5B, quantified in (B), Gap in RNA due to pipetting error. Mutant line 1.2 shows significantly lower expression of eEF1A2 compared to the wildtype (WT) line. (P=0.028). (C), quantified in (D) eEF1A protein expression of the mutant lines in proliferating and differentiated states. eEF1A protein levels in both mutant cell lines are significantly lower than wildtype eEF1A expression in differentiating cells. RPE1 cells used as a control as these are known not to express eEF1A2, but do express eEF1A1. P=0.026 protein 1.2 vs WT, p=0.021 protein 1.11 vs WT.*

(p=0.028) than that seen in the wildtype line. The D252H homozygous line, however, expresses eEF1A2 mRNA at levels comparable to those seen in the wildtype line.

4.5.4.2 Both the D252H homozygous mutant, and mutant line 1.2 express eEF1A proteins at a lower level than wildtype LUHMES.

Probing for eEF1A2 using Western blot can be extremely challenging due to its sequence similarity to eEF1A1 and the fact that many commercial antibodies advertised to be specific to eEF1A2 also pick up eEF1A1. An antibody against eEF1A2 from Genetex, (GTX102326) had previously been shown to be specific to eEF1A2, or at least to pick up two identifiable bands, one of which was eEF1A2. More recently purchased tubes of this antibody appeared to cross-react with eEF1A1 in cell lysate samples from cell culture (it remained specific to eEF1A2 in lysed tissue samples). Despite many attempts at optimisation of another antibody, no suitable replacement was found, making it impossible to check for changes in eEF1A2 at the protein level.

An antibody known to pick up both isoforms of eEF1A (see table 2.19) was used to probe both wildtype and mutant lines, when proliferating and when differentiated. Figure 4.16C shows the western blot and total protein stain of the membrane. The results of the western blot are analysed semi-quantitatively using densitometry in Figure 4.16. Expression of total eEF1A protein in differentiated cells is significantly lower in both the mutant lines than in the wild type line ($p<0.05$). Although there is no evidence to show which isoform of eEF1A protein has reduced expression here, it is reasonable to suggest that the changes in protein eEF1A relate to changes in eEF1A2 expression rather than eEF1A, since it was eEF1A2 that was mutated and eEF1A1 shows no change in expression at the mRNA level (Figure 4.15B)

The mRNA and protein eEF1A2 levels are similarly reduced (compared to wildtype) in the mutant 1.2 line. This is unsurprising given the high likelihood that one eEF1A2 alleles in this line would be null. The homozygous D252H line, in contrast, expresses eEF1A2 mRNA at a similar level to wildtype, however expression of eEF1A at the

protein level is reduced. This fits with the results of earlier experiments which showed that eEF1A2 constructs carrying the epilepsy-causing mutations, transiently transfected into cell lines, were generally expressed comparatively to wildtype constructs at the mRNA level, but had reduced expression at the protein level, which could be rescued by treatment with a proteasome inhibitor (see Section 4.1).

An important caveat of the work here is that the wild type line used in both the RNA and protein analysis above was of a lower passage than the mutant lines (approximately 8 passages fewer) and had not been through clonal selection. eEF1A1 mRNA levels were, however, similar across all three cell lines, showing that expression of this eEF1A isoform is not affected by the difference in passage number.

4.5.4.3 IncuCyte Analysis of LUHMES CRISPR Clones

Having created a line that expresses eEF1A2 containing the D252H mutation, a next step would be development of a high throughput assay based on phenotypic differences found between D252H and wildtype LUHMEs lines, which could eventually be used for drug screening to identify drugs or small molecules with the potential to restore any phenotypic alterations associated with the mutation.

The IncuCyte Zoom is a useful tool for this purpose, able to take live images of unlabelled cells in 96-well plates over a long time period. The IncuCyte Zoom software is able to detect neurites and cell bodies, making it possible to detect changes in cell proliferation and neurite outgrowth over time without either labelling cells or annotating neurites by hand, a process which can take many hours.

4.5.4.3.1 Doubling times of LUHMES clones are variable

The proliferation rate of both mutant cell lines (1.2 and D252H) was calculated by measuring the change in percentage area occupied by proliferating cells over time. The data were plotted on a log scale, and a straight region of the graph analysed, as a straight line indicates the cells were in an exponential growth phase of proliferation.

The proliferation rates of the two mutant lines were measured on two separate occasions, once compared only to a wildtype line of a lower passage than the mutant

lines(Figure 4.17A) , once to both a wildtype line and the control wildtype line that had been through clonal selection, 1.15 (Figure 4.17B). 1.15 is a much more appropriate control for the mutant lines as it is of a similar passage number.

The doubling times for all mutants are expressed alongside the graphs from which they are derived. The doubling time was calculated by using a tool in GraphPad Prism V6 that fits an exponential growth curve to the data using non-linear regression.

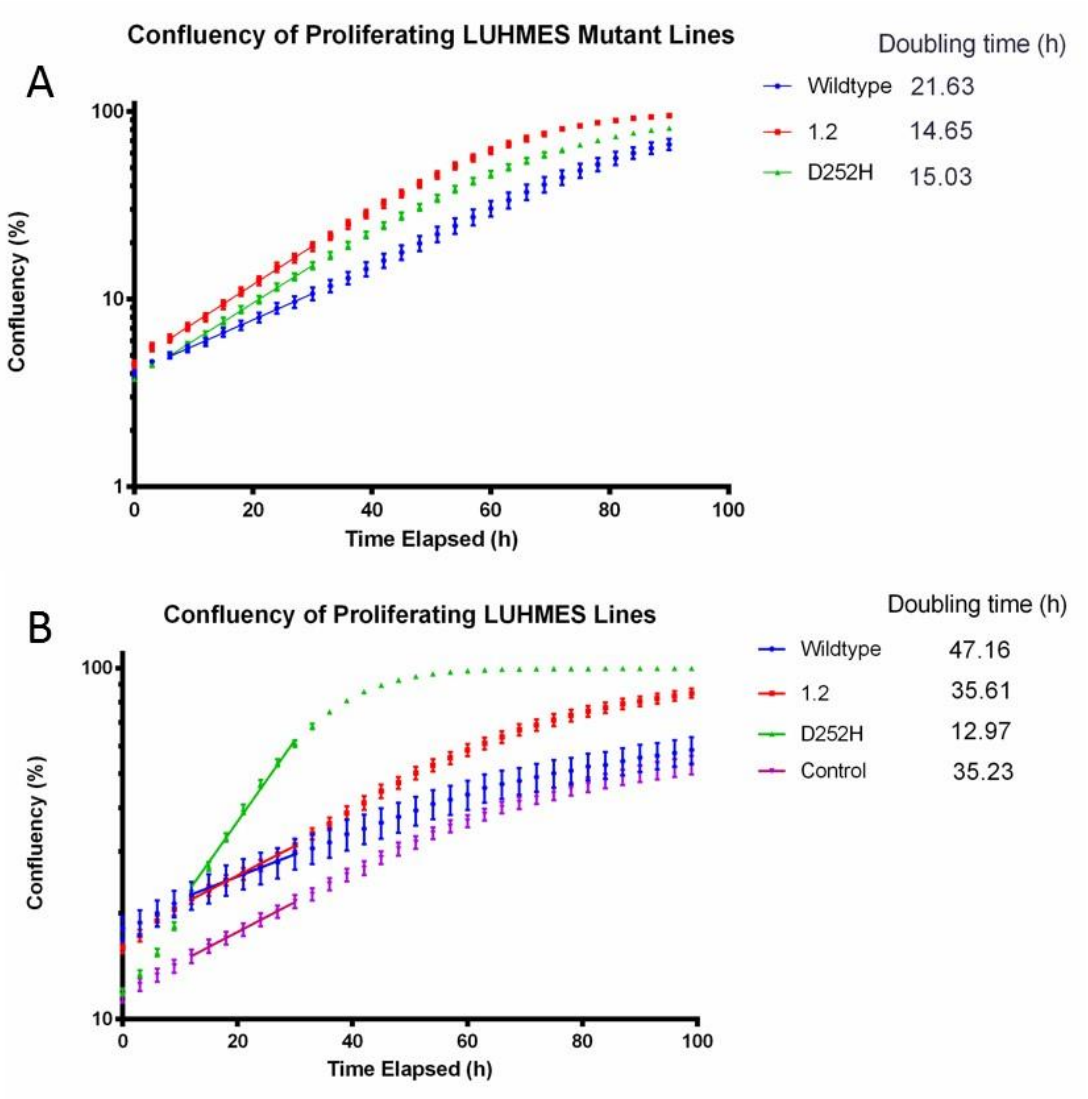

Figure 4.17 Growth Curves for proliferating mutant LUHMES lines, *tested on two separate occasions. Each point represents the mean of six measurements +/-SEM. Lines show the curve of best-fit over a linear section of the graph, from which the doubling time of each cell line can be calculated. Doubling time is expressed in hours to the right of each graph.(A) The first proliferation experiment tested the two mutant LUHMES lines, 1.2 and D252H at passage 24 and some wildtype LUHMES cells of a lower passage, P16. (B) The second proliferation experiment tested the same lines as in (A) but also included a clonal wildtype line of a similar passage to the mutant lines. On this occasion the 1.2 and control lines have an almost identical doubling time, whilst the D252H line proliferates considerably faster.*

The doubling times for the first proliferation experiment are similar for each cell line. In the second proliferation experiment the D252H line has a very much lower doubling time (12.97h) than any of the other cell lines, whilst clonal line 1.2 has the same doubling time as the control line 1.15. The two wildtype lines vary in passage number,

and the clonal line has also been recently derived from a single cell so may have less inherent genetic variability. It is interesting that the error bars for control line 1.15 are smaller than those for the wildtype line. The doubling time is also lower for control line 1.15 than for the wildtype line.

The extreme inter-experiment variability means that proliferation rate is unlikely to be a reliable phenotypic difference between mutant and wildtype lines.

4.5.4.3.2 Differences in Neurite Outgrowth between Mutant Lines

As well as looking for phenotypic differences in proliferating cells, I differentiated the LUHMES mutant lines and used the IncuCyte NeuroTrack software module to analyse neurite dynamics. Photos were taken of the differentiating cells every three hours, nine photos per well, six wells per condition. Analysis was performed by choosing six training images and manually adjusting a number of variables given by the NeuroTrack software to give the optimum selection of neurites within the training photos: maximal recognition of neurites without mistaken recognition of other features such as cell bodies or background objects as neurites. The final 'processing definition' used for analysis is shown in Figure 4.18C, and was applied to all ~27 000 images. Neurite length per field of view was calculated and averaged across each condition.

Mutant lines 1.2 and D252H were differentiated alongside a wildtype LUHMES line. Three different seeding densities were tested, as neuronal cells can behave very differently depending on their growth conditions, so any potential phenotypic differences might be visible at a low seeding density but not high, or vice versa. The neurite lengths over time for each of three seeding densities are shown in Figure 4.18A. At the lowest seeding density the neurite lengths are equal for each cell line, however at the medium, and to a greater degree the high seeding density, the D252H line shows a difference in neurite development over time. D252H line neurite length in the highest seeding density increases in line with the other cell lines until 48 hours into the differentiation, when neurites die back over the next 48 hours, then remaining at a

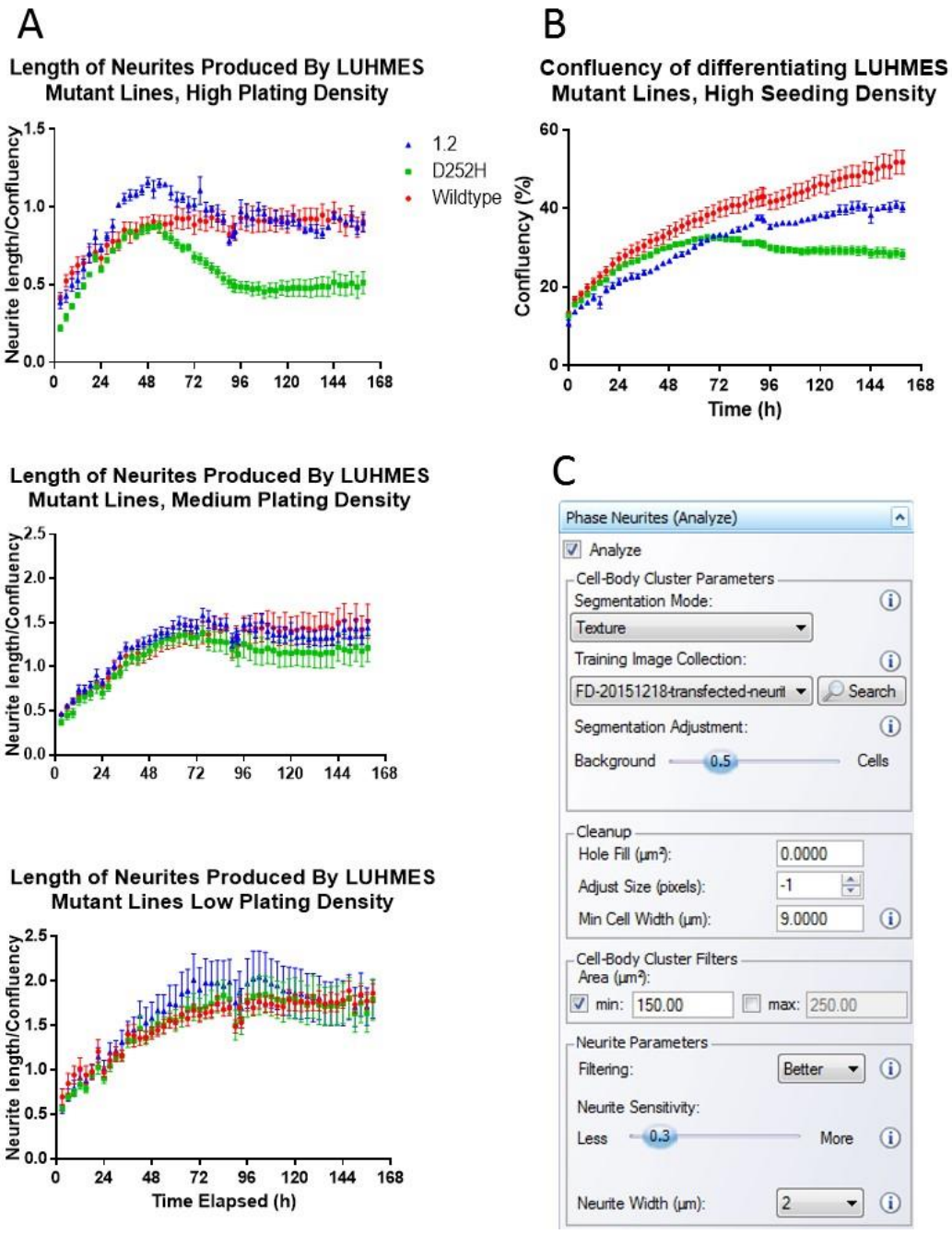

Figure 4.18 Differentiation of Mutant LUHMES lines in the IncuCyte and analysis of neurite length. *(A) Neurite lengths normalised to confluency, measured over seven days in LUHMES mutant lines. 1.2 (blue), 1.11/D252H homozygous mutant line (green) and a wildtype line (red).Six wells of a 96 well plate averaged per condition, nine fields of view per well using a x20 objective Confluency of differentiating LUHMES mutant lines over the same period. (B) Confluency of Cells Used in (A). (C) parameters used in NeuroTrack software.*

steady level for the rest of the experiment. In contrast, neurite lengths of the wildtype LUHMES line continue to increase for the duration of the experiment. The peak neurite length of cells from the 1.2 line, found at 48 hours, is significantly higher than that of wildtype (unpaired t-test, p=0.012).

What causes the apparent die back of neurites in D252H cells? Looking at the confluency of the differentiating cells in Figure 4.18, it is clear that whilst wildtype and 1.2 cells gradually increase over the course of the experiment, confluency of D252H line cells peaks at 72 hours and then dies back. Examining the photos of the time course, representative images shown in Figure 4.19, it can be seen that D252H line neurites did indeed die back, as shown in the inset magnifications. The cell bodies themselves become rounded and develop vacuoles, as shown in the day 3 and day 6 images by red arrows. In all previous differentiation experiments, D252H line cells have not shown this die-back phenotype, in contrast it can continue differentiating without rounding of cells or die-back of neurites for at least 10 days. The die-back seen in this IncuCyte differentiation experiment is therefore likely to be an anomaly, possibly caused by some lack of nutrient or a contaminant in the medium.

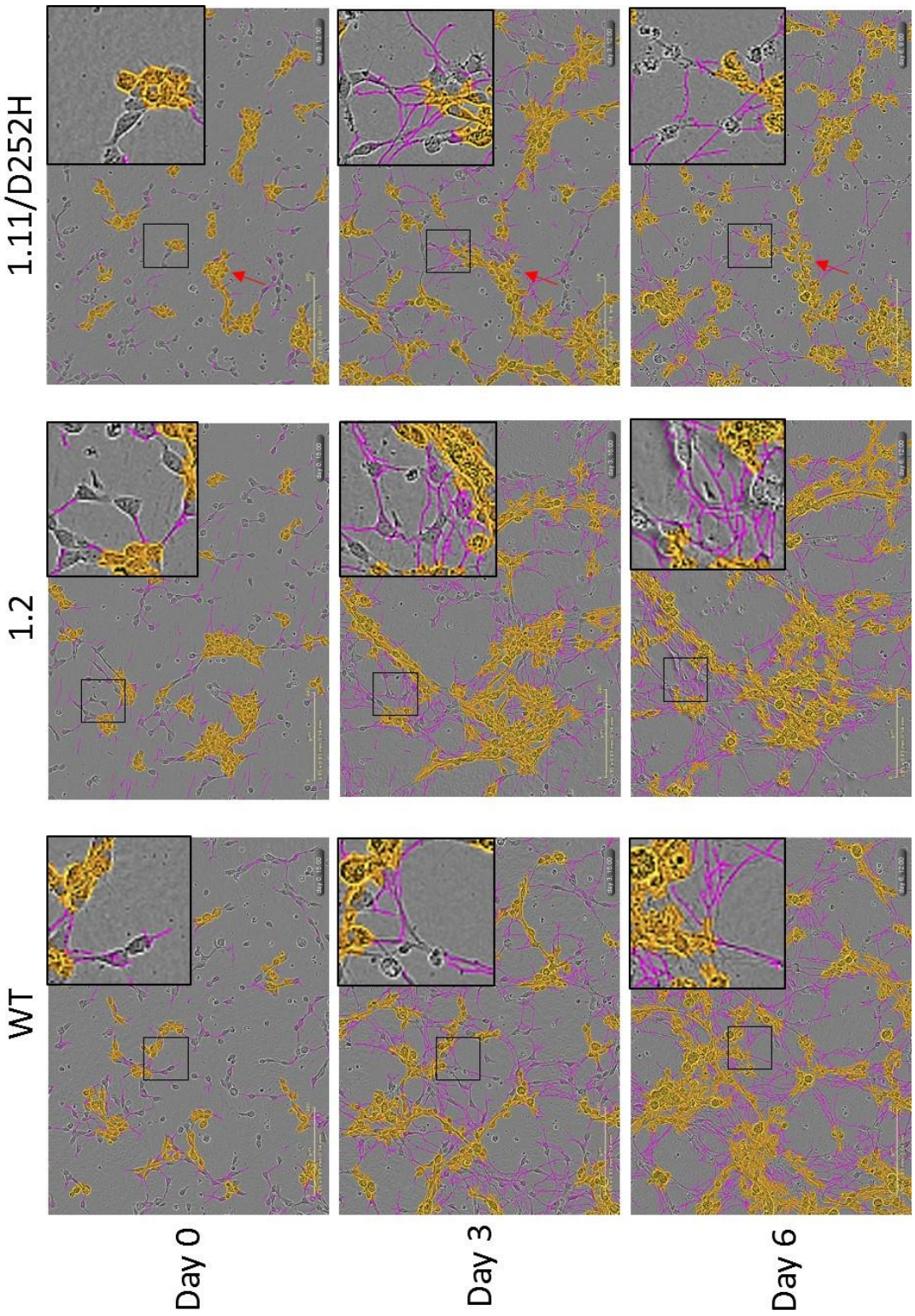

Figure 4.19 Phase contrast photos of LUHMES mutant lines at three differentiation time-points. *Inset squares show details of neurite formation. Red arrows indicate vacuole formation of 1.11 cells over time. IncuCyte NeuroTrack analysis mask applied to images, showing neurites in purple and cell clusters in yellow.*

4.6 Discussion

I have shown that low protein expression of eEF1A2 carrying the R423C mutation in three different cell lines can be rescued by coexpression of wildtype eEF1A2, indicating that the structural instability caused by the mutation, which had been predicted through in-silico modelling is to some degree compensated for by the presence of wildtype eEF1A2.

The NS1 line also appears to follow the same trend, even though it endogenously expresses eEF1A2. This finding was unexpected, as it was presumed that endogenous wildtype eEF1A2 would be as capable of "rescuing" R423C mutant expression as exogenous eEF1A2. The reason for this apparent discrepancy could be down to the nature of the experiment: forced overexpression of eEF1A2 in cell lines. Since NS1 cells endogenously express both eEF1A1 and eEF1A2, levels of endogenous eEF1A2 could be too low to have any measureable effect on exogenous construct expression. Directly comparing levels of endogenous and exogenous eEF1A2 proteins would reveal whether this was the case, however directly comparing relative levels of proteins using different antibodies (anti-V5 and anti-eEF1A2) is not possible, since there is no way of knowing whether the sensitivity of any two antibodies to their epitopes is exactly the same. A strong V5 signal and weaker eEF1A2 signal on a Western blot cannot be said to represent more V5 existing in the cell than eEF1A2,,since the V5 antibody may simply be more sensitive than the eEF1A2 antibody.

In order to be sure that the observed stabilisation effect is indeed due to wildtype-mutant interactions additional evidence on the dimerization of eEF1A2 would be invaluable.

Several lines of evidence exist that indicate that eEF1A2 can form dimers (Bunai et al., 2006; Morita et al., 2008; Sanges et al., 2012) , so it is possible that the R423C mutation destabilises the eEF1A2 molecule in a way that prevents formation of, or destabilises, homodimers of two mutated eEF1A2 molecules but still allows for heterodimers of one mutant molecule and one wildtype. This would explain the lack

of expression in HEK293FT and HCT116 cell lines, which lack endogenous eEF1A2, and the rescue of R423C mutant expression with cotransfection of wildtype eEF1A2.

I next measured protein synthesis levels in HEK293FT cells transfected with wildtype or mutant eEF1A2. This cell line, along with every known immortalised cell line, expresses eEF1A1 endogenously, so a baseline level of protein synthesis was seen in mock transfections due to the action of endogenous eEF1A1. Cells transfected with wildtype eEF1A2 did not have a significantly higher protein synthesis rate than mock transfected cells. This could be due to the toxic effects of transfecting DNA into a cell, or because protein synthesis rates were already maximal. A more suitable control here would have been transfection of an empty vector, rather than the 'no DNA' mock condition I used, as this would have controlled for any such toxicity.

Another limitation of this experiment was the transfection efficiency, since any changes in protein synthesis are not going to be easily detected if only a small percentage of the cells are actually expressing the construct. Although I was able to estimate transfection efficiency by transfecting a GFP-expressing construct into the cells, a high GFP transfection efficiency does not necessarily mean a high eEF1A2 transfection efficiency, given that the two construct backbones are different. A direct measurement such as IHC of V5 would have been more reliable.

A drop in protein synthesis in cells transfected with mutant eEF1A2 would have been evidence of a dominant negative effect, the action of the mutant eEF1A2 interfering with the endogenous translation elongation function of eEF1A; however such a drop was not seen using this model system, suggesting that the mutations do not exert a dominant negative effect over eEF1A1 (but bearing in mind the limitations described above). Beyond this, the results obtained appeared contradictory to each other and to known physiological interactions: the mutations are predicted to have a deleterious effect on EF1Bα or GFP/GTP binding, and this is not likely to increase protein synthesis levels, as appeared to be the case with exogenous expression of the D252H mutant in HEK293FT cells, since translation elongation is reliant on GTP hydrolysis and its GTP exchange factor, of which eEF1Bα is a part.

The difficulties encountered in exogenous protein experiments could partially be overcome through use of a mutant line in which one or both eEF1A2 alleles contains an epilepsy-causing mutation, since this models much more closely the physiological situation. To this end I designed and engineered, using CRISPR, the human neuronal cell line LUHMES to contain the D252H mutation in both copies of eEF1A2, with the intention of both exploring the mechanism of action of the mutation, and creating a screening assay capable of testing small molecules or drugs that may rectify a phenotype caused by the mutation.

I was able to show that the D252H line, when differentiated, expressed eEF1A2 mRNA at similar levels to wildtype (although confirmation of this semi-quantitative analysis using qPCR would be an important continuation of this work), and that protein levels of eEF1A were greatly reduced. This result confirms preliminary work performed in this laboratory using exogenously expressed mutant eEF1A2 constructs.

No clear phenotypic difference between wild type and 'D252H' LUHMES cells has yet been detected using the IncuCyte Zoom. Two potential sources of variability other than the desired genetic alterations may have contributed to this: Firstly, inter-experimental variability, in which the cell lines behave differently in terms of growth rate and differentiation across experiment iterations. This could be related to age of the cell lines, or to uncontrolled variables in the cells' growing environment. LUHMES cells appear particularly prone to changes in morphology and growth rate after passage and plating, exemplified by the large variations in doubling time identified in the two IncuCyte proliferation experiments (Figure 4.17). The second potential source of variability is that introduced by the act of creating a clonal cell line from a single cell. Even if inter-experimental variability can be controlled, in order to create a robust screening assay, a number of clonal lines would need to be tested alongside each other, to control for any natural variation between clones. This would require derivation of more than one D252H line, and comparison of these mutant lines to several independently derived control lines. Ideally more lines would be engineered using CRISPR to model all the mutations discussed here. This was initially planned, however time restraints meant that only one mutation, D252H, was eventually modelled in

LUHMES cells. Since these experiments were performed a mouse line modelling the D252H mutation has been generated using CRISPR.

As well as inter-experimental and clonal line variability, another possible reason for the lack of phenotype between D252H and wildtype LUHMES lines is the presence of eEF1A1 protein in the cells. Although eEF1A1 has been detected in certain neurons *in vivo*, eEF1A2 is the predominant isoform in that cell type after development. In order to more accurately model the human disease condition it might be necessary to find some way of downregulating eEF1A1, which is highly expressed in all immortalised cell lines.

Chapter 5 Modelling disease-causing mutations of eEF1A2 *in vivo*

5.0 Introduction

Since 2012, 13 *de novo* heterozygous missense mutations in *EEF1A2* have been found in 22 patients suffering from epilepsy and intellectual disability (see section 1.2.2**).** Modelling by Dinesh Soares (figure 1.4) has indicated that the majority of mutations are sited in or near either the eEF1Bα or GDP-GTP-binding sites.

A mouse line containing one of the epilepsy-causing mutations would be an invaluable source of information on the mutations and their mode of function. Since it is not yet known whether the mutations are loss- or gain- of function, the wealth of phenotypic and protein expression data from a mutant line would be an important step towards understanding these mutations, and would provide essential background knowledge in the search for a treatment. A heterozygous eEF1A2-null mouse model already exists in the form of the heterozygous wasted mouse. Whilst the homozygous wasted mouse has a muscle wasting phenotype and dies 4 weeks after birth, the heterozygous null does not display any overt epilepsy or motor problems. This suggests that the epilepsy-causing mutations are not a straightforward case of haploinsufficiency.

Being such a highly evolutionarily conserved protein, the amino acid sequences of human and mouse eEF1A2 are identical. The DNA sequences vary slightly, sharing 89% identity (Soares et al., 2009), but the identical amino acid sequences make modelling the equivalent to the human mutations in mice is straightforward.

CRISPR/Cas9 was the obvious choice for a method of mutation induction, since it is quick and simple to design and synthesise both the gRNAs and repair template required (Ran et al., 2013a), and the generation of mice itself is not onerous: CRISPR reagents are microinjected directly into the cytoplasm of mouse embryos at the single-cell stage. Embryos are then implanted into a surrogate mothers, and pups are screened for the desired mutations.

5.0.1 Aims of Mouse CRISPR Experiment

Investigate how the G70S mutation in eEF1A2 affects function by:

- Modelling the G70S mutation in mouse using the CRISPR/Cas9 system by introducing a single point mutation into the eEF1A2 gene of mouse embryos
- Evaluating the phenotype of any mutant mice in terms of behaviour, neurological function, protein expression
- Setting up a breeding colony of mice carrying the G70S mutation to allow for further study

5.0.2 CRISPR Experimental Design

Early trial CRISPR experiments performed by the transgenic unit at the IGMM yielded a very high mutation frequency. In order to reduce the chances of creating homozygous mutant mice, *Eef1a2* $^{G70S/G70S}$, two separate repair templates were designed to be co-injected with the gRNA constructs: both would carry silent PAM site mutations which should prevent re-cutting of the DNA once incorporation had occurred, but one would carry the G70S mutation and the other would be wildtype. HDR-mediated incorporation of the wildtype repair template would prevent further rounds of NHEJ, and so fix the allele as wildtype, increasing the chance of producing heterozygous mice.

The expected phenotype of any *Eef1a2*$^{G70S/+}$ mice may be similar to the human condition: carriers of the G70S mutation suffer from severe intellectual disability and seizures. Although this is the desired genotype, the CRISPR experiment may produce mice carrying any combination of the alleles shown in Figure 4.3B. We know that eEF1A2$^{+/-}$ mice are phenotypically normal, and *Eef1a2*$^{-/-}$ mice are likely to display an identical phenotype to the wasted mouse, which develop tremor, ataxia, wasting and neurological abnormalities from 21 days of age, and die at around 28 days old (Newbery et al.,, 2009). If *Eef1a2*$^{G70S/-}$ and *Eef1a2*$^{G70S/G70S}$ mice show a more severe phenotype than wasted animals, this would indicate toxicity of the G70S allele. In order to make informed decisions about the fate of any mice that may develop a wasted phenotype, and to observe closely any mice with the G70S mutation, it was of great importance to genotype mice as quickly as possible, by PND21 if possible, when the wasted phenotype becomes detectable.

Figure 5.2 G70S mouse gRNA and Repair Template Design. *Exon in uppercase, intron in lower case. (A) Site of repair template coverage shown in purple. gRNA sites indicated by red line, blue line indicates PAM sites. (V) The two repair template designs to be coinjected. Both have a silent mutation which forms a KpnI site, and the G70S repair template also carries the codon carrying the G70S mutation highlighted in green.*

With this in mind, both repair templates also contain a two base pair substitution (TG→GT) 111 bp upstream of the G70S mutation site (Figure 5.2B). This is situated well into the intron, so does not affect the gene, but does create a KpnI restriction site, which could be used to aid genotyping of the mice.

5.0.3 Experimental Outline and Division of Tasks

The workflow of the G70S mouse CRISPR experiment is summarised in Figure 5.3.

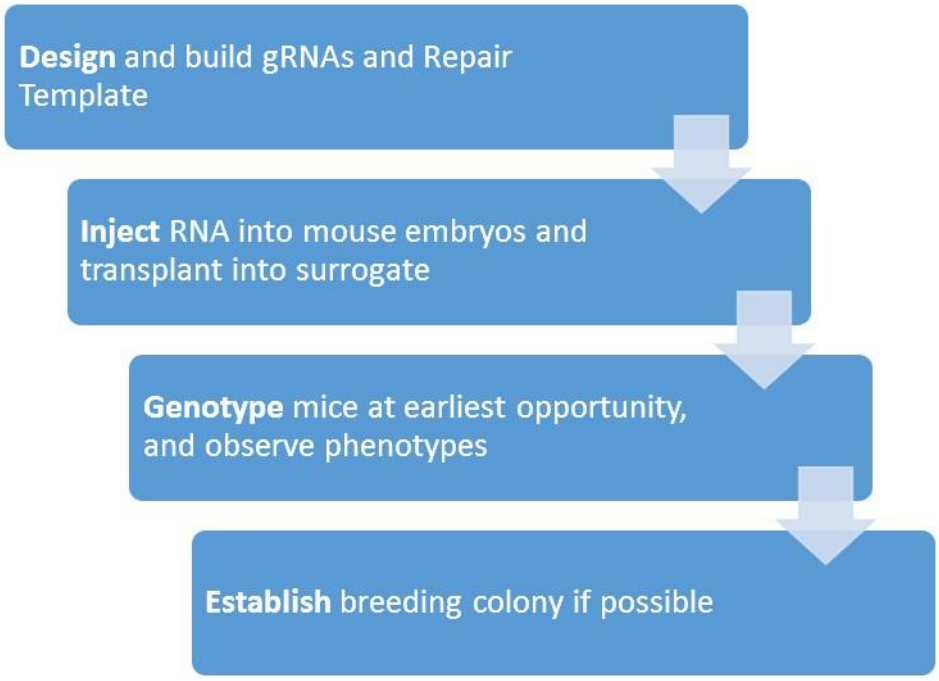

Figure 5.3 Workflow of G70S Mouse CRISPR Experiment.

gRNAs and repair templates had been used in a previous pilot experiment. They were designed by Professor Cathy Abbott and cloned into pSpCas9n(BB)-2A-puro plasmids by Jennifer Doig. DNA was transcribed in RNA by Hemant Bengani. Ear notches from each animal were provided by staff at the Evans Unit, and used to extract DNA for genotyping. Optimisation of the sequencing PCR was jointly performed by Francis Nuñez and me. The sequencing experiments themselves (initial, allele-specific and TOPO) and all subsequent sequencing analyses were performed by me. I also performed the protein expression analysis of muscle samples taken from the mice, while brain protein expression analysis was performed by Fiona McLachlan, a PhD student working in the same group.

5.1 Results

Two microinjection sessions were performed in which gRNA and repair templates, transcribed *in vitro* into RNA were microinjected into the cytoplasm of C57BL/6J

fertilised oocytes which were then transferred into a total of four pseudopregnant surrogate mothers. Thirty-five mice were subsequently born.

5.1.1 A Combination of Sequencing Methods was used to Genotype the CRISPR Mice

A combination of sequencing methods was used to attempt to identify every *Eef1a2* allele within the 35 mouse colony. Sanger sequencing quickly identified wildtype mice and those with homozygous mutations (Figure 5.5), however the vast majority of mice had at least one allele with an indel, which made interpretation of sequencing chromatograms much more challenging. Whilst it is sometimes possible to read the sub-peaks of a chromatogram, and so determine the sequence of both alleles for a mouse, this becomes much harder when there are complex indels, or mice with indels on both alleles, or mosaic mice with more than two alleles. In such cases either allele-specific sequencing, TOPO cloning, or a combination of both were used.

Allele-specific sequencing made use of the preliminary analysis of the basic Sanger sequencing chromatograms. It was possible, for 14 out of 35 mice, to identify small (4 – 40 bp) deletions in one allele by reading only the major peaks on the sequencing chromatogram and ignoring any subpeaks. A forward primer could then be designed to amplify from the deleted region, thereby selectively amplifying the allele without the identified deletion. This product could then be sequenced, so providing a straightforward method to sequence a single allele within a mouse without having to subclone PCR products.

DNA from the 14 mice was classified into three groups depending on position of the indel identified by basic Sanger sequencing, and an allele-specific forward primer designed for each group (see Figure 5.4A) to maximise mismatches at the 3' end of the primer, thereby forcing amplification of the other, uncharacterised allele. A nested PCR was performed as for basic Sanger sequencing, however the forward primer for the second, nested PCR reaction was replaced with the allele-specific forward primer indicated in Figure 5.4A. The first-round and second-round PCR products are shown for each DNA sample in Figure 5.4B. Of note are the PCR products derived from mice #31 and #33, which both show two products of different sizes as first round PCR

products, but only one product in the second round, demonstrating the successful application of this strategy.

DNA samples from eight mice were subject to the same nested PCR as described above, and the PCR products TOPO cloned either because they had not been suitable for allele-specific sequencing, or the allele-specific sequencing results indicated probable mosaicism. DNA taken from mouse #4 was also TOPO cloned for confirmation of genotype, due to the importance of mouse #4 as the only possible homozygous knock-in of the cohort.

Figure 5.4 Allele specific sequencing of 14 G70S mice. *(A) Each allele-specific forward primer is shown in bold, the sequence obtained from each mouse using that primer shown beneath. Alignments of the alleles identified using basic Sanger sequencing are under each primer, to show how the primer sequence is ablated in the identified allele, forcing the amplification of the uncharacterised allele. (B) Nested PCR results. For each mouse the amplified PCR product(s) for the first round of nested PCR are shown, followed by the smaller second round product, which varies in size depending on the allele-specific primer used and the size of any indels. The wildtype sample shows the first round PCR product, followed by three second-round products, one for each allele-specific forward primer, F1, F2, F3. Second round PCR products were sequenced using mG70Sseq1R, a reverse primer.*

5.1.1.1 Two mice could not be satisfactorily genotyped but were probable *Eef1a2*-nulls

The sequences of alleles around the G70S locus in exon 3 of *Eef1a2* were eventually identified for all but two mice in the cohort. G70S mouse #12 could not be sequenced. PCR of the G70S locus indicated two alleles, one with an insertion of approximately 50 bp, another with an insertion of approximately 250 bp, (data not shown) however sequencing of the region remained unclear, with many sub-peaks. Analysis of muscle samples showed eEF1A2 is not expressed at the protein level (Figure 5.7) and the mouse was culled due to a 'wasted' phenotype at PND 25.

The G70S locus of mouse #13 was successfully amplified by PCR (work by Francis Nuñez). The PCR gel shows three amplified bands, indicating likely mosaicism. Two of the bands are much larger than wild type so contain insertions of approximately 400 and 600 bp respectively. The mouse was culled at PND 29 due to a 'wasted' phenotype, and muscle samples taken from this mouse showed no expression of eEF1A2.

All available evidence thus supports the hypothesis that mice #12 and #13 are *Eef1a2*$^{-/-}$ mosaic mice, though this could not be confirmed by any of the sequencing methods used here.

5.1.1.2 Seventy-one Alleles Were Fully Sequenced for the 35 Mice

The DNA sequence of all confirmed alleles of every mouse except the two described above are shown in Appendix B and a box and line figure representing 67 identified alleles is found in Figure 5.5. A further four alleles that could not be represented in the box and line diagram are listed at the bottom of the figure, alongside the two mice described above that could not be sequenced, and one sequence that is probable evidence of mosaicism in a mouse. The total allele count is 71, (excluding the two mice whose DNA was not sequenced, #12 and #13) more than two alleles per mouse because four mice were found to be mosaic.

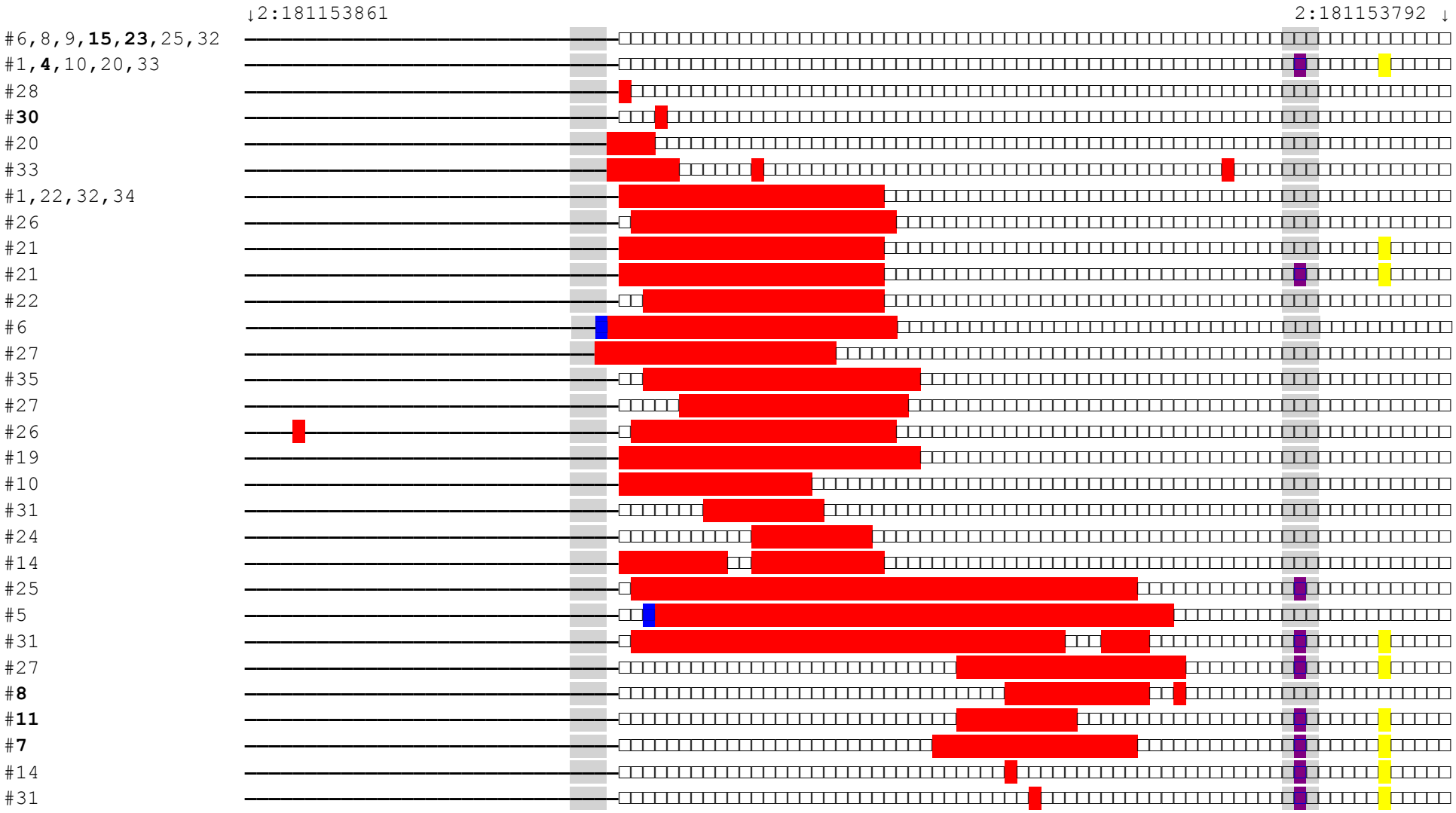
↓2:181153861
2:181153792 ↓
#6,8,9,15,23,25,32
#1,4,10,20,33
#28
#30
#20
#33
#1,22,32,34
#26
#21
#21
#22
#6
#27
#35
#27
#26
#19
#10
#31
#24
#14
#25
#5
#31
#27
#8
#11
#7
#14
#31

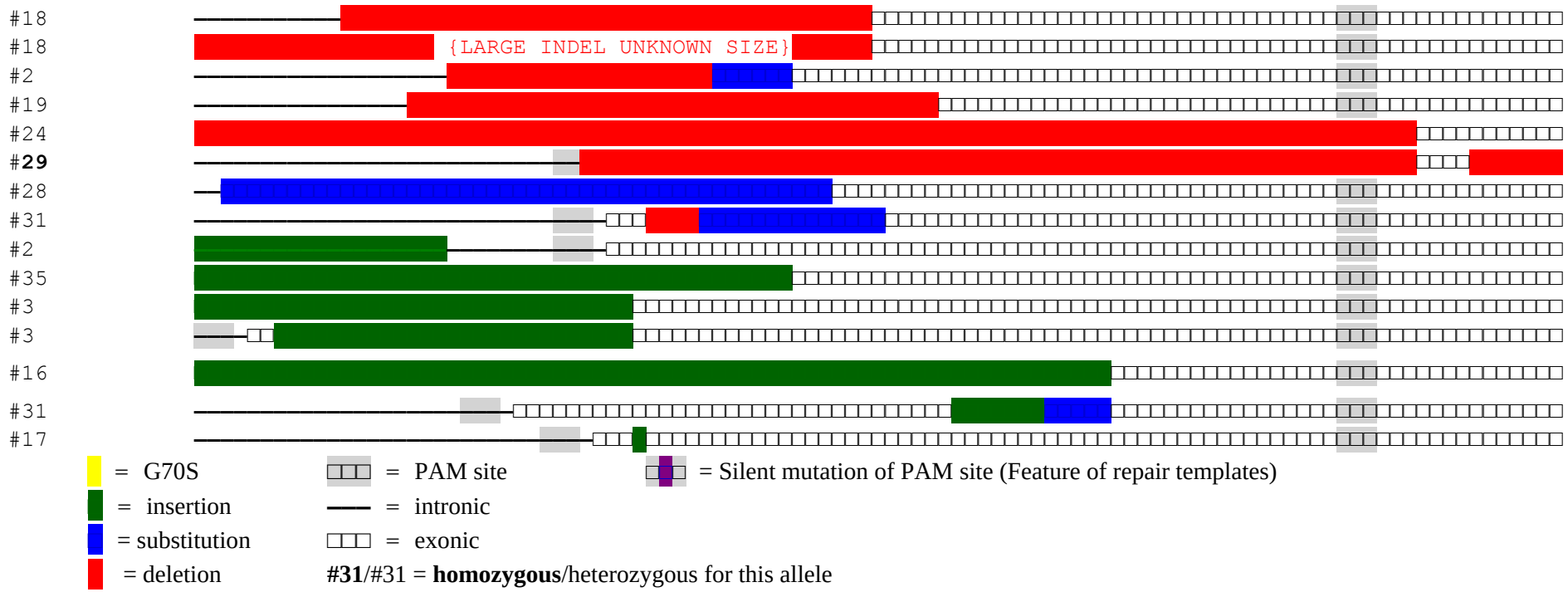

Mouse	Description of allele not included above:
#5	1 bp deletion located 78 bp downstream of G70S site.
#9	22 bp deletion upstream of G70S site, location not known
#12	unable to obtain clean sequence. No G70S incorporation, definite indels, based on PCR band sizes a large insertion on each allele is likely. . eEF1A2 not expressed in muscle sample.
#13	unable to PCR the region. Probably a big deletion. eEF1A2 not expressed in muscle sample.
#16	one allele shown, the other identical across this region but with different indel further upstream.
#21	No G70S incorporation and a 1 bp deletion 150 bp downstream of G70S site
#17	two alleles seen in initial sequencing, only one in TOPO cloning. TOPO cloning null allele shown here, possible G70S allele exists too.

Figure 5.5 Graphical Representation of All Alleles Identified in G70S mouse CRISPR experiment. *Alleles are organised by location of indel, ID of mouse in which allele is found is listed to the left of each allele representation.*

Table 5.1 summarises the CRISPR results. Alleles from the two mice that could not be sequenced are excluded from the total count. 19.5% of alleles had incorporated the G70S mutation, however many of these also contained indels upstream of the G70S site, meaning 9.8% of alleles had perfect incorporation of G70S without indels.

	No. alleles/total sequenced alleles	**Percentage total sequenced alleles**
Alleles with perfect incorporation of G70S mutation and no indel	7/71	9.8%
Alleles with incorporation of G70S plus an indel	9/71	12.7%
Wildtype alleles	9/71	12.7%
Alleles with indels *(including those that also carry G70S mutation)*	**55/71**	**80.5%**
deletions	42	59%
insertions	6	8.5%
substitutions	1	1.5%
multiple indel types	5	7 %

Table 5.1 Incidence of mutation and template incorporation across 35 mice born in a CRISPR experiment designed to incorporate the G70S mutation into eEF1A2. *Two mice, #12 and #13 are excluded from this table as their DNA in the region could not be sequenced. The type of indel seen on each of the 55 alleles found to have indels is listed in the bottommost box of the table.*

The GT→TG mutation situated 111 bp upstream of the G70S site was present on both wildtype and G70S repair templates but was not incorporated into any alleles,

indicating that only certain regions of the repair template were used during homology-directed repair, not the entire template.

Most indels shown are 1-40 bp deletions located close to the 5' PAM site on the intron/exon boundary. Cas9n makes a nick in DNA 3bp 5' to the PAM site. Thirty four of the alleles shown contain indels either over or within 5 bp of the cut site at the intron-exon boundary. This PAM site was not mutated in either the wildtype or G70S repair template due to the presence of the exon 3 splice site acceptor junction and the difficulty of predicting the effect of any artificially introduced mutation. The PAM site closest to the G70S mutation site, however, was in the coding region so was mutated in both repair templates, and there are far fewer indels located close to this PAM site.

Incidence of mutations in experiments designed to incorporate point mutations are not uncommon. Inui et al. (2014) measured the incidence of point mutation and indels in several mouse CRISPR Cas9n experiments and found between 25% and 76.9% of mouse zygotes genotyped to contain indel mutations. Although I found 80.5% of alleles to contain indels, this high incidence, as mentioned above, could well be due to suboptimal design of the repair template: in particular, the fact that only one of two PAM sites was mutated on the repair templates, a design weakness that would be corrected in any future CRISPR experiments.

5.1.2 Phenotypic Observations

Mouse genotype at eEF1A2	No. mice	Mouse ID	Phenotype
G70S/G70S	1	#4	Much smaller than littermates, suffered tremor, culled at PND18
G70S/-	4	#1 #10 (#20) #33	Showed wasted phenotype and were culled
G70S/+	0		
-/-	18	#3 #5 #7 #11 #14 #29 #26 #16 #19 #30 #2 #17 #18 #22 #24 #34 #35	Died after audiogenic seizure Found dead Showed wasted phenotype and were culled
+/+	1	#23	Wildtype. Phenotypically normal
+/-	5	#6 #9 #25 #32 #8	Phenotypically normal Died after audiogenic seizure* (note: very low eEF1A2 expression in muscle)
Mosaicism	4	#21 #27 #28 #31	Found dead (died in transit) Three mosaics culled due to wasted phenotype.
Unknown	2	#12 #13 #15	Showed wasted phenotype Runted. Wildtype at eEF1A2 locus

Table 5.2 Summary of G70S Mouse Genotypes and Phenotype/Cause of death *Mice listed as having a null allele all have an indel in exon 3 of Eef1a2. Expression data is necessary to show for certain that this allele is not expressed. Mice in red were male, mice in blue were female.*

5.1.2.1 All *Eef1a2*$^{G70S/-}$ and *Eef1a2*$^{-/-}$ mice displayed a wasted phenotype

Sixteen of the 35 mice were found to have a wasted phenotype, characterised by failure to gain weight, ataxia and tremor. Such mice were culled as soon as the phenotype became clear. , since the wasted phenotype has been well characterised (Newbery et al., 2005) and culling of wasted mice before they die is a requirement of our project licence.

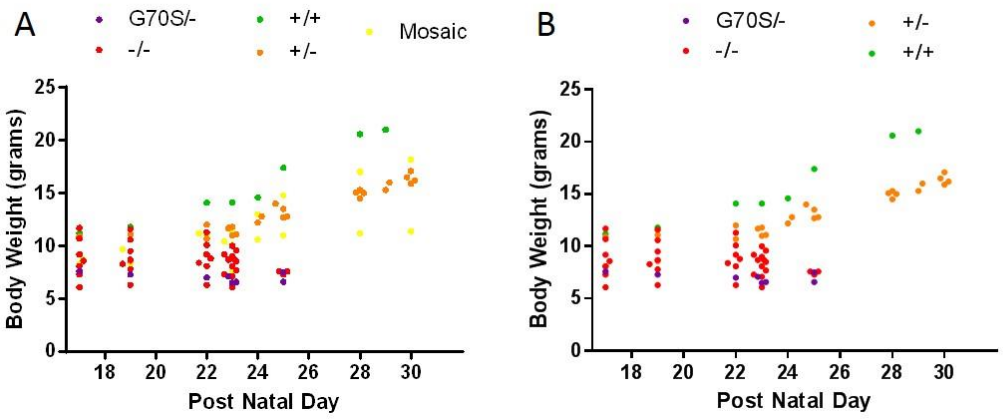

C

Genotype at *Eef1a2* locus	PND 23 Mean Body Weight ± SEM	n
G70S/-	6.73 ± 0.18 *	3
-/-	8.3 ± 0.32 *	9
+/-	11.4 ± 0.20 *	4
+/+	14.1	1
Mosaic	9.85 ± 0.79	4

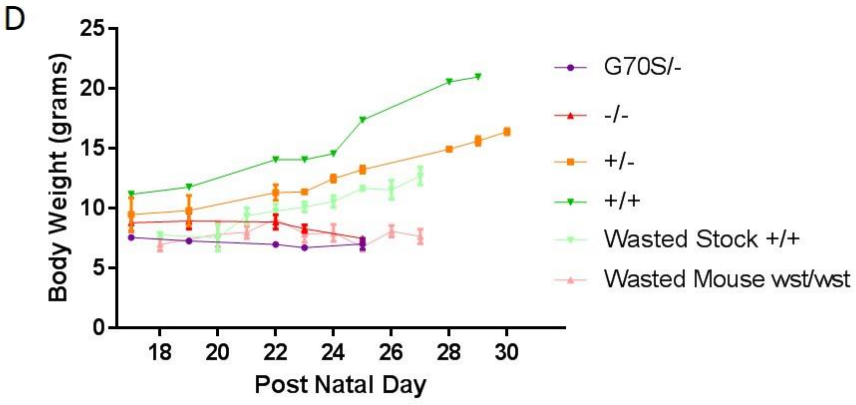

Figure 5.6 G70S mouse weights between PND 17 and 30. *(A) Expressed as one dot per mouse per measurement. Mouse genotype is indicated by colour of dot. (B) Data from (A) without mosaic mice (C) Mean ± SEM of all mice at PND 23. *G70S/- and -/- weights are significantly different (unpaired t-test p=0.033), as are -/- and +/- (p=0.00002). (D) Mean weights ± SEM of all mice grouped by genotype, alongside weights of wasted mice (wst/wst) and wildtype wasted littermates (+/+).*

The first mouse to be culled was #4, the only *Eef1a2*$^{G70S/G70S}$ mouse, at PND 18. It was noticeably smaller than littermates, suffered tremor, had an impaired ability to right itself and was hunched.

Mice were routinely weighed after PND 17. Heterozygous null mice (+/-) gained weight as expected, shown in Figure 5.6A with mosaic mice, and in Figure 5.6B without mosaic mice, for clarity. Although they appear not to have gained weight as quickly as the one wildtype mouse, such a result should not be over interpreted given that there was only one in the wild type group. Previous work has shown that heterozygous wasted mice develop, and gain weight, at the same rate as wildtype mice (3). All the heterozygous null mice from this experiment are still alive, and are fertile.

All three *Eef1a2*$^{G70S/-}$ and all *Eef1a2*$^{-/-}$ failed to gain weight after PND 17. PND 23 is the only day with more than two mice measured in the G70S/- group. By this time point, body weights of *Eef1a2*$^{+/-}$ and *Eef1a2*$^{-/-}$ animals are significantly different ($p=2x10^{-5}$) (Figure 5.6C), with *Eef1a2*$^{-/-}$ animals losing weight after this point. *G70S/-* mice are also significantly smaller than -/- mice on this day (p=0.033). This observation should be interpreted with caution, given the very small number of mice in the group and the fact that at PND 25 the weights of animals in the two groups are the same.

Figure 5.6D shows the weight data of the G70S mouse cohort alongside previously collected body weights from wasted mice and wildtype littermates (Doig et al., 2013). Whilst *wst/wst* mice and *Eef1a2*$^{-/-}$ mice have very similar body weights, heterozygous null and wildtype mice from the present experiment gain weight earlier in development than +/+ mice from the original wasted stock. This could be due to inter-experimental differences such as the balance used, diet, time of weaning or genetic background of the mice.

5.1.2.2 *Eef1a2*$^{-/-}$ mice are susceptible to audiogenic seizures

Whilst examining mice #1 to #21 on PND 18, a loud sound (dispensing of liquid nitrogen in the next room) caused six (#3 #5 #7 #8 #11 #14) of the 21 mice to have audiogenic seizures, characterised by a period of wild running followed by tonic-clonic seizures. Attempts were made to resuscitate the mice, but all died. All six mice began wild running within 30 seconds of the sound beginning, and later measurement of a re-creation of the sound estimated it to be 90 dB. All six mice were *Eef1a2*$^{-/-}$.

On a separate occasion two *Eef1a2*$^{-/-}$ mice (#26 and #29), both of whom were due to be culled as they displayed a wasted phenotype, were being moved in their cage to a

separate room when they suffered audiogenic seizures, apparently triggered by the sound of an automatic door opening. Although not particularly loud, it was a novel sound that the mice were unaccustomed to. Both displayed a short period of wild running followed by tonic-clonic seizures. One died (#26) and the other (#29) recovered after 15 minutes. Three other mice (#31 #33# 35), mosaic, G70S/- and -/- respectively, were also being moved at the same time in a separate cage, underneath the cage containing #26 and #29. None of these mice seized but were arguably more protected from the sound.

The eight mice that suffered audiogenic seizures were all *Eef1a2*$^{-/-}$. Table 5.3 shows that incidence of seizure amongst -/- mice exposed to audio stimuli sufficient to cause seizure in littermates was 47%. Although no other genotype suffered seizures, the small sizes of these groups, and the fact that the observed seizures were accidental in cause, and not performed under proper conditions precludes further statistical analysis, but does suggest a need for further investigation.

Genotype at *Eef1a2* locus	**Seizures (number seized over total exposed)**
-/-	8/17
+/-	0/3
G70S/-	0/3
G70S/G70S	0/1
Mosaic	0/1

Table 5.3 Audiogenic Seizures in G70S mice. *Mice 'exposed' were present in the same room as those that suffered seizures.*

5.1.2.3 Sudden death in four *Eef1a2*$^{-/-}$ mice and one chimaeric mouse with low eEF1A2 protein expression

Three mice (#16 #19 #21) died suddenly on PND 23 when being transferred from the Evans Unit to the adjacent Biomedical Research Facility (BRF). They were alive and well immediately prior to transfer, but dead on arrival. Another two mice (#30 #34) were found dead in their cage on PND 23, no obvious cause of death; they had been checked at PND 22 and appeared healthy. Four of the five mice were *Eef1a2*$^{-/-}$, the

fifth (#21) was a mosaic mouse that showed a low level of expression of eEF1A2 protein, a similar low level of expression as mouse #28, a mosaic who was culled having developed a wasted phenotype. (Figure 5.7).

Mouse #15 was culled at PND 18 as it was a third of the size of littermates, trembly and unsteady. Subsequent genotyping revealed the mouse to be *Eef1a2*$^{+/+}$, and Western blot of skeletal muscle protein lysate confirmed expression of eEF1A2 (Figure 5.7). Off-target endonuclease activity by Cas9n could, in theory, mutate undesired genes or regulatory regions and so cause unexpected phenotypes, however sequencing work by Frances Nuñez (data not shown) found no off-target indels in the five regions most homologous to the gRNA guide sites targeted in this experiment. Since no genetic abnormality was found at the eEF1A2 locus, the likely cause of the runted phenotype is either competitive disadvantage either in the womb or in the litter, or an unidentified genetic abnormality elsewhere, unassociated with the CRISPR experiment. Litter sizes were large because of the high number of embryos implanted into the surrogate mothers, so competitive disadvantage is a distinct possibility. Mouse #15 was excluded from further experiments since its phenotype was unrelated to expression of, or mutations within, eEF1A2.

5.1.3 EEF1A2 Protein Expression Analysis

Protein lysates extracted from muscle samples taken from mice upon death were probed for eEF1A2 expression (Figure 5.7A). Four mice (#1 #10# 20 #33) had been genotyped as *Eef1a2*$^{G70S/-}$ and could be expected to express eEF1A2 based on analysis of a G70S-containing cDNA in transfected cells. Three of the four (#1 #10 #33) expressed eEF1A2 in muscle to some degree, however mouse #20 only expressed eEF1A2 at a negligible level, indicating likely mosaicism or an undetected mutation in the G70S-containing allele (Figure 5.7B). Examination of eEF1A2 protein level in brain showed higher relative expression of eEF1A2 in this tissue than in muscle (work by Fiona McLachlan), meaning mouse #20 is likely a mosaic.

Figure 5.8 shows expression levels of eEF1A2 in a subset of the G70S mice with age-matched heterozygous-null controls. Mice #1 and #21 are both G70S/-, and show

lower levels of eEF1A2 than age matched *Eef1a2*+/- C57BL/6J controls (labelled control 329 to control 331). So the mutant allele in the G70S mice expresses at a lower level than in mice with one wildtype eEF1A2 allele.

Likewise mouse #4, the one *Eef1a2*$^{G70S/G70S}$ mouse shows eEF1A2 protein expression at a lower level than mouse 15, which was wild type at the *Eef1a2* locus and is included as an age-matched comparator. These observations fit with previous work conducted in cells, which showed epilepsy-causing mutations to be unstable at the protein level. (see section 4.1).

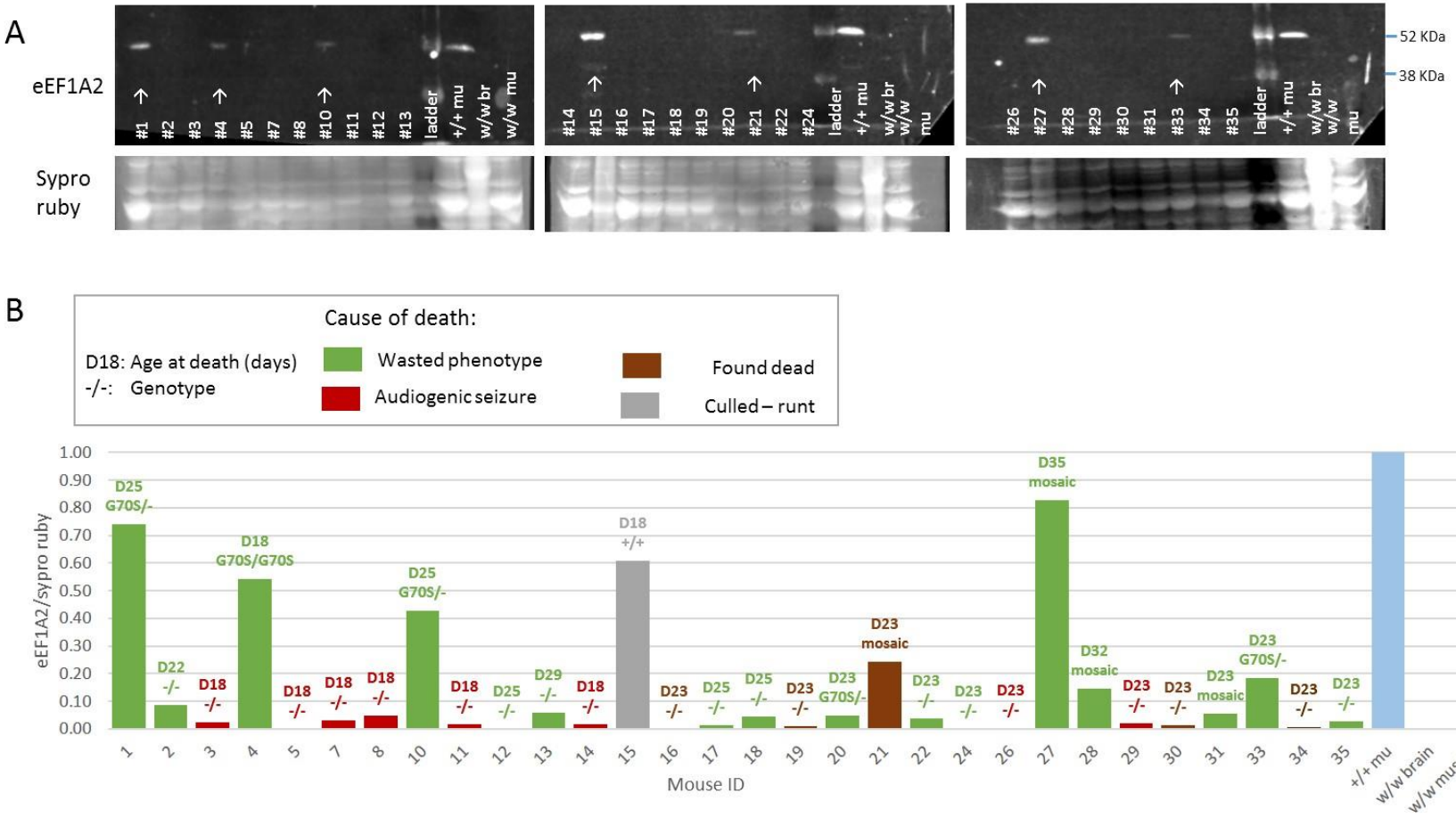

Figure 5.7 eEF1A2 Protein Expression in G70S Mice *(A) Western blots showing G70S mouse protein lysates probed using eEF1A2 antibody and sypro ruby to stain total protein. (B) Graph showing data from (A) quantified to give relative eEF1A2 expression levels. Each bar coloured according to cause of death, post natal day of death and genotype are shown above each bar.*

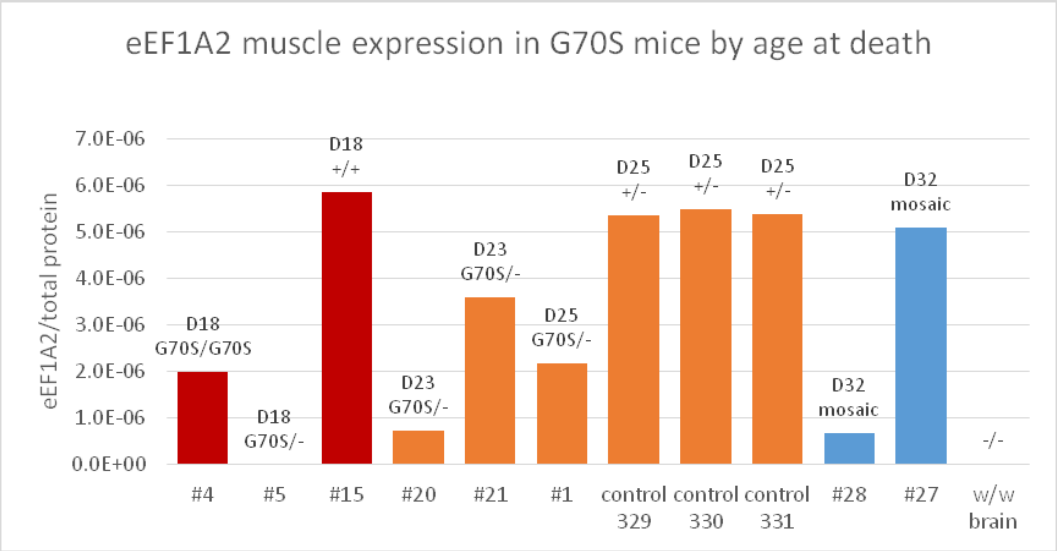

Figure 5.8 eEF1A2 Protein expression in subset of mice from G70S experiment and age matched controls. e*EF1A2 expression shown relative to total protein**. Samples preceded by a hash (#) are mice from the G70S CRISPR experiment. Samples labelled 'control' are heterozygous null (*Eef1a2+/-*) mice, F1 cross of a heterozygous wasted mouse and a pure C57BL/6J mouse. 'w/w' brain is a wasted mouse brain sample which serves as a negative control for EEF1A2. Post natal day of death and genotype are shown above each bar.*

5.2 Discussion

The aims of this chapter were to

1) Model the G70S mutation in mouse

2) Evaluate the phenotype of any mutant mice in terms of behaviour, neurological function, protein expression

3) Set up a breeding colony of mice carrying the G70S mutation to allow for further study

I was partially successful in achieving the first two aims of this part of the project, since I was able to incorporate the G70S mutation cleanly into four separate mice. Due to a high incidence of indels however, I was unable to express the mutation in the desired manner, namely the creation of *Eef1a2*$^{G70S/+}$mice. Whilst the early death of all mice carrying the G70S mutation meant my third aim was out of reach, I was able to collect information on protein expression, pathological phenotype, and weight of the mice,

which has allowed a certain amount of deduction on the effect of the mutation on the function of eEF1A2.

The three *G70S/-* mice suffered from weight loss and tremor similar to that of wasted mice. Protein analysis of muscle samples showed that the mice did express eEF1A2. This points to two possibilities: either eEF1A2 carrying the G70S mutation is not functional, and therefore not sufficient to rescue the wasted phenotype (pointing to G70S being a loss-of-function mutation), or G70S eEF1A2 is functional, but the slightly lower levels of eEF1A2 protein due to the structural instability caused by the G70S mutation mean the level in the cell is less than that seen in heterozygous wasted mice, and not sufficient to rescue wasting, indicating a form of haploinsufficiency

Knowledge of brain EEF1A2 levels are important, given that the wasted phenotype is neurological in origin (Doig et al., 2013). Subsequent work by Fiona McLachlan has shown that eEF1A2 protein levels in brain samples from G70S/- mice are approximately 50% of age-matched wildtype levels (personal communication). Levels of eEF1A2 protein in mice heterozygous for the wasted mutation are likewise found to be 50% of normal but these mice are perfectly healthy (Griffiths et al., 2012). This implies that G70S eEF1A2 is not sufficient to compensate for the loss of wild type eEF1A2 on the other allele, and is therefore functionally compromised.

The one *Eef1a2*$^{G70S/G70S}$ mouse culled at PND 18 was smaller than littermates and suffered tremor at an earlier time point than any other mouse. With the caveat of this only being one mouse, this does provide evidence against the idea that G70S is a simple loss-of-function mutation, since this mouse had a more severe phenotype than *Eef1a2*$^{-/-}$ and *Eef1a2*$^{G70S/-}$ littermates. In support of this hypothesis, the *G70S/-* mice were significantly smaller than -/- at PND 23. Although the small number of mice means this result is vastly underpowered, such a result is compatible with the idea that the G70S mutation could be gain-of-function, since the phenotype in mice with a G70S allele appears to be worse than that of eEF1A2-null mice. A combination of both loss- and gain-of-function of the mutation would therefore fit the observed phenotypes, although with only three *G70S/-* mice and one *G70S/G70S* mouse, a repeat of the current experiment is essential, with modifications to the CRISPR design to ensure that both PAM sites are silently mutated on the repair constructs.

Always bearing in mind the small size of this mouse cohort, it is still striking that almost 50% (8/17) of *Eef1a2*$^{-/-}$ mice exposed to an auditory stimulus suffered fatal (in all but one case) audiogenic seizures, whilst no other mice were observed to suffer seizures. C57BL/6J mice are naturally resistant to audiogenic seizures (Ross et al., 2000) Schreiber, 1977), although mice on this background can be 'primed' by exposure to a loud auditory stimulus between PND 15 and 18. Important to note is that mice exposed to the priming stimulus do not have seizures at the time of priming. Mice that have been primed are then much more likely to have seizures with any subsequent auditory stimuli(Henry, 1967). This cohort of mice received no such priming but nevertheless suffered severe audiogenic seizures, fatal in all but one case, in response to a level of sound well below that typically used to evoke audiogenic seizures in susceptible mice, which in most paradigms is around 120dB (Ross et al., 2000) (Henry, 1967). That seizures here were caused by at most approximately 90dB (this was the measure intensity of the liquid nitrogen stimulus), shows that *Eef1a2*$^{-/-}$ mice are particularly sensitive to this form of seizure induction. The second incidence of audiogenic seizure is striking, given the low intensity of the stimulus. None of the mice that died in the second incidence of audiogenic seizures had been previously exposed to a loud sound as far as we are aware, so priming was not the cause of seizure here.

In forty years of study, no incidence of seizures in wasted mice has ever been reported. One investigator noted that on two occasions a wasted mouse died when being handled (personal communication), however this observation is certainly not consistent with an audiogenic seizure, which has a characteristic period of wild running prior to tonic-clonic seizure, and then death.

Mouse strain could be a factor in this phenotypic difference, since mice used in this experiment were all C57BL/6J, whereas the wasted mouse is on a mixed background. The wasted mouse is also a true *Eef1a2*-null, since the entire promotor region and first, non-coding, exon of the gene is deleted. Although the *Eef1a2*$^{-/-}$ mice generated here using CRISPR did not express EEF1A2 protein as detected using an EEF1A2 antibody, this does not completely preclude the possibility that truncated versions of EEF1A2 were expressed but not picked up by Western blotting. However, no product was seen on the blots at any size below that of wild type EEF1A2 making this explanation unlikely.

The position of the indels induced by CRISPR (the end of intron 2-3 and beginning of exon 3) makes aberrant splicing a possibility, although, as previously shown, no eEF1A2 of any size was picked up in Western blot of muscle samples. Analysis of RNA samples isolated from the mice would allow investigation of this possibility, with primers designed to amplify a region of *Eef1a2* upstream of the deletions in exon 3.

In mice models that are genetically predisposed, a critical time period can exist during which mice are sensitive to seizure. The DBA/2J (Seyfried et al., 1999) and black Swiss (Misawa et al., 2002) mouse strains are susceptible to audiogenic seizure from PND 14, are maximally sensitive around PND 21, then lose sensitivity progressively until adulthood. Although it is in theory possible that wasted mice have an age related susceptibility to seizure that has been missed until now, it seems much more plausible, given the length of time that wasted mice have been in existence, that difference in genetic background is the cause of the seizure phenotype seen here.

No seizures were observed in the three *G70S/-* mice. The seizure rate in -/- mice was just under 50% (8/17), so it is entirely possible that a larger cohort of mice carrying the G70S mutation would have shown a seizure phenotype. Assuming that the lack of seizures in *G70S/-* mice is shown, with further work, to hold true, then *G70S/-* mice do not show an epilepsy phenotype, whilst *G70S/+* human cases do. This could be due to species difference, or it could point to the interaction between wildtype and mutant eEF1A2 being the cause of epilepsy.

Four eEF1A2-null mice (and one mosaic) were found dead in their cages. These deaths were very unlikely to be caused by wasting, since the mice died at PND23, five days before the average time of death in wasted mice, and did not exhibit any of the signs of late-stage wasting such as ataxia, hunching and tremor when checked the previous day. Since their deaths were not observed, it is possible that they suffered from audiogenic seizures. Other eEF1A2-null mice of the cohort seized with very little stimulus. Three of the four died whilst the mice were being transferred between adjacent animal units, and therefore were likely to have been exposed to unexpected noises, making audiogenic seizure a distinct possibility. Another possibility is sudden unexpected death in epilepsy (SUDEP), a known complication of epilepsy sufferers, the mechanism of which is not well understood.

Whilst the audiogenic seizures seen in *Eef1a2-/-* mice are an interesting finding, the small cohort size and unexpected nature of the seizures makes further investigation essential. This is discussed in Chapter 6.

Chapter 6 Discussion

Summary of thesis

eEF1A is a translation elongation factor that exists in two differentially expressed, developmentally regulated isoforms in vertebrates. One or both isoforms also fulfil a number of other, non-canonical functions within the cell. eEF1A2 is the main isoform found in neurons after development, although both isoforms have been shown to be present in brain, and several studies have shown misregulation of eEF1A in brain extracts (Beckelman et al., 2016; Garcia-Esparcia et al., 2015) , or more specifically at the synapse (Sung et al., 2003).

Since 2012, thirteen *de novo* heterozygous missense eEF1A2 mutations across twenty-two cases have been identified in people suffering from epilepsy, intellectual disability and in some cases autism. The mutations are all located close to binding sites of interacting proteins, or at inter-domain contacts.

In this chapter I will examine my progress towards achieving the aims I set out in Chapter 1, the limitations of my work and possible future directions for the project.

Aim 1: Confirm and extend the finding that cilostazol potentiates neurite outgrowth in PC12 cells in an eEF1A1-dependent manner

This background to this aim was largely based on the findings of Hashimoto and Ishima (2011), who showed that cilostazol, a phosphodiesterase type-3 inhibitor and licensed treatment for intermittent claudication, potentiates NGF-induced neurite outgrowth in PC12 cells in an eEF1A1-dependent manner. I was not able to confirm Hashimoto's results, although I did vary his protocol slightly in using NS1 cells, a subclone of PC12, as their lower propensity for self-aggregation made them easier to adapt to semi-automated neurite outgrowth assays.

The mechanism of action for a cilostazol was posited not to be due to the downstream effects of PDE-3 inhibition, since two other PDE-3 inhibitors, cilostamide and milrinone, did not show the same neurite outgrowth potentiation effects. I have found

that cilostazol does differ from cilostamide and milrinone in two ways however. Firstly, it is somewhat effective against PDE5 (IC50 4.4µM), (Schrör, 2002; Sudo et al., 2000), a property not shared by either cilostamide or milrinone. PDE5 inhibition has been shown to be neuroprotective in cultured rat motor neurons exposed to chronic Glu-induced neurotoxicity or acute ROS-induced toxicity (Nakamizo et al., 2003). If PDE5 inhibition is cilostazol's mode of action in PC12 cell neuritogenesis it would be interesting to test a specific PDE5 inhibitor to see if the effect I could not detect using cilostazol is detectable under this method.

Apart from its inhibitory action on PDEs, cilostazol also inhibits uptake of adenosine with an IC50 of 5-10µM (Liu et al., 2000). Inhibition of adenosine uptake leads to enhanced adenosine action because of increased extracellular adenosine. Is this relevant in PC12 cells? This cell type has been shown to express adenosine receptors (Arslan and Fredholm, 1999). O'Driscoll and Gorman (2005), found that hypoxia induces neurite outgrowth in PC12 cells, not mediated by TrkA through which NGF causes neurite outgrowth, but through activation of adenosine A2A receptors. So it is possible that cilostazol's potentiating effects on neurite outgrowth are a result of its inhibition of adenosine uptake. PC12 cells have been shown to release adenosine into the medium under normal growth conditions (Rabin et al., 1993). It is probable, though not proven, that PC12 cells release adenosine under differentiating conditions, indicating another possible mechanism by which cilostazol acts: reducing the uptake of adenosine, which increases its extracellular concentration, causing an adenosine-mediated increase in neurite outgrowth.

Neither of these proposed mechanisms (PDE5 inhibition or adenosine uptake inhibition) account directly for the role of eEF1A1 in cilostazol's effects, though they give possible explanations for why this PDE3 inhibitor, though not others, may potentiate neurite outgrowth. Further investigations along this line of research would most likely benefit from a high-throughput approach in which a number of potential modulating factors are tested in parallel. The neurite outgrowth assays I optimised would be amenable to this sort of approach, as discussed at the end of chapter 3.

The second part of my work around eEF1A1 and neuritogenesis involved examining the direct effects of knocking down eEF1A1 and eEF1A2 expression on neuritogenesis. Hashimoto had not found any effect, however I found the converse to be true –

knockdown of eEF1A1 but not eEF1A2 causes a decrease both in neurite length, and proportion of cells that develop neurites. An explanation for this discrepancy may lie in technical details of the experiments: I was able to knock down expression of each isoform by at least 50% using RNAi, whilst Hashimoto was not able to affect baseline levels of eEF1A1 at all.

That eEF1A1 is involved in neuritogenesis is not surprising, given the requirement for protein synthesis at the neuronal growth cone, however it was interesting that eEF1A2 was not able to compensate for the loss of eEF1A1, perhaps pointing to the different roles of the two isoforms. A recently published paper has found that prenatal methylmercury exposure in rats causes an impairment of neurite outgrowth as shown by a decrease in expression of neurofilament H. The TrkA signalling pathway was found to be suppressed in exposed rats, as were protein levels of eEF1A1 in the cerebellum. Knockdown of eEF1A1 in PC12 cells was shown to have a similar suppressive effect on neurite outgrowth (as measured by neurofilament H protein levels) (Fujimura et al., 2016).

I would be interested to check levels of protein synthesis within the cells after knockdown of each isoform to investigate whether the observed effects on neuritogenesis are due to reduced protein synthesis or some other of eEF1A1's functions.

In terms of my aim for this part of the project, although my results did not confirm those of Hashimoto and Ishima (2011), I was able to optimise a neurite outgrowth assay which could be utilised in future mutant cell line experiments.

Aim 2: Model the Epilepsy-causing eEF1A2 mutations in neuronal cell lines, with the intention of developing a phenotypic assay to screen for drugs capable of correcting the observed phenotype

Although my attempts to use the CRISPR/Cas9n system to induce mutations in SHSY5Y and NS1 cell lines were ultimately not successful, the process of optimisation and refinement of protocols meant that I was able to use LUHMES, a human neuronal cell line, to create a mutant line carrying the D252H mutation. LUHMES cells are capable of differentiation into post-mitotic neurons, making them more physiologically relevant than many other immortalised neuronal lines. The mutant cell line I engineered is homozygous for the mutation, however all epilepsy-causing eEF1A2 mutations so far found in humans have been heterozygous, so I would hope to continue this investigation by the creation of more mutant lines using CRISPR. Although it might be expected that homozygous mutant lines would have a more severe phenotype than heterozygous line, given how little is still know about the mutant protein function, it is possible that wildtype eEF1A2 forms a dimer with, and therefore stabilises, the mutant protein. If the mutant protein also has a toxic function in the cell, it is conceivable that cells heterozygous for the mutation could have a worse phenotype than cells homozygous for the mutation, since the presence of wildtype eEF1A2 may stabilise the expression of mutant, damaging eEF1A2.

Another reason for creating more mutant lines is because any identified phenotypes would need to be shown to hold true across several independently derived mutant lines to be of significance. As well as more mutant lines, wild type lines of a similar passage number to the mutant lines would be required to act as baseline controls.

Basic analysis of the mutant lines for phenotypic differences relating to the epilepsy-causing mutations have not thus far yielded any differences, however the search for phenotypic differences was cut short by time restraints. Future analysis would include running a protein synthesis assay on the mutant lines and comparable control lines to determine whether overall levels of protein synthesis are changed by the presence of the mutation, and performing qPCR to determine conclusively whether there is a

quantitative change in eEF1A2 mRNA expression in D252H lines compared to wild type lines. If an eEF1A2-specific antibody can be identified, then isoform-specific western blots could be performed on the cells which would be able to show definitively whether eEF1A2 expression is reduced in the mutant line. Given the epilepsy phenotype in humans, I could also examine the electrophysiological characteristics of mutant and control cells, and relative levels and distribution of synaptic proteins.

The location of many of the epilepsy-causing mutations on or near known interactor binding sites suggests that the observed phenotypes are not due to a general destabilisation of the protein, but more specific effects on the ability of the eEF1A2 to interact with binding partners. The observed differences in phenotype between carriers of different eEF1A2 mutations may therefore be due to changes in the interactome of eEF1A2, which have an effect either on protein synthesis in the cell, on some other non-canonical function of eEF1A2, or on differences in genetic background between patients. Sahni et al. (2015) describe how an understanding of the genotype-phenotype relationship in genetic disease in many cases requires an analysis of perturbations in the interactomes of affected genes, termed the edgotype . Proteomic analysis of mutant lines by mass spectrometry would reveal whether the level of interaction between eEF1A2 and other proteins is changed by the D252H mutation – this is highly likely given the position of D252H at the eEF1Bα binding site. Since eEF1Bα functions as a catalyst of guanine nucleotide exchange for eEF1A2 (and eEF1A1), a reduction in binding between eEF1A and eEF1Bα may reduce the ability of eEF1B to catalyse GDP/GTP exchange, essential for the translation elongation function of eEF1A2. Of the two eEF1A isoforms, eEF1A2 may be more reliant on eEF1B for GDP/GTP exchange, since it has a higher affinity for GDP than GTP (the converse is true in eEF1A1), meaning a reduction in eEF1Bα binding in eEF1A2 could have a larger effect on translation elongation function than it would in eEF1A1.

Relating the mutation back to the human phenotype, of the two cases reported to carry D252H, one developed seizures from the age of eight years old, and the other, though only three years old, has as yet reported no seizures, placing D252H at the milder end of the spectrum of phenotypic severity for eEF1A2 mutations. This later onset of symptoms combined with the fact that LUHMES cells express eEF1A1 as well as

eEF1A2 (a characteristic of developing cells *in vivo* and all known cells *in vitro*) may mean that longer term culture of cells is necessary to identify a disease phenotype. Long term culture (greater than one year) of spinal motor neurons derived from human embryonic stem cells can lead to changes in gene expression from embryonic to more mature forms (Sposito et al., 2015), and CORTECON, a temporal RNA-seq database of neurons derived from human embryonic stem cells shows upregulation of eEF1A2 after 9 days in culture, continuing past 70 days, although levels of eEF1A1 remain high throughout (van de Leemput et al., 2014). A longitudinal analysis of the transcriptome during neurogenesis of cortical glutamatergic neurons from murine embryonic stem cells showed a steady decrease in eEF1A1 mRNA over 28 days. These data together suggest that eEF1A1 downregulation *in vitro* is coupled to development, as it is *in vivo.*

Although not conducive to drug screening assay development, a long term culture of LUHMES mutant lines may allow for more physiologically-relevant detection of phenotypic changes induced by the mutations, which could reveal more about their mode of action. The published maximum duration of LUHMES cells once differentiated had been said to be 12 days (Scholz et al., 2011), but a recent paper published a protocol for 3-D culture of LUHMES cells which can continue culture up to 22 days or beyond by allowing aggregates of LUHMES cells to detach from the surface of the culture vessel and develop in suspension (Smirnova et al., 2015).

With regards to my aim for this section of the PhD, I was ultimately successful in modelling an eEF1A2 epilepsy-causing mutation in a neuronal cell line, and showed expression of eEF1A to be reduced at the protein level in this mutant line compared to wildtype LUHMES. Although much work remains to analyse this line, create more independently-derived mutant lines and work towards a phenotypic assay for drug screening, the work performed here to optimise CRISPR for this locus and cell line, and phenotype the D252H mutant line lays the essential groundwork for further much needed research.

Aim 3: Model the epilepsy-causing eEF1A2 mutations in mouse to better understand the mechanisms behind the human phenotype

Whilst none of the mice engineered using CRISPR were found to replicate the human disease genotype, *Eef1a2*$^{G70S/+}$, the wealth of data gathered has opened up a number of interesting possibilities for future projects.

The priority for future work would be redesigning the CRISPR gRNAs and repair templates to avoid the creation of indels, and so increase the likelihood of producing founder mice for an *Eef1a2* mutant line. In the future I would like to shift my focus from G70S to D252H, the mutation I modelled in LUHMES cells, to provide an *in vivo* model system to complement the *in vitro* work. The advantage of the D252H mutation in terms of mouse modelling is that the human phenotype for carriers of this mutation is not as severe as that of G70S. This may mean the difference between being able to set up a breeding colony of *Eef1a2* mutant mice, and having to analyse founders individually, who die before reaching breeding age.

If I were able to establish such a colony, I would focus initially on characterising the mice in terms of susceptibility to seizure. This could be achieved using wireless telemetry EEG monitoring or analysis of video observations of mice to look for signs of seizure. I would also look for signs of autistic behaviours since these are found in the human carriers of these mutations. Such signs could be found using behavioural testing paradigms such as the marble burying task, social preference tests and repetitive behaviour analysis (Silverman et al., 2010). I would also like to perform proteomics analysis of the brain and/or spinal cord to determine levels of both eEF1A2 and other related proteins in mutant mice compared to wildtype, in the hope of unravelling the pathways affected by these mutations.

Mosaicism was another issue identified in this CRISPR mouse experiment, with at least four mice being found with more than two *Eef1a2* alleles. Singh and colleagues (2015) speculate that mosaicism in CRISPR experiments could be due to the timing of the target locus replication in the zygote. Early replicating loci would have a higher chance of generating mosaicism as there are potentially four copies of the locus for Cas9n to

act on. Replication timings have been measured for the entire human genome using a method that sequences Brd-U tagged nascent proteins at various stages of the cell cycle in a number of different human cell lines. eEF1A2 is shown by this method to be an early replicating gene (Hansen et al., 2010) (Data available on the USCS genome browser under the 'Replication Timing by Repli-seq' track).

Using TOPO cloning certainly enabled me to find more alleles than through Sanger sequencing alone, however in one case I found an allele through allele-specific sequencing that was not then recovered from the TOPO cloning. Sequencing more clones per mouse DNA sample should remedy such a situation but an alternative method would be to use Next-Generation Sequencing of PCR-amplified target loci. Since this is a high-throughput approach, all founder mice in an experiment, or mice from several experiments, could be included in one barcoded amplicon library, enabling simultaneous detection of a higher number of alleles per mouse than is feasible with TOPO cloning.

Regarding my aim for this section, although I was unable to model the exact human genotype in mice, I am confident that the technical reasons for this have been analysed and can be easily rectified in future CRISPR experiments. More is now understood about the effect that the G70S mutation has on eEF1A2 function, given that one copy of the G70S *Eef1a2* allele was shown to be not sufficient to prevent wasting in the *Eef1a2*$^{G70S/-}$ mice. This indicates that the protein, although expressed, was likely not functional; but a concomitant gain of function for the protein cannot be discounted given the severe phenotype of the one mouse homozygous for G70S.

Other future Directions

Work investigating the role that oligomeric state plays in the function of eEF1a isoforms suggests that eEF1A isoforms may perform elongation translation as a monomeric unit (Behrmann et al., 2015) , but other roles, specifically that of actin binding, as a dimer (Vlasenko et al., 2015).

The questions of whether the eEF1A2 isoform specifically dimerises in neurons and for what purpose, whether the epilepsy-causing mutations have an impact on any such dimerisation, and what functional effect this has, remain to be answered. The X-ray crystal structure of eEF1A2 was found to have resolved as a dimer by Crepin et al (2014) , but if elongation translation functions are indeed performed as a monomer then dimerization could well be related to some other, non-canonical function. *In vitro* chemical cross-linking assays using epitope-tagged mutant and wildtype eEF1A2 constructs would be one way of examining potential dimerization disruption.

It would be also be illuminating to investigate the exact distribution of eEF1A2 protein in various neuronal sub-types across development, a task that has been hindered thus far by the difficulty in obtaining reliable isoform-specific antibodies. One way to avoid the need for isofom-specific antibodies would be to epitope-tag *Eef1a2 in vivo* using CRISPR, a method that has been successfully utilised at other loci (Yang et al., 2013), perhaps also multiplexing the CRISPR to create epitope-tagged mutant *Eef1a2* carrying an epilepsy-causing mutation, allowing examination of eEF1A2 localisation across development in health and disease. This could also be performed *in vitro* in LUHMES cells, and in the mutant D252H LUHMES line to examine potential differences in eEF1A2 protein localisation within cells.

In conclusion, as evidence in the role of eEF1A isoforms in neurological disease becomes stronger, increasing our knowledge of the role played by each isoform within the brain becomes ever more important. I and others will use the work I have completed in this project as a building block on which we can increase our understanding, and continue to tease out the functions of eEF1A1 and eEF1A2 in health and disease.

Appendices

Appendix A – Attempts to Mutate eEF1A1 in NS1 Cells

Since I had previously used NS1 cells extensively to develop a neurite outgrowth assay, the production of an epilepsy mutation-carrying NS1 would be incredibly useful, since work to characterise possible neurite outgrowth phenotypes had already been optimised. New gRNAs and repair templates were necessary since NS1 is a rat cell line.

A1.1 Design and Preparation of Rat gRNAs and Repair Templates against D252H and G70S eEF1A2 mutations

I expanded the experiment at this point to include two epilepsy causing mutations – G70S, as before, plus D252H.

A1.1 G70S

As in the initial CRISPR experiment using SHSY5Y cells, I designed gRNAs using the CRISPR.mit.edu design tool to generate gRNA pair possibilities. I chose the top two pairs recommended and ran them through the excel spreadsheet I designed to generate the oligonucleotides to order.

The repair template was designed to cover 100 bp either side of the G70S mutation and included one silent mutation to prevent gRNAs from cutting the template once integrated, by mutating the PAM recognition site for one of the gRNAs from NGG to NGN. This mutation is indicated in Figure A1 in pink. gRNAs were cloned into the pSPCas9n(BB)-2A-puro plasmid and sequenced directly to confirm correct insertion of the oligonucleotides. Diagnostic PCRs such as those used in the initial CRISPR experiment in SHSY5Y were not used here, since every colony picked there had contained the correct insertion. The system works so efficiently that for the remainder of the CRISPR experiments, one colony was picked for each gRNA and sequenced after maxiprepping. In every case the sequence was correct.

Figure A0.1 Rat eEF1A2 exon 3 (capitals) with surrounding introns (lower case). *Two pairs of rat G70S gRNAs shown in red and blue, as well as green and yellow. The repair template is shown in purple, and two sites where the repair template deviates from wild type are indicated. One is to introduce the G70S mutation, the other is to mutate a PAM site to ensure the gRNAs do not cut the newly integrated repair template.*

A1.2 D252H

The D252H mutation lies within exon 5 of eEF1A2. gRNAs were designed, ordered and cloned into the Cas9n plasmid as previously described in section 2.1.6 The repair template was 200 bp long and centred around the D252H mutation. gRNAs and repair template location are shown in Figure A2

Figure A0.2 Rat eEF1A2 exon 5 (capitals) with surrounding introns (lower case). *Two pairs of rat D252H gRNAs shown in red and blue, as well as green and yellow. The repair template is shown in purple.*

A1.3 NS1 Transfection Optimisation

Initially, NS1 transfections were performed using peqFECT (PEQLAB). The optimum ratio of DNA to transfection reagent was determined by transfecting a range of DNA and reagent ratios in 80% confluent NS1 cells. DNA used was pMaxGFP. After 24 hours, the cells were imaged using a fluorescent microscope to detect GFP. Figure A3A shows the results of peqFECT optimisation. The most efficient transfection, as determined by extent of GFP expression, was found using 1µg DNA and 2.5µl peqFECT, so this ratio of reagent to DNA was used in subsequent experiments up until production of peqFECT was discontinued.

At this point two other transfection reagents were tested, Lipofectamine 2000 (Figure A3B) and Fugene (Figure A3C). Lipofectamine 2000 was found to give a much higher transfection efficiency than peqFECT had, at a range of DNA/reagent ratios. 2µg DNA and 4µl lipofectamine 2000 were then used for the remainder of the NS1 CRISPR experiments.

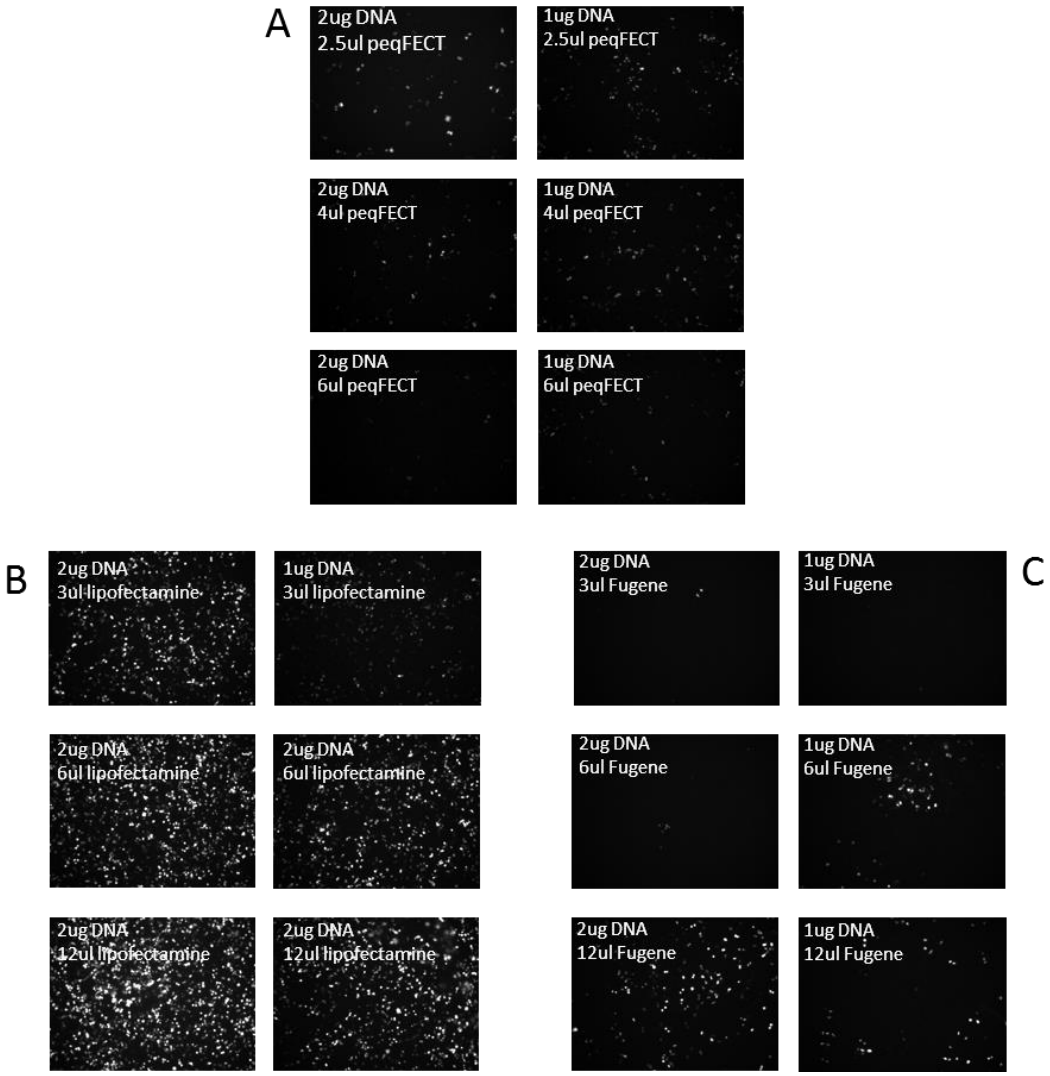

Figure A0.3 Optimisation of three different transfection reagents in NS1 cells. *peqFECT (A), lipofectamine 2000 (B) and fugene (C) were added, along with pMaxGFP DNA, to 80% confluent NS1 cells in one well of a 12-well plate, per manufacturers' instructions. After 24 hours each well was imaged using an inverted fluorescent microscope to detect GFP, shown here in white.*

A1.4 Transfection of gRNAs and Repair Templates into NS1 Cells

Transfection of gRNAs and repair templates designed against the G70S and D252H mutations was conducted using the same transfection conditions as those described in section 2.1.11.2. 24 hours after transfection, a control well which had been transfected with pMaxGFP only was examined using a fluorescent microscope to confirm that the

transfection was successful. 0.5 μg/μl puromycin was then applied to all wells. 48 hours later, all cells were dead. The experiment was repeated with the same result, so on the third attempt three different doses of puromycin were given to triplicate wells: 0μg/μl, 0.25μg/μl and 0.5μg/μl.

One set of triplicate wells in this experiment was cotransfected with one of gRNAs and pmaxGFP. This triplicate was used to give a readout of puromycin activity. If the puromycin treatment was working, the percentage of wells expressing GFP should rise after puromycin treatment. 24 hours post transfection, the GFP control wells were examined and GFP-positive and –negative cells counted. 16% of cells expressed GFP.

48 hours after puromycin treatment, the cell were counted again. The well with no puromycin treatment now had 22% of cells GFP positive, whilst the 0.25 μg/μl and 0.5 μg/μl wells had 35% and 31% GFP positive respectively. These percentages are only an estimate, since only one field of view was counted for each well, however they seemed to show slight enrichment of transfected cells using puromycin, though not as large an enrichment as expected.

One day later, all cells treated with the highest level of puromycin were dead. Some remained from the 0.25 μg/μl treatment, so these were serially diluted into 96-well plates, and any spare cells after this were plated out into T25 plates to grow up for a few days before the DNA was extracted for Screen 1.

One week later the wells containing just one colony were counted, and between 9 and 12 colonies were identified per 96-well plate. Not long after this a bacterial infection was found in several of the plates, so all plates were discarded to prevent the spread of infection.

At this point it was found that peqFECT reagent had been discontinued, so after the testing and optimisation described in section A1.3, lipofectamine 2000 was chosen as a replacement. Using the new transfection reagent, gRNAs and repair templates against G70S and D252H were again transfected in NS1 cells, and a transfection efficiency of 37% was achieved (as measured by percentage of cells expressing GFP in a control well 24 hours post transfection). After 48 hours of 0.25μg/μl puromycin treatment, GFP expression was 41%. Puromycin treatment had had little or no enrichment effect. DNA was taken as before for Screen 1, and cells plated out in 96-

well plates using serial dilution. One week later, bacterial infection again appeared in the outmost wells of some 96-well plates, so all were discarded.

Despite deep cleaning of the tissue culture room, replacement of all media and reagents, new plates and use of an earlier passage of NS1 cells, every subsequent attempt to perform CRISPR using this cell line over a number of months ended in bacterial infection. Eventually, since the source of the infection could not be found, it was decided to focus entirely on a different cell line, LUHMES.

A1.5 PAGE-based Mutation Assay Shows Cutting Activity in NS1 Mixed Cell Populations

Prior to the loss of all potential mutant lines, the DNA taken from mixed populations of transfected and untransfected cells was tested for presence of mutations (screen 1) using the PAGE-based heteroduplex assay.

Six samples were available, from two separate experiments. The first four samples were from an experiment that used peqFECT, the second two samples used lipofectamine 2000. The proportion of cells transfected was higher in the samples that used lipofectamine 2000, and both lipofectamine-treated samples show mutations (red arrows in figure A0.4A for exon 3 gRNA pair, and figure A0.4B for exon 5 gRNA pair). The only peqFECT treated sample to show evidence of mutation was gRNA pair 74/130, which targeted exon 5. (Figure A0.4B, left hand red arrow)

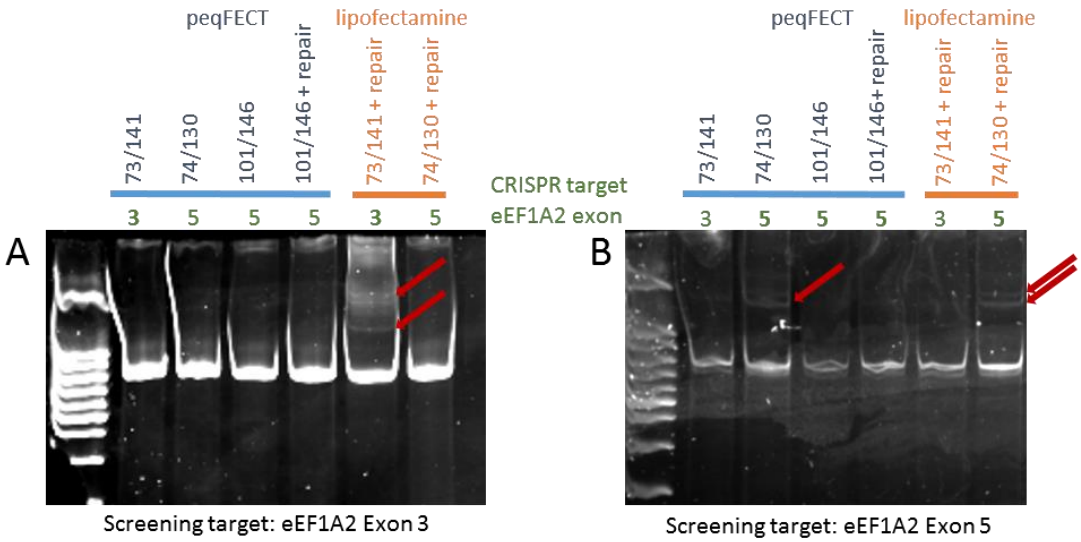

***Figure A0.4 Screen 1 of two separate NS1 CRISPR experiments**, one using peqFECT to transfect gRNAs into cells, the other using lipofectamine 2000. Both experiments transfected gRNAs, and in some wells repair templates designed to incorporate either G70S (exon 3) or D252H (exon 5) mutations. (A) PCR amplified a region around eEF1A2 exon 3. Evidence of mutations (marked by red arrows) can be seen in the lipofectamine-transfected sample that targeted exon 3, but no other samples. (B) PCR amplified a region around eEF1A2 exon 5. Evidence of mutations (marked by red arrows) can be seen in the lipofectamine-transfected sample that targeted exon 5, and one of the peqFECT transfected samples that targeted exon 5 (gRNA pair 74/130).*

A1.6 Diagnostic Digests Show No Evidence of Repair Template Incorporation

In NS1 cells, incorporation of the rat G70S repair template in exon 3 causes the formation of a BbvI recognition site, and incorporation of the D252H template at exon 5 causes the formation of a BtsCI recognition site. The two lipofectamine-treated samples, both of which showed evidence of mutations (Figure A0.4), were amplified using either exon 3 primers, or exon 5 primers, and then used in restriction digests using the restriction enzymes discussed above. The digests were run out on a gel, and in neither case was any evidence of repair template incorporation found.

Since repeated infections could not be avoided, CRISPR work with this cell line was abandoned in favour of LUHMES cells.

Appendix B: G70S CRISPR Mice. Sequences by Mouse Around G70S Locus

INSERTIONS SUSBSTITUTIONS DELETIONS G70S EXONS introns

```
G70S #1          cttatcctgagttgtgcctctacccttccagATGGGGAAGGGCTCTTTTAAATATGCCTGGGTGCTGGACAAGCTGAAGGCCGAGCGTGAACGAAGCATCACC
G70S #1          cttatcctgagttgtgcctctacccttccag----------ATGCCTGGGTGCTGGACAAGCTGAAGGCCGAGCGGGAACGAGGCATCACC

G70S #2          cttatcctgagttgtgcct----------TACTCTTTTTAAATATGCCTGGGTGCTGGACAAGCTGAAGGCCGAGCGGGAACGAGGCATCACC
G70S #2          AGTACTACATCACCATCATctacccttccagATGGGGAAGGGCTCTTTTAAATATGCCTGGGTGCTGGACAAGCTGAAGGCCGAGCGGGAACGAGGCATCACC

G70S #3          +++{LARGE INSERTION EX3 FRAGMENT}GGGGAAGGGCTCTTTTAAATATGCCTGGGTGCTGGACAAGCTGAAGGCCGAGCGGGAACGAGGCATCACC
G70S #3          tcagATGCCTGGGTGCTGGACAAGCTGAAGGCCGGGGAAGGGCTCTTTTAAATATGCCTGGGTGCTGGACAAGCTGAAGGCCGAGCGGGAACGAGGCATCACC

G70S #4          cttatcctgagttgtgcctctacccttccagATGGGGAAGGGCTCTTTTAAATATGCCTGGGTGCTGGACAAGCTGAAGGCCGAGCGTGAACGAAGCATCACC
G70S #4          cttatcctgagttgtgcctctacccttccagATGGGGAAGGGCTCTTTTAAATATGCCTGGGTGCTGGACAAGCTGAAGGCCGAGCGTGAACGAAGCATCACC

G70S #5          cttatcctgagttgtgcctctacccttccagATC----------AGGCCGAGCGGGAACGAGGCATCACC
G70S #5          cttatcctgagttgtgcctctacccttccagATGGGGAAGGGCTCTTTTAAATATGCCTGGGTGCTGGACAAGCTGAAGGCCGAGCGTGAACGAAGCATCACC

G70S #6          cttatcctgagttgtgcctctacccttcct----------TGCCTGGGTGCTGGACAAGCTGAAGGCCGAGCGGGAACGAGGCATCACC
G70S #6          cttatcctgagttgtgcctctacccttccagATGGGGAAGGGCTCTTTTAAATATGCCTGGGTGCTGGACAAGCTGAAGGCCGAGCGGGAACGAGGCATCACC

G70S #7          cttatcctgagttgtgcctctacccttccagATGGGGAAGGGCTCTTTTAAATATGC----------TGAAGGCCGAGCGTGAACGAAGCATCACC
G70S #7          SECOND ALLELE EITHER A WILDTYPE ALLELE OR ANOTHER LIKE ABOVE. OR BOTH (MOSAIC).

G70S #8          cttatcctgagttgtgcctctacccttccagATGGGGAAGGGCTCTTTTAAATATGCCTGGGT----------GA-GGCCGAGCGGGAACGAGGCATCACC
G70S #8          SECOND ALLELE EITHER A WILDTYPE ALLELE OR ANOTHER LIKE ABOVE. OR BOTH (MOSAIC).

G70S #9          cttatcctgagttgtgcctctacccttccagATGGGGAAGGGCTCTTTTAAATATGCCTGGGTGCTGGACAAGCTGAAGGCCGAGCGGGAACGAGGCATCACC
G70S #9          14BP DELETION ON ONE ALLELE BUT CANNOT SEE WHERE IT ORIGINATES.

G70S #10         cttatcctgagttgtgcctctacccttccag----------TTAAATATGCCTGGGTGCTGGACAAGCTGAAGGCCGAGCGGGAACGAGGCATCACC
G70S #10         cttatcctgagttgtgcctctacccttccagATGGGGAAGGGCTCTTTTAAATATGCCTGGGTGCTGGACAAGCTGAAGGCCGAGCGTGAACGAAGCATCACC
```

```
G70S #11          cttatcctgagttgtgcctctacccttccagATGGGGAAGGGCTCTTTTAAATATGCCT----------CAAGCTGAAGGCCGAGCGTGAACGAAGCATCACC
G70S #11          SECOND ALLELE EITHER A WILDTYPE ALLELE OR ANOTHER LIKE ABOVE. OR BOTH (MOSAIC).

G70S #12          Probable large insertions on both alleles, ~50bp on one, ~150bp on the other from PCR of region.

G70S #13          Probable large deletions on both alleles, region could not be amplified using PCR

G70S #14          cttatcctgagttgtgcctctacccttccagATGGGGAAGGGCTCTTTTAAATATGCCTGGGT-CTGGACAAGCTGAAGGCCGAGCGTGAACGAAGCATCACC
G70S #14          cttatcctgagttgtgcctctacccttccagATGGGGAAGGG----------CTGGACAAGCTGAAGGCCGAGCGGGAACGAGGCATCACC

G70S #15          cttatcctgagttgtgcctctacccttccagATGGGGAAGGGCTCTTTTAAATATGCCTGGGTGCTGGACAAGCTGAAGGCCGAGCGGGAACGAGGCATCACC
G70S #15          cttatcctgagttgtgcctctacccttccagATGGGGAAGGGCTCTTTTAAATATGCCTGGGTGCTGGACAAGCTGAAGGCCGAGCGGGAACGAGGCATCACC

G70S #16          ++++++++++++++++++++++++++++++++++++++++++++++++{125BP insertion}++++++CAAGCTGAAGGCCGAGCGGGAACGAGGCATCACC
G70S #16          ++++++++++++++++++++++++++++++++++++++++++++++++{125BP insertion}++++++CAAGCTGAAGGCCGAGCGGGAACGAGGCATCACC

G70S #17          ttatcctgagttgtgcctctacccttccagATGGGGGAAGGGCTCTTTTAAATATGCCTGGGTGCTGGACAAGCTGAAGGCCGAGCGTGAACGAAGCATCACC
G70S #17          SECOND ALLELE EITHER A WILDTYPE ALLELE OR ANOTHER LIKE ABOVE. OR BOTH (MOSAIC).

G70S #18          cttatcctgag----------------------------------------ATATGCCTGGGTGCTGGACAAGCTGAAGGCCGAGCGGGAACGAGGCATCACC
G70S #18          --------------------------{UNKNOWN LARGE INDEL}------TGCCTGGGTGCTGGACAAGCTGAAGGCCGAGCGGGAACGAGGCATCACC

G70S #19          cttatcctgagttgtgcctctacccttccag-------------------------CCTGGGTGCTGGACAAGCTGAAGGCCGAGCGGGAACGAGGCATCACC
G70S #19          cttatcctgagttgtg-----------------------------------------CCTGGGTGCTGGACAAGCTGAAGGCCGAGCGGGAACGAGGCATCACC

G70S #20          cttatcctgagttgtgcctctacccttcca----GGGAAGGGCTCTTTTAAATATGCCTGGGTGCTGGACAAGCTGAAGGCCGAGCGGGAACGAGGCATCACC
G70S #20          cttatcctgagttgtgcctctacccttccagATGGGGAAGGGCTCTTTTAAATATGCCTGGGTGCTGGACAAGCTGAAGGCCGAGCGTGAACGAAGCATCACC

G70S #21          cttatcctgagttgtgcctctacccttccag----------------------ATGCCTGGGTGCTGGACAAGCTGAAGGCCGAGCGTGAACGAAGCATCACC
G70S #21          cttatcctgagttgtgcctctacccttccag----------------------ATGCCTGGGTGCTGGACAAGCTGAAGGCCGAGCGGGAACGAAGCATCACC
G70S #21          ALSO AN ALLELE WITH G70S INCORPORATION AND A 1BP  INTRONIC DELETION 258BP DOWNSTREAM OF G70S LOCATION

G70S #22          cttatcctgagttgtgcctctacccttccagAT--------------------ATGCCTGGGTGCTGGACAAGCTGAAGGCCGAGCGGGAACGAGGCATCACC
G70S #22          cttatcctgagttgtgcctctacccttccag----------------------ATGCCTGGGTGCTGGACAAGCTGAAGGCCGAGCGGGAACGAGGCATCACC
```

```
G70S #23          cttatcctgagttgtgcctctacccttccagATGGGGAAGGGCTCTTTTAAATATGCCTGGGTGCTGGACAAGCTGAAGGCCGAGCGGGAACGAGGCATCACC
G70S #23          cttatcctgagttgtgcctctacccttccagATGGGGAAGGGCTCTTTTAAATATGCCTGGGTGCTGGACAAGCTGAAGGCCGAGCGGGAACGAGGCATCACC

G70S #24          cttatcctgagttgtgcctctacccttccagATGGGGAAGGG----------TATGCCTGGGTGCTGGACAAGCTGAAGGCCGAGCGGGAACGAGGCATCACC
G70S #24          ----------------------------------------{180BP DELETION}----------------------------------GAGGCATCACC

G70S #25          cttatcctgagttgtgcctctacccttccagA----------------------------------------TGAAGGCCGAGCGTGAACGAGGCATCACC
G70S #25          cttatcctgagttgtgcctctacccttccagATGGGGAAGGGCTCTTTTAAATATGCCTGGGTGCTGGACAAGCTGAAGGCCGAGCGGGAACGAGGCATCACC

G70S #26          ctta-cctgagttgtgcctctacccttccagA----------------------TGCCTGGGTGCTGGACAAGCTGAAGGCCGAGCGGGAACGAGGCATCACC
G70S #26          cttatcctgagttgtgcctctacccttccagA----------------------TGCCTGGGTGCTGGACAAGCTGAAGGCCGAGCGGGAACGAGGCATCACC

G70S #27          cttatcctgagttgtgcctctacccttccagATGGGGAAGGGCTCTTTTAAATATGCCT--------------------GGCCGAGCGTGAACGAAGCATCACC
G70S #27          cttatcctgagttgtgcctctacccttcc--------------------AAATATGCCTGGGTGCTGGACAAGCTGAAGGCCGAGCGGGAACGAGGCATCACC
G70S #27          cttatcctgagttgtgcctctacccttccagATGGG--------------------GCCTGGGTGCTGGACAAGCTGAAGGCCGAGCGGGAACGAGGCATCACC

G70S #28          cttatcctgagttgtgcctctacccttccagATGGGGAAGGGCTCTTTTAAATATGCCTGGGTGCTGGACAAGCTGAAGGCCGAGCGGGAACGAGGCATCACC
G70S #28          cttatcctgagttgtgcctctacccttccagATG-GGAAGGGCTCTTTTAAATATGCCTGGGTGCTGGACAAGCTGAAGGCCGAGCGGGAACGAGGCATCACC
G70S #28          cttTAAATATCTCGACATTAGGTGAAGGCCTGGGTGCTGGACATTAGGTAAATATGCCTGGGTGCTGGACAAGCTGAAGGCCGAGCGGGAACGAGGCATCACC

G70S #29          cttatcctgagttgtgcctctacccttcc------------------------------------------------------------------GAGG-------
G70S #29          cttatcctgagttgtgcctctacccttcc------------------------------------------------------------------GAGG-------

G70S #30          cttatcctgagttgtgcctctacccttccagATG-GGAAGGGCTCTTTTAAATATGCCTGGGTGCTGGACAAGCTGAAGGCCGAGCGGGAACGAGGCATCACC
G70S #30          cttatcctgagttgtgcctctacccttccagATG-GGAAGGGCTCTTTTAAATATGCCTGGGTGCTGGACAAGCTGAAGGCCGAGCGGGAACGAGGCATCACC

G70S #31          tgagttgtgcctctacccttccagATGGGGAAGGGCTCTTTTAAATATGCCTGGGTGAAGATCGTACTTCAAGCTGAAGGCCGAGCGGGAACGAGGCATCACC
G70S #31          cttatcctgagttgtgcctctacccttccagATGGGGAAGGGCTCTTTTAAATATGCCTGGGTGC-GGACAAGCTGAAGGCCGAGCGTGAACGAAGCATCACC
G70S #31          cttatcctgagttgtgcctctacccttccagATG----ATGCCTGGGTATCATATGCCTGGGTGCTGGACAAGCTGAAGGCCGAGCGGGAACGAGGCATCACC
G70S #31          cttatcctgagttgtgcctctacccttccagATGGGGA----------TAAATATGCCTGGGTGCTGGACAAGCTGAAGGCCGAGCGGGAACGAGGCATCACC
G70S #31          cttatcctgagttgtgcctctacccttccagA-----------------------------------ACA----GAAGGCCGAGCGTGAACGAAGCATCACC

G70S #32          cttatcctgagttgtgcctctacccttccag----------------------ATGCCTGGGTGCTGGACAAGCTGAAGGCCGAGCGGGAACGAGGCATCACC
G70S #32          cttatcctgagttgtgcctctacccttccagATGGGGAAGGGCTCTTTTAAATATGCCTGGGTGCTGGACAAGCTGAAGGCCGAGCGGGAACGAGGCATCACC
```

```
G70S #33          cttatcctgagttgtgcctctacccttcca------GAAGGG-TCTTTTAAATATGCCTGGGTGCTGGACAAGCTGAAGGC-GAGCGGGAACGAGGCATCACC
G70S #33          cttatcctgagttgtgcctctacccttccagATGGGGAAGGGCTCTTTTAAATATGCCTGGGTGCTGGACAAGCTGAAGGCCGAGCGTGAACGAAGCATCACC


G70S #34          cttatcctgagttgtgcctctacccttccag----------------------ATGCCTGGGTGCTGGACAAGCTGAAGGCCGAGCGGGAACGAGGCATCACC
G70S #34          cttatcctgagttgtgcctctacccttccag----------------------ATGCCTGGGTGCTGGACAAGCTGAAGGCCGAGCGGGAACGAGGCATCACC

G70S #35          cttatcctgagttgtgcctctacccttccagAT----------------------CCTGGGTGCTGGACAAGCTGAAGGCCGAGCGGGAACGAGGCATCACC
G70S #35          ++++++++++++++++++++{48BP INSERTION}++++++++TTTTAAATATGCCTGGGTGCTGGACAAGCTGAAGGCCGAGCGGGAACGAGGCATCACC
```

Bibliography

Andersen, G.R., Valente, L., Pedersen, L., Kinzy, T.G., and Nyborg, J. (2001). Crystal structures of nucleotide exchange intermediates in the eEF1A-eEF1Balpha complex. Nat Struct Biol 8, 531–534.

Antonellis, A., Ellsworth, R.E., Sambuughin, N., Puls, I., Abel, A., Lee-Lin, S.Q., Jordanova, A., Kremensky, I., Christodoulou, K., Middleton, L.T., et al. (2003). Glycyl tRNA synthetase mutations in Charcot-Marie-Tooth disease type 2D and distal spinal muscular atrophy type V. Am J Hum Genet 72, 1293–1299.

Arai, H., and Takahashi, T. (2009). A combination therapy of donepezil and cilostazol for patients with moderate Alzheimer disease: pilot follow-up study. Am J Geriatr Psychiatry 17, 353–4.

Arslan, G., and Fredholm, B.B. (1999). Adenosine and P2 receptors in PC12 cells. Genotypic, phenotypic and individual differences. Prog Brain Res 120, 301–10.

Auerbach, B.D., Osterweil, E.K., and Bear, M.F. (2011). Mutations causing syndromic autism define an axis of synaptic pathophysiology. Nature 480, 63–68.

Bassell, G.J., and Warren, S.T. (2008). Fragile X syndrome: loss of local mRNA regulation alters synaptic development and function. Neuron 60, 201–214.

Beckelman, B.C., and Ma, T. (2015). Synaptic Pathology in Alzheimer's Disease' ' 300.10/C43. In 2015 Neuroscience Meeting Planner, (Washington, DC: Society for Neuroscience),.

Beckelman, B.C., Zhou, X., Keene, C.D., and Ma, T. (2016). Impaired Eukaryotic Elongation Factor 1A Expression in Alzheimer's Disease. Neurodegener Dis 16, 39–43.

Behrmann, E., Loerke, J., Budkevich, T.V., Yamamoto, K., Schmidt, A., Penczek, P.A., Vos, M.R., Bürger, J., Mielke, T., Scheerer, P., et al. (2015). Structural snapshots of actively translating human ribosomes. Cell 161, 845–857.

Bender, A.C., Morse, R.P., Scott, R.C., Holmes, G.L., and Lenck-Santini, P.P. (2012). SCN1A mutations in Dravet syndrome: impact of interneuron dysfunction on neural networks and cognitive outcome. Epilepsy Behav 23, 177–186.

Bernard, C., Cossart, R., Hirsch, J. C., Esclapez, M. and Ben-Ari, Y. (2000). What is GABAergic inhibition? How is it modified in epilepsy? Epilepsia 41 Suppl 6S90–5.

Bhakar, A.L., Dölen, G., and Bear, M.F. (2012). The pathophysiology of fragile X (and what it teaches us about synapses). Annu Rev Neurosci 35, 417–443.

Bluem, R., Schmidt, E., Corvey, C., Karas, M., Schlicksupp, A., Kirsch, J., and Kuhse, J. (2007). Components of the translational machinery are associated with juvenile glycine receptors and are redistributed to the cytoskeleton upon aging and synaptic activity. J Biol Chem 282, 37783–37793.

Boeckers, T. M., Bockmann, J., Kreutz, M. R. and Gundelfinger, E. D. (2002). ProSAP/Shank proteins - a family of higher order organizing molecules of the postsynaptic density with an emerging role in human neurological disease. Journal of Neurochemistry 81(5), 903–910.

Borck, G., Shin, B.S., Stiller, B., Mimouni-Bloch, A., Thiele, H., Kim, J.R., Thakur, M., Skinner, C., Aschenbach, L., Smirin-Yosef, P., et al. (2012). eIF2γ mutation that disrupts eIF2 complex integrity links intellectual disability to impaired translation initiation. Mol Cell 48, 641–646.

Bosutti, A., Scaggiante, B., Grassi, G., Guarnieri, G., and Biolo, G. (2007). Overexpression of the elongation factor 1A1 relates to muscle proteolysis and proapoptotic p66(ShcA) gene transcription in hypercatabolic trauma patients. Metab Clin Exp 56, 1629–1634.

Bunai, F., Ando, K., Ueno, H., and Numata, O. (2006). Tetrahymena eukaryotic translation elongation factor 1A (eEF1A) bundles filamentous actin through dimer formation. J Biochem 140, 393–399.

Cajigas, I.J., Tushev, G., Will, T.J., tom Dieck, S., Fuerst, N., and Schuman, E.M. (2012). The local transcriptome in the synaptic neuropil revealed by deep sequencing and high-resolution imaging. Neuron 74, 453–466.

Carvill, G.L., Weckhuysen, S., McMahon, J.M., Hartmann, C., Møller, R.S., Hjalgrim, H., Cook, J., Geraghty, E., O'Roak, B.J., Petrou, S., et al. (2014). GABRA1 and STXBP1: Novel genetic causes of Dravet syndrome. Neurology.82(14), 1245-1253

Chambers DM, Peters J, Abbott CM. The lethal mutation of the mouse wasted (wst) is a deletion that abolishes expression of a tissue-specific isoform of translation elongation factor 1alpha, encoded by the Eef1a2 gene. Proc Natl Acad Sci U S A. 1998 Apr 14;95(8):4463–4468.

Chang, R., and Wang, E. (2007). Mouse translation elongation factor eEF1A-2 interacts with Prdx-I to protect cells against apoptotic death induced by oxidative stress. J Cell Biochem 100, 267–278.

Chieffo, D., Ricci, D., Baranello, G., Martinelli, D., Veredice, C., Lettori, D., Battaglia, D., Dravet, C., Mercuri, E., and Guzzetta, F. (2011). Early development in Dravet syndrome; visual function impairment precedes cognitive decline. Epilepsy Res 93, 73–79.

Cho, S.J., Lee, H., Dutta, S., Seog, D.H., and Moon, I.S. (2012). Translation elongation factor-1A1 (eEF1A1) localizes to the spine by domain III. BMB Rep 45, 227–32.

Choi, Y., Sims, G.E., Murphy, S., Miller, J.R., and Chan, A.P. (2012). Predicting the functional effect of amino acid substitutions and indels. PLoS ONE 7, e46688.

Chuang, S.M., Chen, L., Lambertson, D., Anand, M., Kinzy, T.G., and Madura, K. (2005). Proteasome-mediated degradation of cotranslationally damaged proteins involves translation elongation factor 1A. Mol Cell Biol 25, 403–413.

Claes, L.R., Ceulemans, B., Audenaert, D., Deprez, L., Jansen, A., Hasaerts, D., Weckx, S., Claeys, K.G., Del-Favero, J., Van Broeckhoven, C., et al. (2004). De novo KCNQ2 mutations in patients with benign neonatal seizures. Neurology 63, 2155–2158.

Crepin, T., Shalak, V.F., Yaremchuk, A.D., Vlasenko, D.O., McCarthy, A., Negrutskii, B.S., Tukalo, M.A., and El'skaya, A.V. (2014). Mammalian translation elongation factor eEF1A2: X-ray structure and new features of GDP/GTP exchange mechanism in higher eukaryotes. Nucleic Acids Res 42, 12939–12948.

Dard, R., Mignot, C., Durr, A., Lesca, G., Sanlaville, D., Roze, E. and Mochel, F. (2015). Relapsing encephalopathy with cerebellar ataxia related to an ATP1A3 mutation. Developmental Medicine and Child Neurology 57(12), 1183–1186.

Doig J, Griffiths LA, Peberdy D, Dharmasaroja P, Vera M, Davies FJ, et al. *In vivo* characterization of the role of tissue-specific translation elongation factor 1A2 in protein synthesis reveals insights into muscle atrophy. FEBS J. 2013 Dec;280(24):6528–6540.

Engel, J., and International League Against Epilepsy (ILAE) (2001). A proposed diagnostic scheme for people with epileptic seizures and with epilepsy: report of the ILAE Task Force on Classification and Terminology. Epilepsia 42, 796–803.

Epi4K Consortium, Epilepsy Phenome/Genome Project, Allen, A.S., Berkovic, S.F., Cossette, P., Delanty, N., Dlugos, D., Eichler, E.E., Epstein, M.P., Glauser, T., et al. (2013). De novo mutations in epileptic encephalopathies. Nature 501, 217–221.

Fujimura, M., Usuki, F., Cheng, J., and Zhao, W. (2016). Prenatal low-dose methylmercury exposure impairs neurite outgrowth and synaptic protein expression and suppresses TrkA pathway activity and eEF1A1 expression in the rat cerebellum. Toxicol Appl Pharmacol 298, 1–8.

Garcia-Esparcia, P., Hernández-Ortega, K., Koneti, A., Gil, L., Delgado-Morales, R., Castaño, E., Carmona, M., and Ferrer, I. (2015). Altered machinery of protein synthesis is region- and stage-dependent and is associated with α-synuclein oligomers in Parkinson's disease. Acta Neuropathol Commun 3, 76.

Gauthier, J., Champagne, N., Lafrenière, R. G., Xiong, L., Spiegelman, D., Brustein, E., Lapointe, M., Peng, H., Côté, M., Noreau, A., Hamdan, F. F., Addington, A. M., Rapoport, J. L., Delisi, L. E., Krebs, M.-O., Joober, R., Fathalli, F., Mouaffak, F., Haghighi, A. P., Néri, C., Dubé, M.-P., Samuels, M. E., Marineau, C., Stone, E. A., Awadalla, P., Barker, P. A., Carbonetto, S., Drapeau, P., Rouleau, G. A. and S2D

Team (2010). De novo mutations in the gene encoding the synaptic scaffolding protein SHANK3 in patients ascertained for schizophrenia. Proceedings of the National Academy of Sciences of the United States of America 107(17), 7863–7868

Giustetto, M., Hegde, A.N., Si, K., Casadio, A., Inokuchi, K., Pei, W., Kandel, E.R., and Schwartz, J.H. (2003). Axonal transport of eukaryotic translation elongation factor 1alpha mRNA couples transcription in the nucleus to long-term facilitation at the synapse. Proc Natl Acad Sci U S A 100, 13680–13685.

Goto, S. (2005). Cilostazol: potential mechanism of action for antithrombotic effects accompanied by a low rate of bleeding. Atheroscler Suppl 6, 3–11.

Greer, P. L., Hanayama, R., Bloodgood, B. L., Mardinly, A. R., Lipton, D. M., Flavell, S. W., Kim, T.-K., Griffith, E. C., Waldon, Z., Maehr, R., Ploegh, H. L., Chowdhury, S., Worley, P. F., Steen, J. and Greenberg, M. E. (2010). The Angelman Syndrome protein Ube3A regulates synapse development by ubiquitinating arc. Cell 140(5), 704–716.

Griffiths, L. Investigating the role of eEF1A2 in motor neuron degeneration. Doctoral dissertation 2011 University of Edinburgh

Griffiths, L.A., Doig, J., Churchhouse, A.M., Davies, F.C., Squires, C.E., Newbery, H.J., and Abbott, C.M. (2012). Haploinsufficiency for translation elongation factor eEF1A2 in aged mouse muscle and neurons is compatible with normal function. PLoS ONE 7, e41917.

Hansen, R.S., Thomas, S., Sandstrom, R., Canfield, T.K., Thurman, R.E., Weaver, M., Dorschner, M.O., Gartler, S.M., and Stamatoyannopoulos, J.A. (2010). Sequencing newly replicated DNA reveals widespread plasticity in human replication timing. Proc Natl Acad Sci U S A 107, 139–144.

Hashimoto, K., and Ishima, T. (2011). Neurite outgrowth mediated by translation elongation factor eEF1A1: a target for antiplatelet agent cilostazol. PLoS ONE 6, e17431.

Helbig, K.L., Farwell Hagman, K.D., Shinde, D.N., Mroske, C., Powis, Z., Li, S., Tang, S., and Helbig, I. (2016). Diagnostic exome sequencing provides a molecular diagnosis for a significant proportion of patients with epilepsy. Genet Med. 18(9), 898-905

Helbig K Delineation of the EEF1A2-epileptic encephalopathy phenotypic spectrum Poster presented at the American Epilepsy Association 2015 Meeting, Pennsylvania Convention Center, Philadelphia, PA

Henry KR. Audiogenic Seizure Susceptibility Induced in C57B1/6J Mice by Prior Auditory Exposure. Science. 1967 Nov 17;158(3803):938–940.

Huang, F., Chotiner, J.K., and Steward, O. (2005). The mRNA for elongation factor 1alpha is localized in dendrites and translated in response to treatments that induce long-term depression. J Neurosci 25, 7199–7209.

Huber, K.M., Kayser, M.S., and Bear, M.F. (2000). Role for rapid dendritic protein synthesis in hippocampal mGluR-dependent long-term depression. Science 288, 1254–1257.

Inui, T., Kobayashi, S., Ashikari, Y., Sato, R., Endo, W., Uematsu, M., Oba, H., Saitsu, H., Matsumoto, N., Kure, S., et al. (2015). Two cases of early-onset myoclonic seizures with continuous parietal delta activity caused by EEF1A2 mutations. Brain Dev. 38(5), 520-524

Inui, M., Miyado, M., Igarashi, M., Tamano, M., Kubo, A., Yamashita, S., Asahara, H., Fukami, M., and Takada, S. (2014). Rapid generation of mouse models with defined point mutations by the CRISPR/Cas9 system. Sci Rep 4, 5396.

Jamain, S., Quach, H., Betancur, C., Råstam, M., Colineaux, C., Gillberg, I. C., Soderstrom, H., Giros, B., Leboyer, M., Gillberg, C., Bourgeron, T. and Paris Autism Research International Sibpair Study (2003). Mutations of the X-linked genes encoding neuroligins NLGN3 and NLGN4 are associated with autism. *Nature Genetics* 34(1), 27–29.

Janikiewicz, J. (2011). Tissue-specific variants of translation elongation factor eEF1A and their role in cancer. Doctoral Dissertation University of Edinburgh

Jinek, M., Chylinski, K., Fonfara, I., Hauer, M., Doudna, J. A. and Charpentier, E. (2012). A programmable dual-RNA-guided DNA endonuclease in adaptive bacterial immunity.*Science (New York)* 337(6096), 816–821.

Jordanova, A., Irobi, J., Thomas, F.P., Van Dijck, P., Meerschaert, K., Dewil, M., Dierick, I., Jacobs, A., De Vriendt, E., Guergueltcheva, V., et al. (2006). Disrupted function and axonal distribution of mutant tyrosyl-tRNA synthetase in dominant intermediate Charcot-Marie-Tooth neuropathy. Nat Genet 38, 197–202.

Kahns, S., Lund, A., Kristensen, P., Knudsen, C.R., Clark, B.F., Cavallius, J., and Merrick, W.C. (1998). The elongation factor 1 A-2 isoform from rabbit: cloning of the cDNA and characterization of the protein. Nucleic Acids Res 26, 1884–1890.

Khacho, M., Mekhail, K., Pilon-Larose, K., Pause, A., Côté, J., and Lee, S. (2008). eEF1A is a novel component of the mammalian nuclear protein export machinery. Mol Biol Cell 19, 5296–5308.

Khalyfa, A., Bourbeau, D., Chen, E., Petroulakis, E., Pan, J., Xu, S., and Wang, E. (2001). Characterization of elongation factor-1A (eEF1A-1) and eEF1A-2/S1 protein expression in normal and wasted mice. J Biol Chem 276, 22915–22922.

Khalyfa, A., Carlson, B.M., Dedkov, E.I., and Wang, E. (2003). Changes in protein levels of elongation factors, eEF1A-1 and eEF1A-2/S1, in long-term denervated rat muscle. Restor Neurol Neurosci 21, 47–53.

Kjeldgaard, M., Nissen, P., Thirup, S., and Nyborg, J. (1993). The crystal structure of elongation factor EF-Tu from Thermus aquaticus in the GTP conformation. Structure 1, 35–50.

De Kovel, C. G. F., Brilstra, E. H., van Kempen, M. J. A., Van't Slot, R., Nijman, I. J., Afawi, Z., De Jonghe, P., Djémié, T., Guerrini, R., Hardies, K., Helbig, I., Hendrickx, R., Kanaan, M., Kramer, U., Lehesjoki, A.-E. E., Lemke, J. R., Marini, C., Mei, D., Møller, R. S., Pendziwiat, M., Stamberger, H., Suls, A., Weckhuysen, S., EuroEPINOMICS RES Consortium and Koeleman, B. P. C. (2016). Targeted

sequencing of 351 candidate genes for epileptic encephalopathy in a large cohort of patients. Molecular genetics & genomic medicine 4(5), 568–580

Kugel, J.F., and Goodrich, J.A. (2006). Beating the heat: A translation factor and an RNA mobilize the heat shock transcription factor HSF1. Mol Cell 22, 153–154.

Lam, W.W.K., Millichap, J.J., Soares, D.C., Chin, R., McLellan, A., Fitzpatrick, D.R., Elmslie, F., Lees, M.M., Schaefer, G.B., D D D S, et al. (2016). Novel de novo EEF1A2 missense mutations causing epilepsy and intellectual disability. Mol Genet Genomic Med.4(4), 465-74.

Lawson-Yuen, A., Saldivar, J.-S., Sommer, S. and Picker, J. (2008). Familial deletion within NLGN4 associated with autism and Tourette syndrome. European Journal of Human Genetics 16(5), 614–618

Lee, J.W., Beebe, K., Nangle, L.A., Jang, J., Longo-Guess, C.M., Cook, S.A., Davisson, M.T., Sundberg, J.P., Schimmel, P., and Ackerman, S.L. (2006). Editing-defective tRNA synthetase causes protein misfolding and neurodegeneration. Nature 443, 50–55.

Lee, S., Francoeur, A.M., Liu, S., and Wang, E. (1992). Tissue-specific expression in mammalian brain, heart, and muscle of S1, a member of the elongation factor-1 alpha gene family. J Biol Chem 267, 24064–24068.

Van de Leemput, J., Boles, N.C., Kiehl, T.R., Corneo, B., Lederman, P., Menon, V., Lee, C., Martinez, R.A., Levi, B.P., Thompson, C.L., et al. (2014). CORTECON: a temporal transcriptome analysis of *in vitro* human cerebral cortex development from human embryonic stem cells. Neuron 83, 51–68.

Li, D., Wei, T., Abbott, C.M., and Harrich, D. (2013). The unexpected roles of eukaryotic translation elongation factors in RNA virus replication and pathogenesis. Microbiol Mol Biol Rev 77, 253–266.

De Ligt, J., Willemsen, M.H., van Bon, B.W., Kleefstra, T., Yntema, H.G., Kroes, T., Vulto-van Silfhout, A.T., Koolen, D.A., de Vries, P., Gilissen, C., et al. (2012). Diagnostic exome sequencing in persons with severe intellectual disability. N Engl J Med 367, 1921–1929.

Liu, G., Tang, J., Edmonds, B.T., Murray, J., Levin, S., and Condeelis, J. (1996). F-actin sequesters elongation factor 1alpha from interaction with aminoacyl-tRNA in a pH-dependent reaction. J Cell Biol 135, 953–963.

Liu, Y., Fong, M., Cone, J., Wang, S., Yoshitake, M., and Kambayashi, J. (2000). Inhibition of adenosine uptake and augmentation of ischemia-induced increase of interstitial adenosine by cilostazol, an agent to treat intermittent claudication. J Cardiovasc Pharmacol 36, 351–360.

Lopes, F., Barbosa, M., Ameur, A., Soares, G., de Sá, J., Dias, A.I., Oliveira, G., Cabral, P., Temudo, T., Calado, E., et al. (2016). Identification of novel genetic causes of Rett syndrome-like phenotypes. J Med Genet. 53(3), 190-199

Lund, A., Knudsen, S.M., Vissing, H., Clark, B., and Tommerup, N. (1996). Assignment of human elongation factor 1alpha genes: EEF1A maps to chromosome 6q14 and EEF1A2 to 20q13.3. Genomics 36, 359–361.

Misawa H, Sherr EH, Lee DJ, Chetkovich DM, Tan A, Schreiner CE, et al. Identification of a monogenic locus (jams1) causing juvenile audiogenic seizures in mice. J Neurosci. 2002 Dec 1;22(23):10088–10093.

Morita, K., Bunai, F., and Numata, O. (2008). Roles of three domains of Tetrahymena eEF1A in bundling F-actin. Zool Sci 25, 22–29.

Mouse Models in the Study of Genetic Neurological Disorders [Internet]. illustrated. Springer Science & Business Media; 2012.

Najmabadi, H., Hu, H., Garshasbi, M., Zemojtel, T., Abedini, S.S., Chen, W., Hosseini, M., Behjati, F., Haas, S., Jamali, P., et al. (2011). Deep sequencing reveals 50 novel genes for recessive cognitive disorders. Nature 478, 57–63.

Nakajima, J., Okamoto, N., Tohyama, J., Kato, M., Arai, H., Funahashi, O., Tsurusaki, Y., Nakashima, M., Kawashima, H., Saitsu, H., et al. (2015). De novo EEF1A2 mutations in patients with characteristic facial features, intellectual disability, autistic behaviors and epilepsy. Clin Genet 87, 356–361.

Nakamizo, T., Kawamata, J., Yoshida, K., Kawai, Y., Kanki, R., Sawada, H., Kihara, T., Yamashita, H., Shibasaki, H., Akaike, A., et al. (2003). Phosphodiesterase inhibitors are neuroprotective to cultured spinal motor neurons. J Neurosci Res 71, 485–495.

Newbery, H.J., Gillingwater, T.H., Dharmasaroja, P., Peters, J., Wharton, S.B., Thomson, D., Ribchester, R.R., and Abbott, C.M. (2005). Progressive loss of motor neuron function in wasted mice: effects of a spontaneous null mutation in the gene for the eEF1 A2 translation factor. J Neuropathol Exp Neurol 64, 295–303.

Newbery, H.J., Loh, D.H., O'Donoghue, J.E., Tomlinson, V.A., Chau, Y.Y., Boyd, J.A., Bergmann, J.H., Brownstein, D., and Abbott, C.M. (2007). Translation elongation factor eEF1A2 is essential for post-weaning survival in mice. J Biol Chem 282, 28951–28959.

Numata, O., Kurasawa, Y., Gonda, K., and Watanabe, Y. (2000). Tetrahymena elongation factor-1 alpha is localized with calmodulin in the division furrow. J Biochem 127, 51–56.

Orhan, G., Bock, M., Schepers, D., Ilina, E.I., Reichel, S.N., Löffler, H., Jezutkovic, N., Weckhuysen, S., Mandelstam, S., Suls, A., et al. (2014). Dominant-negative effects of KCNQ2 mutations are associated with epileptic encephalopathy. Ann Neurol 75, 382–394.

Osterweil, E.K., Krueger, D.D., Reinhold, K., and Bear, M.F. (2010). Hypersensitivity to mGluR5 and ERK1/2 leads to excessive protein synthesis in the hippocampus of a mouse model of fragile X syndrome. J Neurosci 30, 15616–15627.

Osterweil, E.K., Chuang, S.C., Chubykin, A.A., Sidorov, M., Bianchi, R., Wong, R.K., and Bear, M.F. (2013). Lovastatin corrects excess protein synthesis and prevents epileptogenesis in a mouse model of fragile X syndrome. Neuron 77, 243–250.

O'Driscoll, C.M., and Gorman, A.M. (2005). Hypoxia induces neurite outgrowth in PC12 cells that is mediated through adenosine A2A receptors. Neuroscience 131, 321–329.

Paciorkowski, A. R., McDaniel, S. S., Jansen, L. A., Tully, H., Tuttle, E., Ghoneim, D. H., Tupal, S., Gunter, S. A., Vasta, V., Zhang, Q., Tran, T., Liu, Y. B., Ozelius, L. J., Brashear, A., Sweadner, K. J., Dobyns, W. B. and Hahn, S. (2015). Novel mutations in ATP1A3 associated with catastrophic early life epilepsy, episodic prolonged apnea, and postnatal microcephaly. Epilepsia 56(3), 422–430.

Park, S.H., Kim, J.H., Bae, S.S., Hong, K.W., Lee, D.S., Leem, J.Y., Choi, B.T., and Shin, H.K. (2011). Protective effect of the phosphodiesterase III inhibitor cilostazol on amyloid β-induced cognitive deficits associated with decreased amyloid β accumulation. Biochem Biophys Res Commun 408, 602–608.

Pedersen, L., Andersen, G.R., Knudsen, C.R., Kinzy, T.G., and Nyborg, J. (2001). Crystallization of the yeast elongation factor complex eEF1A-eEF1B alpha. Acta Crystallogr D Biol Crystallogr 57, 159–161.

Phelan, K. and McDermid, H. E. (2012). The 22q13.3 deletion syndrome (Phelan-McDermid syndrome). Molecular syndromology 2(3-5), 186–201.

Phillips, G.R., Florens, L., Tanaka, H., Khaing, Z.Z., Fidler, L., Yates, J.R., and Colman, D.R. (2005). Proteomic comparison of two fractions derived from the transsynaptic scaffold. J Neurosci Res 81, 762–775.

Popp, M.W., and Maquat, L.E. (2013). Organizing principles of mammalian nonsense-mediated mRNA decay. Annu Rev Genet 47, 139–165.

Rabin, R.A., Fiorella, D., and Van Wylen, D.G. (1993). Role of extracellular adenosine in ethanol-induced desensitization of cyclic AMP production. J Neurochem 60, 1012–1017.

Ran, F.A., Hsu, P.D., Wright, J., Agarwala, V., Scott, D.A., and Zhang, F. (2013b). Genome engineering using the CRISPR-Cas9 system. Nat Protoc 8, 2281–2308.

Ran, F.A., Hsu P.D., Lin C.Y., Gootenberg, J.S. Konermann S., T A.E., Scott D.A., Inoue A., Matoba S., Zhang Y., Zhang F. (2013a). Double nicking by RNA-guided CRISPR Cas9 for enhanced genome editing specificity. Cell 154, 1380–1389

Ross KC, Coleman JR. Developmental and genetic audiogenic seizure models: behavior and biological substrates. Neurosci Biobehav Rev. 2000 Aug;24(6):639–653.

Ruest, L.B., Marcotte, R., and Wang, E. (2002). Peptide elongation factor eEF1A-2/S1 expression in cultured differentiated myotubes and its protective effect against caspase-3-mediated apoptosis. J Biol Chem 277, 5418–5425.

Sahni, N., Yi, S., Taipale, M., Fuxman Bass, J.I., Coulombe-Huntington, J., Yang, F., Peng, J., Weile, J., Karras, G.I., Wang, Y., et al. (2015). Widespread macromolecular interaction perturbations in human genetic disorders. Cell 161, 647–660.

Samocha, K. E., Robinson, E. B., Sanders, S. J., Stevens, C., Sabo, A., McGrath, L. M., Kosmicki, J. A., Rehnström, K., Mallick, S., Kirby, A., Wall, D. P., MacArthur, D. G., Gabriel, S. B., DePristo, M., Purcell, S. M., Palotie, A., Boerwinkle, E., Buxbaum, J. D., Cook, E. H., Gibbs, R. A., Schellenberg, G. D., Sutcliffe, J. S., Devlin, B., Roeder, K., Neale, B. M. and Daly, M. J. (2014). A framework for the interpretation of de novo mutation in human disease. Nature Genetics 46(9), 944–950.

Sandbaken, M.G., and Culbertson, M.R. (1988). Mutations in elongation factor EF-1 alpha affect the frequency of frameshifting and amino acid misincorporation in Saccharomyces cerevisiae. Genetics 120, 923–934.

Sanges, C., Scheuermann, C., Zahedi, R.P., Sickmann, A., Lamberti, A., Migliaccio, N., Baljuls, A., Marra, M., Zappavigna, S., Reinders, J., et al. (2012). Raf kinases mediate the phosphorylation of eukaryotic translation elongation factor 1A and regulate its stability in eukaryotic cells. Cell Death Dis 3, e276.

Scheper, G.C., van der Knaap, M.S., and Proud, C.G. (2007). Translation matters: protein synthesis defects in inherited disease. Nat Rev Genet 8, 711–723.

Shamovsky, I., Ivannikov, M., Kandel, E.S., Gershon, D., and Nudler, E. (2006). RNA-mediated response to heat shock in mammalian cells. Nature 440, 556–560.

Schildknecht, S., Karreman, C., Pöltl, D., Efrémova, L., Kullmann, C., Gutbier, S., Krug, A., Scholz, D., Gerding, H.R., and Leist, M. (2013). Generation of genetically-modified human differentiated cells for toxicological tests and the study of neurodegenerative diseases. ALTEX 30, 427–444.

Scholz, D., Pöltl, D., Genewsky, A., Weng, M., Waldmann, T., Schildknecht, S., and Leist, M. (2011). Rapid, complete and large-scale generation of post-mitotic neurons from the human LUHMES cell line. J Neurochem 119, 957–971.

Schreiber RA. Effects of stimulus intensity and stimulus duration during acoustic priming on audiogenic seizures in C57BL/6J mice. Dev Psychobiol. 1977 Jan;10(1):77–85.

Schrör, K. (2002). The pharmacology of cilostazol. Diabetes Obes Metab 4 Suppl 2, S14–S19.

Shultz, L. D., Sweet, H. O., Davisson, M. T. and Coman, D. R. (1982). “Wasted”, a new mutant of the mouse with abnormalities characteristic to ataxia telangiectasia. Nature297(5865), 402–404.

Silverman, J. L., Yang, M., Lord, C. and Crawley, J. N. (2010). Behavioural phenotyping assays for mouse models of autism. Nature Reviews. Neuroscience 11(7), 490–502.

Singh, P., Schimenti, J.C., and Bolcun-Filas, E. (2015). A mouse geneticist’s practical guide to CRISPR applications. Genetics 199, 1–15.

Smirnova, L., Harris, G., Delp, J., Valadares, M., Pamies, D., Hogberg, H.T., Waldmann, T., Leist, M., and Hartung, T. (2015). A LUHMES 3D dopaminergic neuronal model for neurotoxicity testing allowing long-term exposure and cellular resilience analysis. Arch Toxicol 90(11), 2725-2743

Soares, D.C., Barlow, P.N., Newbery, H.J., Porteous, D.J., and Abbott, C.M. (2009). Structural models of human eEF1A1 and eEF1A2 reveal two distinct surface clusters of sequence variation and potential differences in phosphorylation. PLoS ONE 4, e6315.

Sposito, T., Preza, E., Mahoney, C.J., Setó-Salvia, N., Ryan, N.S., Morris, H.R., Arber, C., Devine, M.J., Houlden, H., Warner, T.T., et al. (2015). Developmental regulation of tau splicing is disrupted in stem cell-derived neurons from frontotemporal dementia patients with the 10 + 16 splice-site mutation in MAPT. Hum Mol Genet 24, 5260–5269.

Steinlein, O. K. (2004). Genetic mechanisms that underlie epilepsy. Nature Reviews. Neuroscience 5(5), 400–408.

Sudo, T., Tachibana, K., Toga, K., Tochizawa, S., Inoue, Y., Kimura, Y., and Hidaka, H. (2000). Potent effects of novel anti-platelet aggregatory cilostamide analogues on recombinant cyclic nucleotide phosphodiesterase isozyme activity. Biochem Pharmacol 59, 347–356.

Sung, Y.J., Dolzhanskaya, N., Nolin, S.L., Brown, T., Currie, J.R., and Denman, R.B. (2003). The fragile X mental retardation protein FMRP binds elongation factor 1A mRNA and negatively regulates its translation in vivo. J Biol Chem 278, 15669–15678.

Svobodová, K., Horák, P., Stratil, A., Bartenschlager, H., Van Poucke, M., Chalupová, P., Dvořáková, V., Knorr, C., Stupka, R., Čítek, J., et al. (2015). Porcine EEF1A1 and EEF1A2 genes: genomic structure, polymorphism, mapping and expression. Mol Biol Rep 42, 1257–1264.

Takahashi, K., and Mikuni, M. (2012). [Augmentation therapy with cilostazol for the intractable geriatric major depressive disorder patients with deep white matter hyperintensities on T2-weighted brain MRI]. Seishin Shinkeigaku Zasshi 114, 297–302.

Taylor, A.M., Berchtold, N.C., Perreau, V.M., Tu, C.H., Li Jeon, N., and Cotman, C.W. (2009). Axonal mRNA in uninjured and regenerating cortical mammalian axons. J Neurosci 29, 4697–4707.

Timchenko, A.A., Novosylna, O.V., Prituzhalov, E.A., Kihara, H., El'skaya, A.V., Negrutskii, B.S., and Serdyuk, I.N. (2013). Different oligomeric properties and

stability of highly homologous A1 and proto-oncogenic A2 variants of mammalian translation elongation factor eEF1. Biochemistry 52, 5345–5353.

Topol, A., English, J.A., Flaherty, E., Rajarajan, P., Hartley, B.J., Gupta, S., Desland, F., Zhu, S., Goff, T., Friedman, L., et al. (2015). Increased abundance of translation machinery in stem cell-derived neural progenitor cells from four schizophrenia patients. Translational Psychiatry 5, e662.

Tsai, N.P., Wilkerson, J.R., Guo, W., Maksimova, M.A., DeMartino, G.N., Cowan, C.W., and Huber, K.M. (2012). Multiple autism-linked genes mediate synapse elimination via proteasomal degradation of a synaptic scaffold PSD-95. Cell 151, 1581–1594.

Tuchman, R. and Rapin, I. (2002). Epilepsy in autism. Lancet Neurology 1(6), 352–358.

Veeramah, K.R., Johnstone, L., Karafet, T.M., Wolf, D., Sprissler, R., Salogiannis, J., Barth-Maron, A., Greenberg, M.E., Stuhlmann, T., Weinert, S., et al. (2013). Exome sequencing reveals new causal mutations in children with epileptic encephalopathies. Epilepsia 54, 1270–1281.

Vera, M., Pani, B., Griffiths, L.A., Muchardt, C., Abbott, C.M., Singer, R.H., and Nudler, E. (2014). The translation elongation factor eEF1A1 couples transcription to translation during heat shock response. Elife 3, e03164.

Vlasenko, D.O., Novosylna, O.V., Negrutskii, B.S., and El'skaya, A.V. (2015). Truncation of the A,A(∗),A' helices segment impairs the actin bundling activity of mammalian eEF1A1. FEBS Lett 589, 1187–1193.

Weckhuysen, S., Mandelstam, S., Suls, A., Audenaert, D., Deconinck, T., Claes, L.R., Deprez, L., Smets, K., Hristova, D., Yordanova, I., et al. (2012). KCNQ2 encephalopathy: emerging phenotype of a neonatal epileptic encephalopathy. Ann Neurol 71, 15–25.

Yang, H., Wang, H., Shivalila, C.S., Cheng, A.W., Shi, L., and Jaenisch, R. (2013). One-step generation of mice carrying reporter and conditional alleles by CRISPR/Cas-mediated genome engineering. Cell 154, 1370–1379.

Yang, Y., Muzny, D.M., Xia, F., Niu, Z., Person, R., Ding, Y., Ward, P., Braxton, A., Wang, M., Buhay, C., et al. (2014). Molecular findings among patients referred for clinical whole-exome sequencing. JAMA 312, 1870–1879.

Zoghbi, H. Y. and Bear, M. F. (2012). Synaptic dysfunction in neurodevelopmental disorders associated with autism and intellectual disabilities. Cold Spring Harbor Perspectives in Biology 4(3),